GEOPHYSICAL STUDIES OF SALINE FLUIDS IN THE DEEP CRUST

by

Guy Marquis
B.Sc., Université du Québec à Chicoutimi, 1986
M.Sc., University of Victoria, 1988

ACCEPTED
FACULTY OF GRADUATE STUDIES

DEAN
DATE Sept 28/92

A Dissertation Submitted in Partial Fulfilment of the
Requirements for the Degree of

DOCTOR OF PHILOSOPHY

in the School of Earth and Ocean Sciences

We accept this thesis as conforming
to the required standard

Dr. Roy D. Hyndman, Co-Supervisor (School of Earth & Ocean Sciences)

Dr. George D. Spence, Co-Supervisor (School of Earth & Ocean Sciences)

Dr. Christopher R. Barnes, Departmental Member (School of Earth & Ocean Sciences)

Dr. Harry W. Dosso, Outside Member (Department of Physics and Astronomy)

Dr. Alan G. Jones, External Examiner (Geological Survey of Canada)

University of Victoria

Supervisors: Drs Roy D. Hyndman and George D. Spence

ABSTRACT

Geophysical studies have shown that the lower continental crust, especially in Phanerozoic areas, is commonly more conductive and reflective and has a lower seismic velocity than what is expected from the composition of xenoliths and exposed lower crustal terrains. These anomalous in situ properties can be explained by the presence of small amounts of free aqueous fluids in the intergranular space. A compilation of lower crustal geophysical data shows a correlation between electrical resistivity and seismic velocity, in agreement with physical properties models of porous rocks, as well as a general decrease of inferred porosity with geological age. Correlations with geothermal data also show that the reflective and conductive layers usually have their tops near the 400-450°C isotherms suggesting an association with the brittle-ductile transition. The rheology at depth might have an effect on the trapping of the fluids that are in textural equilibrium pores in the ductile crust. Alternatively metamorphic reactions may constrain free fluids to below this depth. Model for the effects of porosity in textural equilibrium pores on seismic and electrical properties of rocks have been developed, and are also in good agreement with the data compilation. Re-processed LITHOPROBE South Cordillera magnetotelluric and seismic reflection data in the Intermontane Belt support a coincidence between the top of low resistivity and high reflectivity of the crust at depths of about 20 km in the west, and about 15 km in the east of the Belt, corresponding to temperatures around 450°C. Two models for reconciling the low vertical permeability required for maintaining the porosity at depth with the interconnection required to reduce the electrical resistivity are presented: one involves the deformation of equilibrium pores by small deviatoric stresses that pinch off the vertical interconnection, the other the flattening and alignment of pores by lower crustal shear processes. A difficulty is recognized in reconciling free aqueous fluids in the lower crust with the expected retrograde metamorphism that should take up any free water. This process can be avoided if the fluids are of high salinity. High-salinity fluids

are in liquid phase in the lower crust, not in supercritical phase as often thought.

Examiners:

Dr. Roy D. Hyndman, Co-Supervisor (School of Earth & Ocean Sciences)

Dr. George D. Spence, Co-Supervisor (School of Earth & Ocean Sciences)

Dr. Christopher R. Barnes, Departmental Member (School of Earth & Ocean Sciences)

Dr. Harry W. Dosso, Outside Member (Department of Physics and Astronomy)

Dr. Alan G. Jones, External Examiner (Geological Survey of Canada)

TABLE OF CONTENTS

LIST OF TABLES

LIST OF FIGURES

ACKNOWLEDGEMENTS

First and foremost, I want to thank my research supervisor, Dr. Roy Hyndman. Roy has shown great patience in dealing with my somewhat unusual working methods and was always available to discuss any idea I might have, as well as providing the seeds for a lot of the work presented here. I just hope that putting up with me for three years will not deter him from taking another Ph.D. student... I have received tremendous help from a lot of people as I worked my way into that project: seismic data utilities from George Spence, seismic processing support at Lithoprobe from Kris Vasudevan and Rolf Maier, MT data and processing advice from Alan Jones, MT inversion programs from J.T. Weaver and A.K. Agarwal, and help with ANSYS from Minh Ly and Subu Ramamani. I benefited greatly from discussions with Tark Hamilton, Lawrie Law, Trevor Lewis, and Leonid Vanyan. Still, the best thing about Grad School remains the fellow students: thanks to Tianson Yuan for general geophysical consulting, Chinese tutoring, and support in our daily battles against computer equipment, to Chris Spindler for computer help and radio savvy, to Stewart Langton for discussions/arguments on any topic under the sun, and to Steve Fallows for long discussions on the philosophical implications of alternative rock lyrics. I also wish to thank two other students from ultra-Rockies, John Varsek and Mike Burianyk, for data, results, suggestions, and interest in my work.

Really huge thank you to Richard Baldwin for computer help, rides to PGC, and for his understanding and friendship.

Of course, thanks to NSERC and SCBC for fellowships that put food on my table for all those years and for NSERC grants to Roy that paid for various travel needs and research expenses. Thanks also to the Geological Survey of Canada that provided a variety of services (computer time, office space, supplies, drafting) at no charge.

DEDICATION

A Gilles et Géraldine, qui m'ont toujours encouragé faire ce qui me plaisait, même si les bénéfices sont parfois longs à venir...

"... besides, I expect nothing better from geophysicists anyway."

Anonymous petrologist, reviewing Marquis and Hyndman (1992)

CHAPTER I INTRODUCTION

The lower continental crust is the least understood part of the lithosphere. Its instrumental role in most tectonic processes such as crustal shortening, extensional zones and rifts, and thrust and normal fault décollements has long been recognized, but the lack of direct geological data prevented geologists from developing well constrained compositional models. Most early models were based on such limited evidence that almost any composition could be fit to the data.

With the advent of more modern geophysical and geological measurement and analysis techniques in the past two decades, it became possible to obtain more detailed information on the deeper part of the crust. Reflection and refraction seismology, electromagnetic methods, better heat-flow and heat generation data, isotope studies, fluid inclusions, geothermometry and geobarometry (especially on xenoliths and in exposed cross-sections), and many other techniques provide important constraints around which new geological models have been built. These new data have spurred interest in the lower crust and there have been special volumes focusing on the geophysics and the geology of the lower crust (Dawson et al., 1986; Mereu et al., 1989). In this first chapter, I briefly review the geological and geophysical information on the nature and the physical properties of deep-crustal rocks, and how these results can be reconciled in a single model.

i. Geological information on the deep crust

There are two major direct sampling sources of material of lower crustal origin:

xenoliths and high-grade metamorphic terrains. The latter are interpreted as coming from the lower crust since their mineralogy can only be produced under high pressure-temperature conditions, i.e. 5-10 kbar, 600-900°C (Taylor and McLennan, 1984). Kay and Kay (1986) have presented an overview of data from both of these sources. Geochemical results of relevance for this thesis topic are summarized here.

1.1 Xenoliths

Xenoliths are found in volcanic pipes and in kimberlites. They are entrained and brought to the surface by magmas and fluidized solids, usually of mantle origin, traversing the crust. The rapid transport of xenoliths should ensure that they have not been subjected to retrograde metamorphism by long exposures to mid and upper crustal temperatures and pressures. They may have been near the surface for long periods of time but the slow reaction kinetics at such low temperatures prevents them from retrograding. For these reasons "they are probably the least equivocal samples of the lower crust to which we have access" (Taylor and McLennan, 1984). They provide a good aerial sampling of the deep crust since they can be found in many different tectonic environments: converging plate margins, rift valleys, continental intraplate regions, and volcanic plateaux. The main problems in interpreting xenolith data are that they are small, and hence it is difficult to obtain large-scale correlations, and the vertical resolution can be quite poor, as xenoliths from different horizons have been scrambled. There is also uncertainty in correlating the observed mineralogies to actual depths of origin. Xenoliths are primarily produced in high temperature volcanic terrains so they may be at higher metamorphic facies than typical rocks of the present lower crust, i.e. most xenoliths being in granulite facies does not imply that the lower crust everywhere is in granulite facies at present time. In most crustal areas present-day temperatures in the lower crust are well below the onset of granulite facies metamorphism.

Griffin and O'Reilly (1987) have surveyed lower crustal xenolith data from all over the world. Most xenoliths have been collected from basalt outcrops in Phanerozoic terrains or from kimberlites in Precambrian cratons. Precambrian xenoliths appear to be somewhat less mafic in composition than Phanerozoic ones. In both environments however, the overwhelming majority of the xenoliths surveyed have mineralogies typical

of mafic granulites (see Table 1). Griffin and O'Reilly (1987) conclude that most of the crustal material added since the Precambrian is mafic, and that the lower crust in Phanerozoic areas is especially mafic. They also note that the lower crustal composition inferred from xenoliths is more mafic than suggested by the seismic velocity data (see Chapter III).

	Mafic	Felsic	Granulite	Eclogite	Other
Precambrian	13	3	13	2	1
Phanerozoic	44	13	40	5	12

Table 1 Xenolith data compilation from Griffin and O'Reilly (1987)

Caution should be exercised in interpreting the results above as evidence that most of the lower crust is in granulite facies. As stated earlier, xenoliths are usually produced in high temperature volcanic environments, so their metamorphic grade may be higher than that of typical lower crust.

1.2 Exposed cross-sections

Even though the information from xenoliths is usually admitted to be more reliable sampling of the lower crust (Kay and Kay, 1986), the most accessible samples of large volumes of lower crustal rocks are the exposed granulite terrains, whose mineralogy requires that they have been formed in the deep crust. These terrains all show increasing metamorphic grades at present deeper crustal levels (Fountain and Salisbury, 1981), regardless of chemical composition. One objection to the extrapolation of such sections to the deep crust as a whole is that most have been exposed by overthrusting at continental collision zones, which is certainly not the typical history of most crustal sections (Kay and Kay, 1986). In addition, the pressure-temperature conditions at which these rocks have been metamorphosed, as well as structural relationships, indicate that they may not come from the lowermost crust, but often from

the middle crust, at their peak metamorphic conditions. This has been shown to be the case for the Kapuskasing structural zone, until recently considered of very deep crustal origin. Structural (Percival and Card, 1985) and seismic (Percival et al., 1989) evidence now indicates that it actually originates from the middle crust . Granulite facies rocks as a whole range from mafic to silicic in composition. In the Ivrea Zone (Italy) and in Australia, lower crustal rocks are predominantly mafic, while in Manitoba (Pikwitonei subprovince) they are intermediate to silicic. However, even in the latter section there are mafic-ultramafic bodies present in the deeper levels.

The most famous sample of the deep crust is the Lewisian gneiss complex in Scotland. It comprises a block of granulite facies rocks surrounded by amphibolite-facies gneisses. A comparison of granulite vs amphibolite gneiss composition (Weaver and Tarney, 1984) shows that the inferred lower crustal rocks in the complex are more mafic (~12% Fe, Mg minerals) than the middle crustal rocks (~8%). In comparison, xenoliths in general are even more mafic. This indicates that the deeper portions of the crust are more mafic than the composition of the exposed granulite terrains (Taylor and McLennan, 1984), and therefore also more mafic than suggested by the seismic velocity data.

ii. Geophysical information on the deep crust

Over the past few decades, a large number of geophysical measurements have provided information on the lower crust. The main contributors are the large national seismic reflection programs such as COCORP, BIRPS, LITHOPROBE, and many others that have produced huge amounts of geophysical data from almost all kinds of geological environments. Yet despite the diversity of those environments, three surprising results have been commonly obtained:

(1) seismic reflection profiles commonly show a transparent upper and middle crust, but a highly reflective lower crust, particularly in Phanerozoic areas. Examples of such reflective patterns have been presented by Matthews (1986) for the British Isles (see "typical Birp" in Figure 1a), where reflectivity is increased between 5 to 10 s two-way traveltime, by Allmendinger et al. (1987) for the Basin and Range Province (Figure

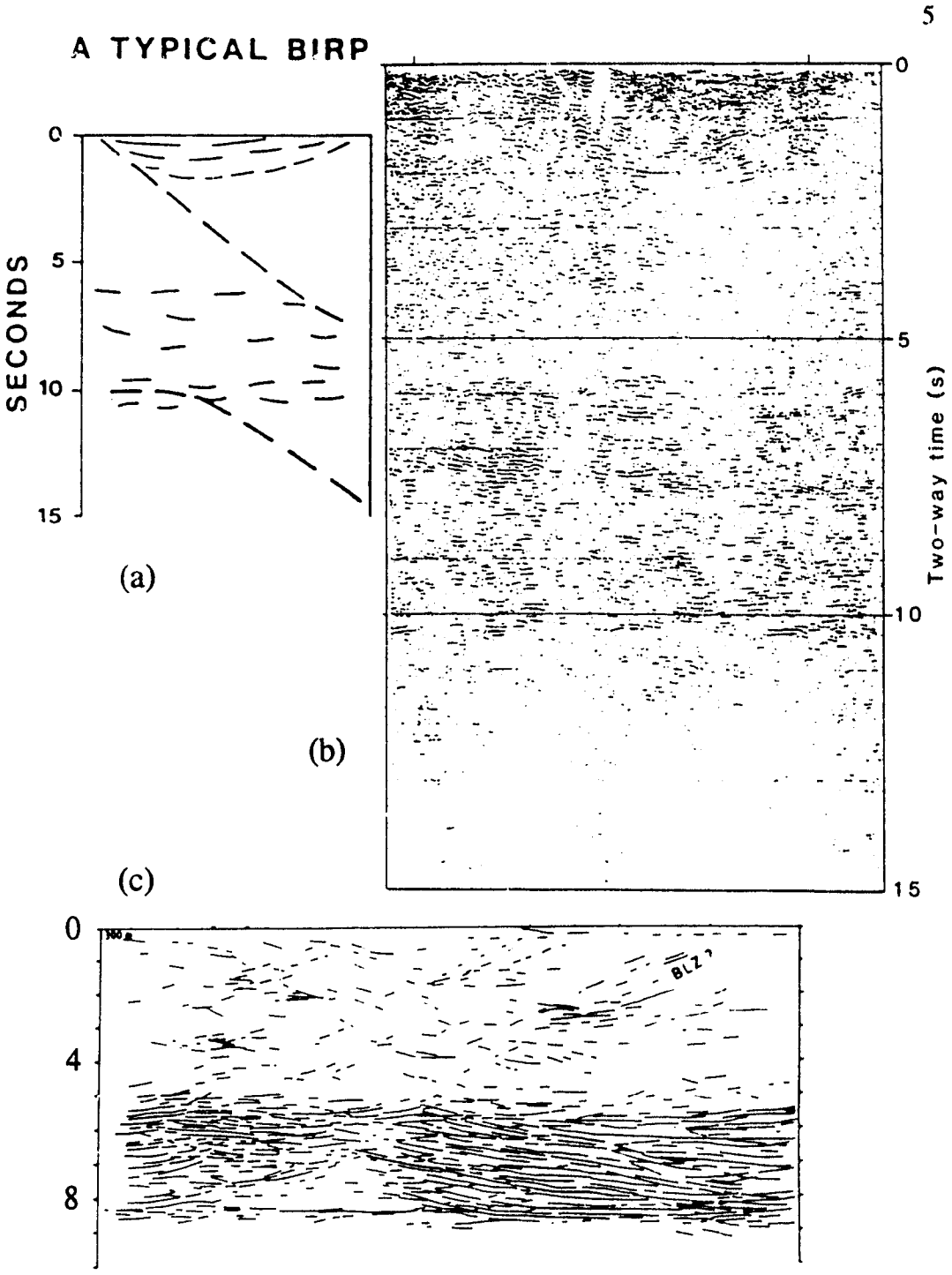

Figure 1 Examples of deep crustal reflectivity: (a) "typical Birp" for the British Isles, (b) Basin and Range Province, (c) southwest Germany.

1b), and by Lüschen et al. (1987) for southwest Germany (Figure 1c). For other examples of enhanced reflectivity in the deep crust, the reader is referred to the volumes on Seismic Reflection Profiling of the Lithosphere (Barazangi and Brown (eds.), 1986a, b; Matthews (ed.), *Geophysical Journal of the Royal Astronomical Society*, **89**, 1987; Leven et al. (eds.), *Tectonophysics*, **173**, 1990; Meissner et al. (eds.), 1991). While more recent data and analyses have shown the division of a non-reflective upper crust and a reflective lower crust to be rather too simple, a higher reflectivity in the lower crust is usually observed.

(2) seismic refraction profiles have defined lower crustal velocities commonly less than 7.0 km/s (e.g. Meissner, 1986), lower than expected for the otherwise inferred dominant mafic composition from xenoliths and exposed terrains as discussed above (e.g. Hyndman and Klemperer, 1989). A few examples are shown in Figure 2: Basin and Range, U.S.A. (Benz et al., 1991; Figure 2a), Black Forest, Germany (Gajewski and Prodehl, 1987; Figure 2b), North Sea (Barton and Wood, 1984; Figure 2c).

(3) magnetotelluric and controlled-source surveys have revealed that the lower crust generally has very low electrical resistivity compared to rocks thought to be common in the lower crust as measured dry in the laboratory (e.g. Shankland and Ander, 1983). Some examples of deep crustal low-resistivity zones are shown in Figure 3: Scotland (Hutton et al., 1980; Figure 3a), Basin and Range (Lienert and Bennett, 1976; Figure 3b), and the Canadian Cordillera (Jones et al., 1992; Figure 3c). Many reviews and compilations on the resistivity of the deep crust have been published over the years: Jones (1981), Gregori and Lanzerotti (1982), Shankland and Ander (1983), Haak and Hutton (1986), Ádám (1987), Hyndman and Shearer (1989). There is little doubt that the lower crust, especially in Phanerozoic areas, has very low resistivity.

iii. How can they be reconciled?

Many hypotheses have been presented to explain these properties of the lower crust, but most of them apply to only a single anomalous property. Reflective patterns have often been associated with sub-horizontal compositional boundaries, basalt sills, horizontal shear zones or mylonitic fabrics. The lower deep crustal velocities have been

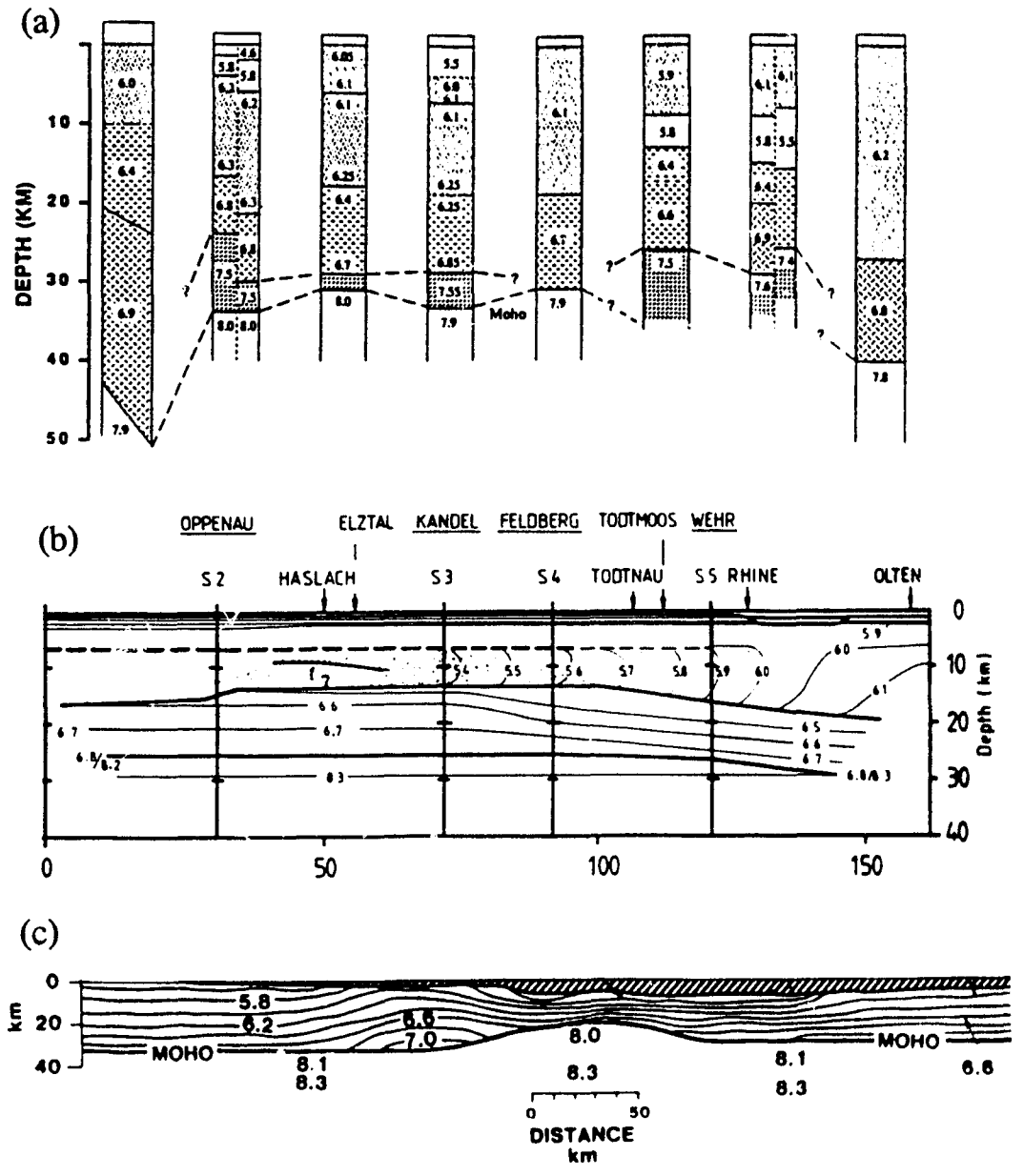

Figure 2 Examples of deep crustal low-velocity zones: (a) Basin and Range Province, (b) Black Forest, Germany, (c) North Sea.

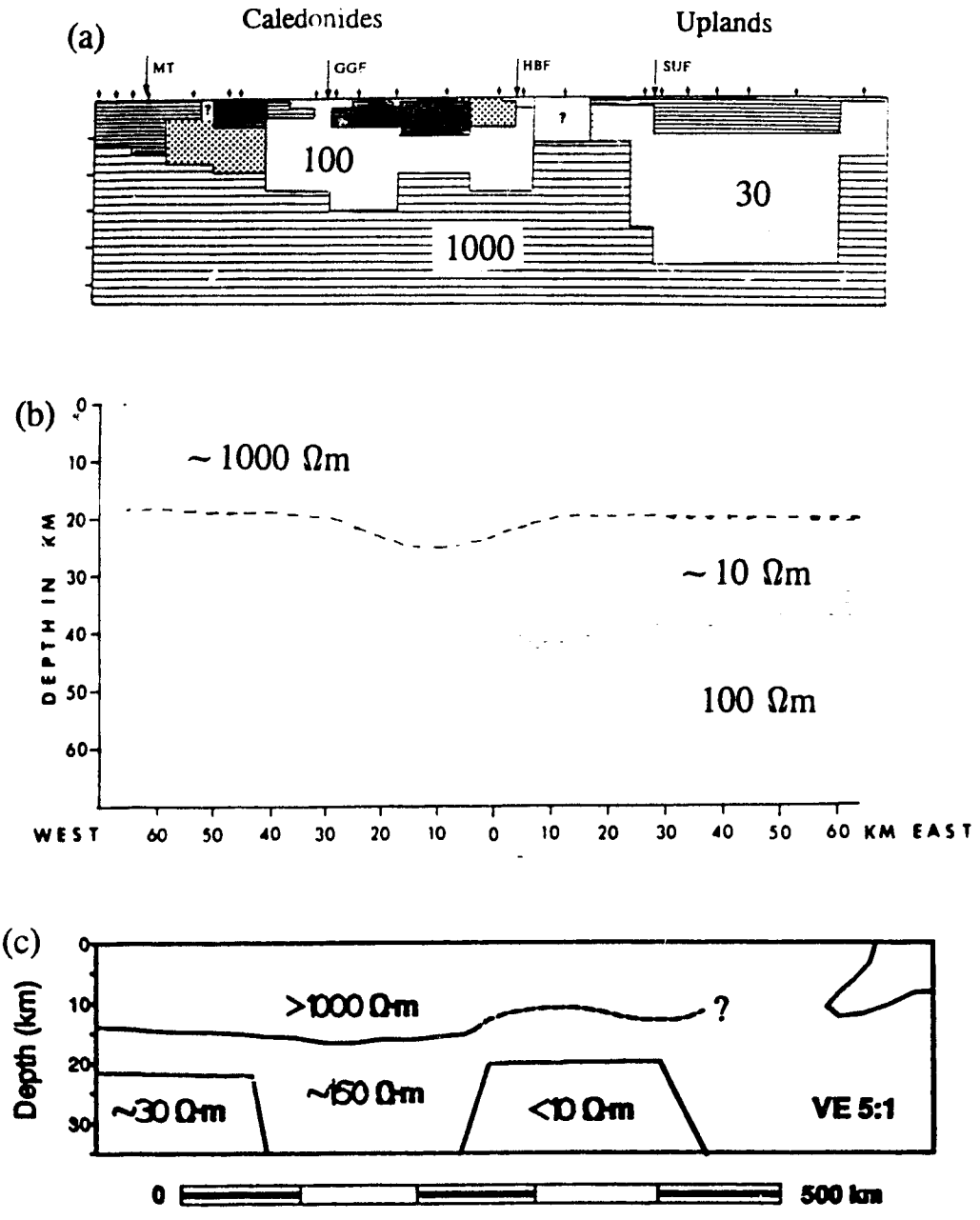

Figure 3 Examples of deep crustal low-resistivity zones: (a) Scotland, (b) Basin and Range Province, (c) southern Canadian Cordillera.

interpreted as an intermediate composition for the deep crust. None of these mechanisms can explain the low-resistivity in the deep crust, as rocks show very little variation in electrical resistivity with composition. Low-resistivity layers have been interpreted variously as zones of partial melting, graphitic inclusions or films, iron oxides, but none of these should have any noticeable effect on the seismic properties of rocks. One hypothesis that appears to reconcile both seismic and electrical observations is the presence of horizontally layered zones of aqueous fluids in the lower crust (e.g., Hyndman and Hyndman, 1968; Shankland and Ander, 1983; Haak and Hutton, 1986; Gough, 1986; Hyndman and Shearer, 1989). The primary objective of the research reported in this thesis is to investigate whether aqueous fluids are present in the lower continental crust.

In order to test the hypothesis of free aqueous fluids in the deep crust, three questions have to be answered. First, what are the effects of aqueous fluids on the physical properties of deep crustal rocks? This will be discussed in Chapter II. Second, are the physical properties of lower-crustal rocks observed in situ consistent with the porosity models? This will be discussed for global data in Chapter III and in Chapter IV on a smaller local scale. Third, are there any other conditions that must be met in the deep-crustal porosity model? This will be discussed in Chapters V and VI. Some of the possible alternatives to the aqueous fluid hypothesis for a conductive, low-velocity and reflective lower crust will be presented in Chapter VII.

CHAPTER II MODELLING OF PHYSICAL PROPERTIES

i. Effects of porosity on elastic properties of rocks

The effects of porosity on the elastic properties of rocks under lower crustal conditions have been discussed by many authors. The elastic behaviour of low-porosity crystalline rocks is controlled mainly by the matrix composition, but it is also affected by the amount of fluid present, the magnitude of the effect depending on the geometry of the pore spaces. The first commonly used velocity-porosity relation was the time-average equation of Wyllie et al. (1956):

$$\frac{1}{V} = \frac{1-\phi}{V_m} - \frac{1}{V_f}$$

where
- V porous rock velocity,
- V_m matrix velocity,
- V_f pore fluid velocity,
- ϕ porosity ($\phi < 1$).

It is still widely used today in the petroleum industry for sedimentary rocks, but is only a first-order approximation, since it does not take into account the pore shapes. More representative models applicable to crystalline rocks have been developed for spherical pores (Watt et al., 1976), ellipsoidal pores (Kuster and Toksöz, 1974; O'Connell and Budiansky, 1977), for tubular porosity (Mavko, 1980), and for combinations of various pore shapes (Schmelling, 1985). It has been shown by Shearer (1988) that these various formalisms all give similar results. The formalism of Kuster and Toksöz (1974) has been used here, mostly for its mathematical ease and flexibility. It describes the effects of ellipsoidal pores with varying minimum to maximum axis ratio (aspect ratio). It has been pointed out by Holbrook et al. (1991) that this formalism is valid only for isolated pores, and therefore might not be valid for interconnected porosity. Schmelling (1985) modelled the effects of the degree of pore interconnection on elastic properties and found that they are very small, even at high degrees of interconnection. It will be argued later that the porosity in the ductile lower crust should be in textural equilibrium pores. These

pores are fluid pockets at grain corners, interconnected by very narrow channels at grain boundaries. If such a porous medium is deformed at seismic frequencies, the fluid phase will not be displaced into the narrow channels. Therefore, the fluid phase is in an unrelaxed state as an elastic deformation goes through the rock, which is similar to the case for isolated pores. Using the formalism of Kuster and Toksöz is thus applicable. In addition, Hyndman and Shearer (1989) present laboratory data that show good agreement with this theory for both P-velocity (V_p) and Poisson's ratio vs porosity.

Figure 4 shows P-velocity versus porosity relations for a mafic rock with V_p = 7.2 km/s containing ellipsoidal pores with a range of aspect ratios. The most important property of these relations is that thinner pores have a much more pronounced effect on velocity than more equidimensional pores for the same porosity.

A zero-porosity velocity of 7.2 km/s has been chosen, assuming a mafic composition for the lower crust, as suggested by the results mentioned in the previous section. The compilation of Christensen (1982) shows that gabbros, metagabbros, and amphibolites have laboratory velocities averaging about 7.2 km/s at lower crustal pressure conditions (10 kbar). Intermediate compositions generally have slower velocity, about 6.5 to 6.7 km/s (Christensen, 1979; 1982). Most of the velocity inferences described below depend upon the lower crust being dominantly mafic in composition, with a zero-porosity velocity of about 7.2 km/s.

To the left of Figure 4 is a histogram of seismic refraction velocity estimates for the lower crustal layers compiled in Table 3. The right part of Figure 4 illustrates the inferred porosity for a range of pore aspect ratios. The number of sites in this compilation is limited by the requirement of nearly coincident magnetotelluric measurements (see Chapter III), but the velocity pattern is similar to other compilations (e.g. Hyndman and Klemperer, 1989).

The models presented above are dependent upon two assumptions: the first, as already mentioned, is that of a mafic composition; the second is that of a uniform pore geometry. Pore shapes are however never uniform, but are distributed depending on grain sizes and shapes, which are determined by localised, microscopic igneous crystallization and metamorphic conditions (e.g. Jurewicz and Jurewicz, 1986). Because

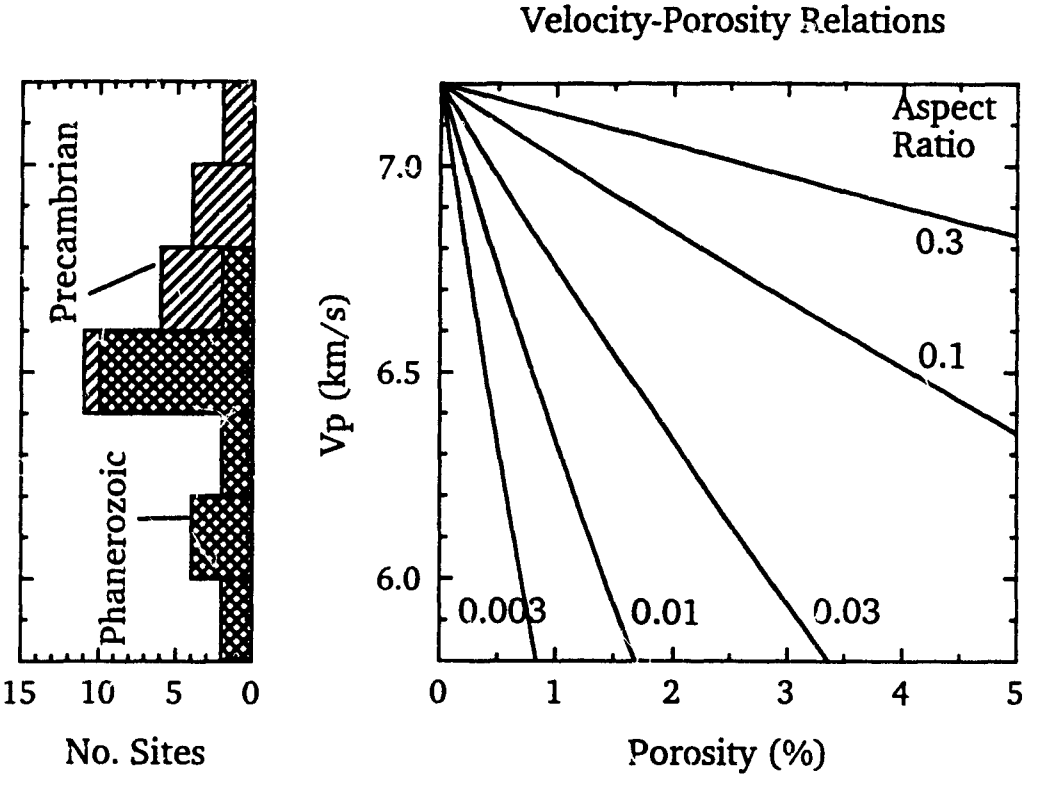

Figure 4 Velocity-porosity relations for a mafic rock containing ellipsoidal pores of selected aspect ratios. To the left, histogram of velocity values from Table 3.

there is undoubtedly a distribution of pore geometries present, elastic parameters have also been calculated for various distributions of pore aspect ratio (Figure 5). Lognormal distributions with standard deviation of up to 0.5 are realistic (Jurewicz and Jurewicz, 1986), since it is unlikely that more than two orders of magnitude of pore aspect ratio are present in significant amounts in the lower crust, because the expected tendency towards equilibrium pore geometries will limit the range of effective aspect ratios. Elastic parameters have been recalculated using a weighted average of the effects for each value of pore aspect ratio. The theory of Kuster and Toksöz (1974) is still used here. Figure 6 shows how P-velocity is influenced by various distributions centred on selected values of mean pore aspect ratio: thicker mean pores show a greater variation in effects, from moderate (s=0) to large (s=1) distributions. A wide distribution of aspect ratios always has a larger effect on the elastic parameters because even a small fraction of very thin pores affects them dramatically.

Another important parameter that is sensitive to pore geometry and which is receiving increasing attention in deep crustal surveys is Poisson's Ratio (related to V_p/V_s). A critical factor in the interpretation of deep crustal Poisson's ratio from seismic data in terms of porosity and pore geometry is its zero-porosity value. This value depends on the assumed composition and on the extrapolation of the available laboratory data to zero porosity. Most laboratory measurements on rocks that are likely candidates for the lower crust, at high confining pressure and low temperature, give Poisson's ratios ranging from 0.27 to 0.32. Low- to medium grade mafic rocks (e.g. gabbro, metagabbro) have Poisson's ratios generally in the higher part of the range, 0.29 to 0.32, while mafic granulites' values are in the lower part of the range from 0.27 to 0.29 (see summary in Goodwin and McCarthy, 1990). These Poisson's ratio values must be corrected to zero porosity. There does not seem to be any laboratory study of the effects of porosity on Poisson's ratio for gabbros, metagabbros or mafic granulites that allow us to extrapolate with confidence to zero porosity. The porosity of the samples is usually not given, but the few reported range from 0.2 to 1%. Laboratory measurements for basalts are given in Hyndman and Shearer (1989). The relatively small range in Poisson's ratios for a probable factor of 5 in porosity for lower crustal type rocks

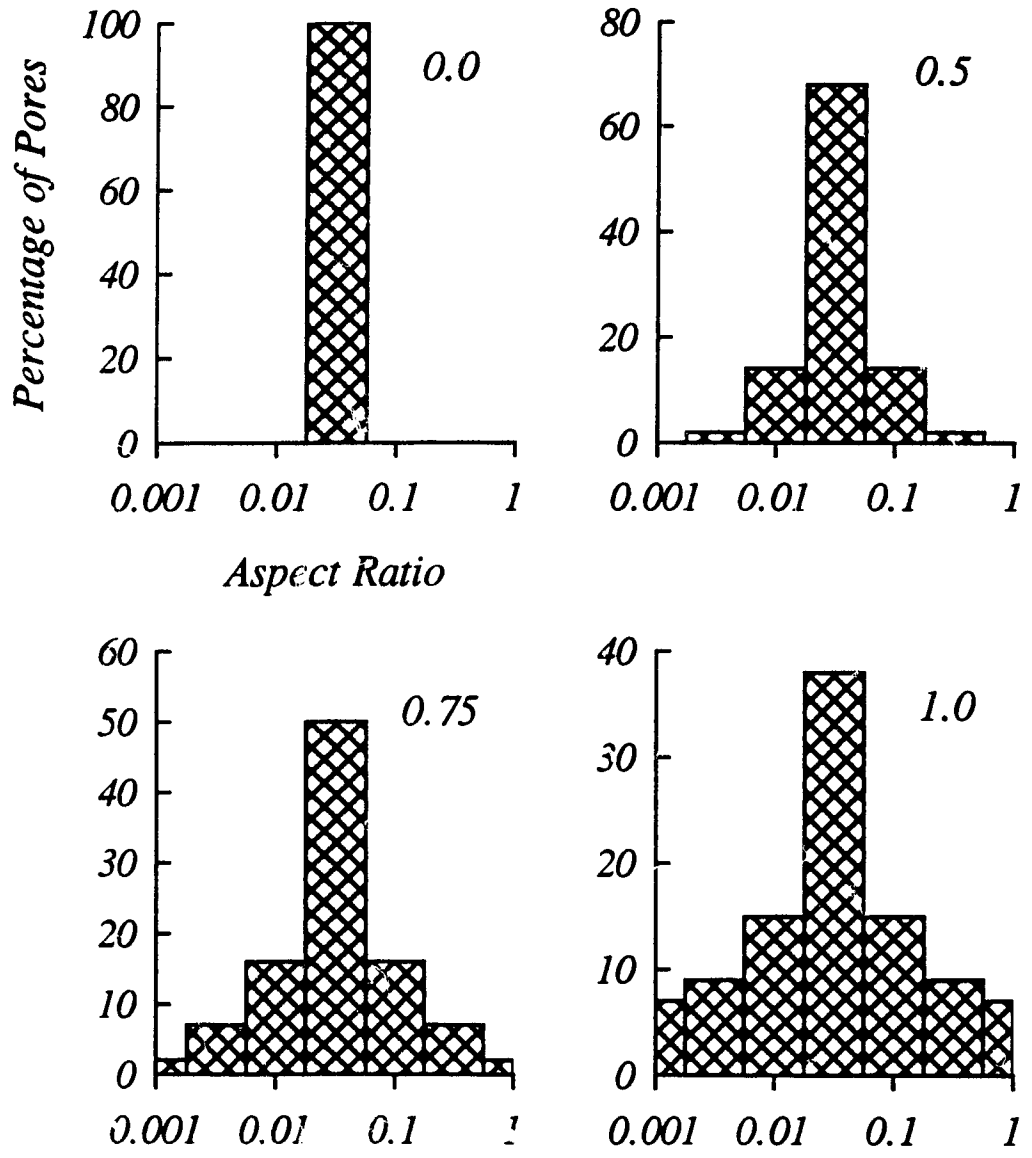

Figure 5 Pore aspect ratio distribution for calculating P-velocity and Poisson's ratio values in Figures 6 and 8. s=standard deviation of lognormal distribution

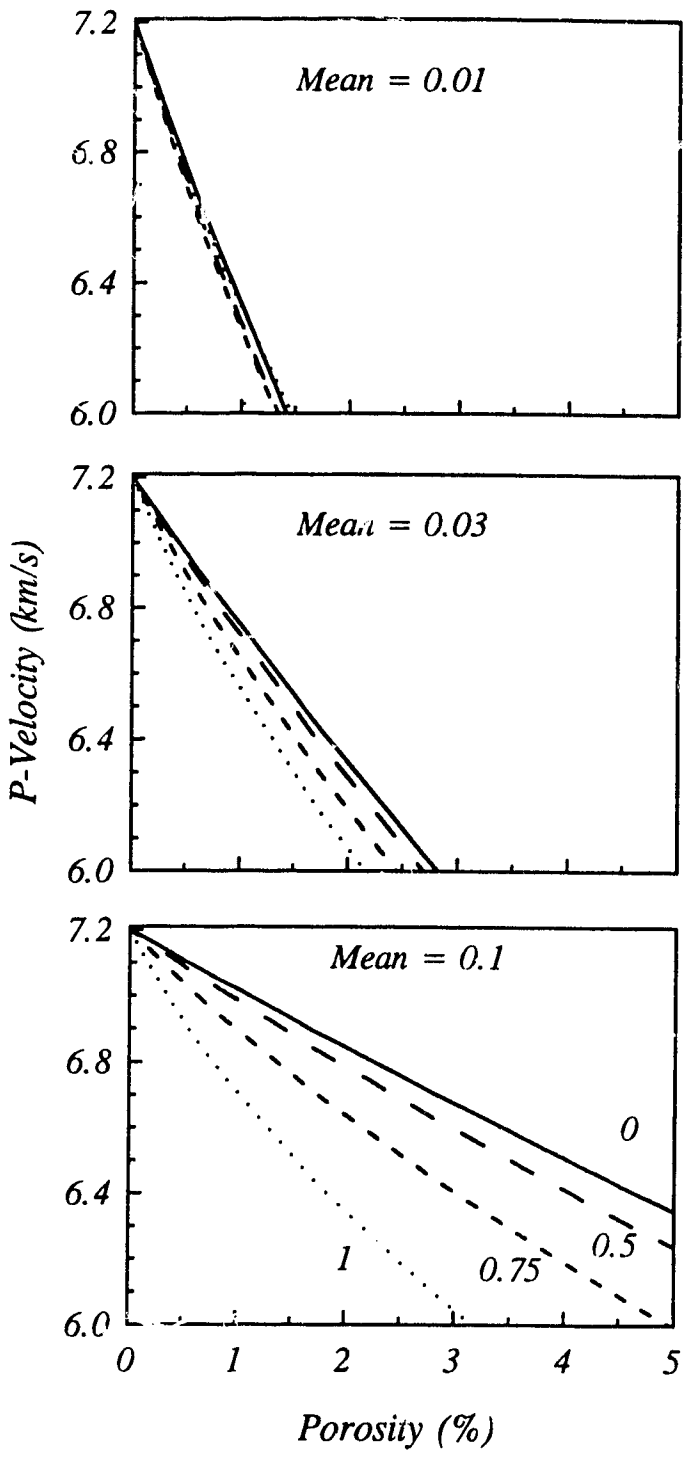

Figure 6 Velocity-Porosity relations for distributed pore aspect ratios. The numbers refer to the lognormal standard deviations as in Figure 5.

suggests that under low temperature and the high confining pressure laboratory conditions that close the thinner pores (above 0.5 kbars or 50 MPa), the effects of porosity are small, i.e. the effective aspect ratios are more equidimensional than 0.03. The effect of temperature on Poisson's ratio is negligible for the lithologies of interest (variation of less than 1% for temperature increase of 500°C using data from Christensen, 1979). A zero-porosity Poisson's ratio of 0.29 is thus a reasonable average value for lower crustal conditions, with a range of 0.27 to 0.31.

Figure 7b shows the variation in Poisson's ratio against porosity for selected pore aspect ratios, using the formalism of Kuster and Toksöz (1974). The figure illustrates that for pores of small aspect ratios Poisson's ratio increases rapidly with increasing porosity, while pores of larger more equidimensional aspect ratio it tends to decrease with increasing porosity (see also Shearer, 1988). It is important to note that quite thin pores or cracks are required for Poisson's ratio to increase strongly with increasing porosity at the porosities of interest in the lower crust (i.e., aspect ratios < 0.01 required). Thus the absence of high Poisson's ratio cannot be taken as evidence against porosity in the lower crust (Hyndman, Lewis and Marquis, 1991). The effect of a distribution of pore aspect ratios are shown in Figure 8. It is seen that for thin average aspect ratio pore (mean 0.01) a substantial spread in pore geometries results in a more rapid increase in Poisson's ratio with increasing porosity (top of Figure 8). For more equidimensional mean pore aspect ratio (e.g. 0.1) there is a smaller effect on Poisson's ratio; the change with increasing porosity remains negative except for quite wide distributions. Again wide distribution of pore aspect ratio have dramatic effect on Poisson's ratio because of the large contribution of the few very thin pores.

Even though the ellipsoidal pore models used above are in close agreement with experimental results for near-surface porous rocks, pore geometries may be fundamentally different for rocks in the ductile lower crust. At these depths, pore fluids, if present, are expected to be in textural equilibrium with the rock matrix. Equilibrium pore geometries differ greatly from ellipsoidal pore shapes. In order to obtain a velocity-resistivity relation for equilibrium pore geometries, the effect of such pores on the elastic properties of a rock have been modelled numerically .

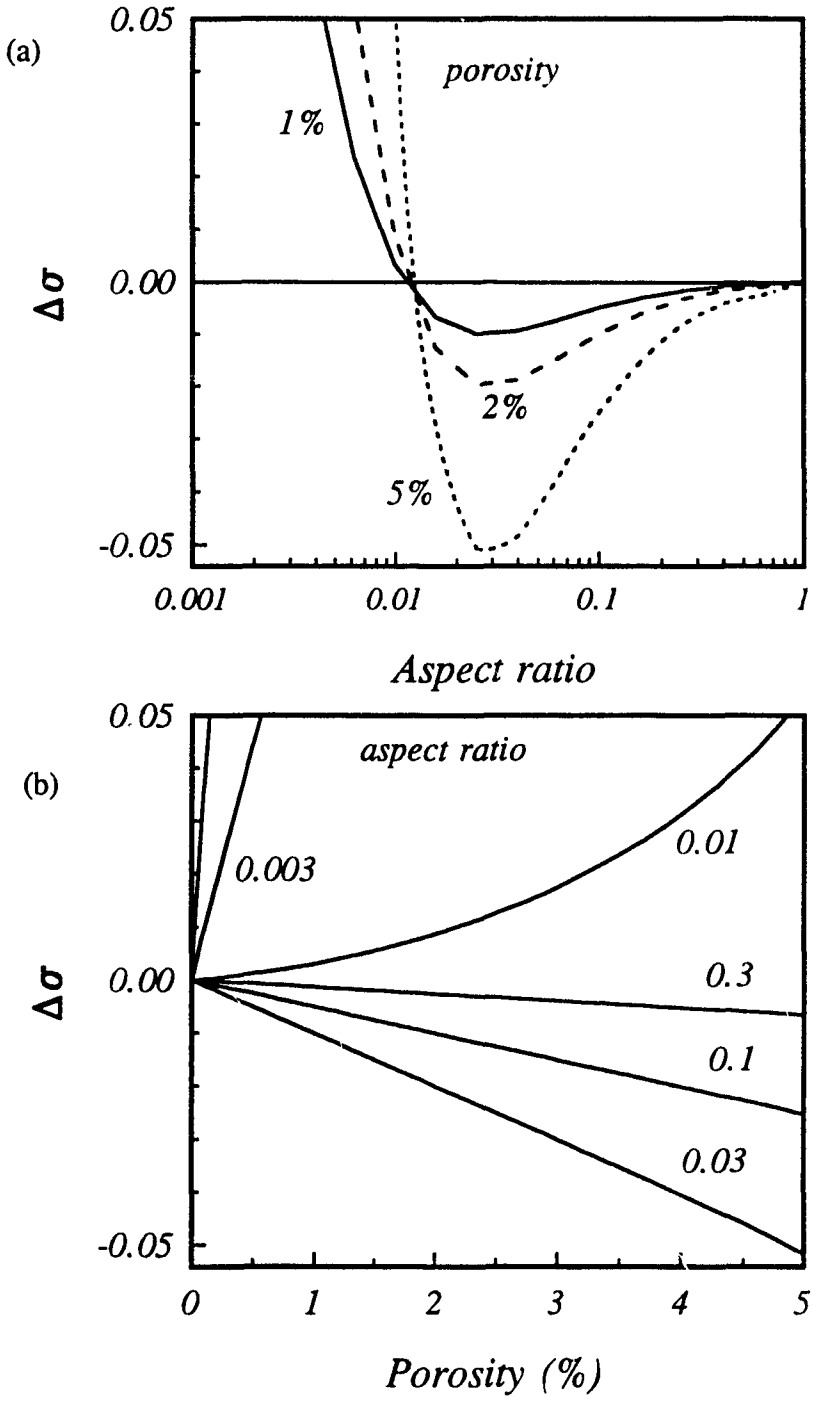

Figure 7 (a) Influence of pore aspect ratio on Poisson's ratio for 1,2 and 5% porosity. (b) Poisson's ratio vs porosity relations for selected pore aspect ratios.

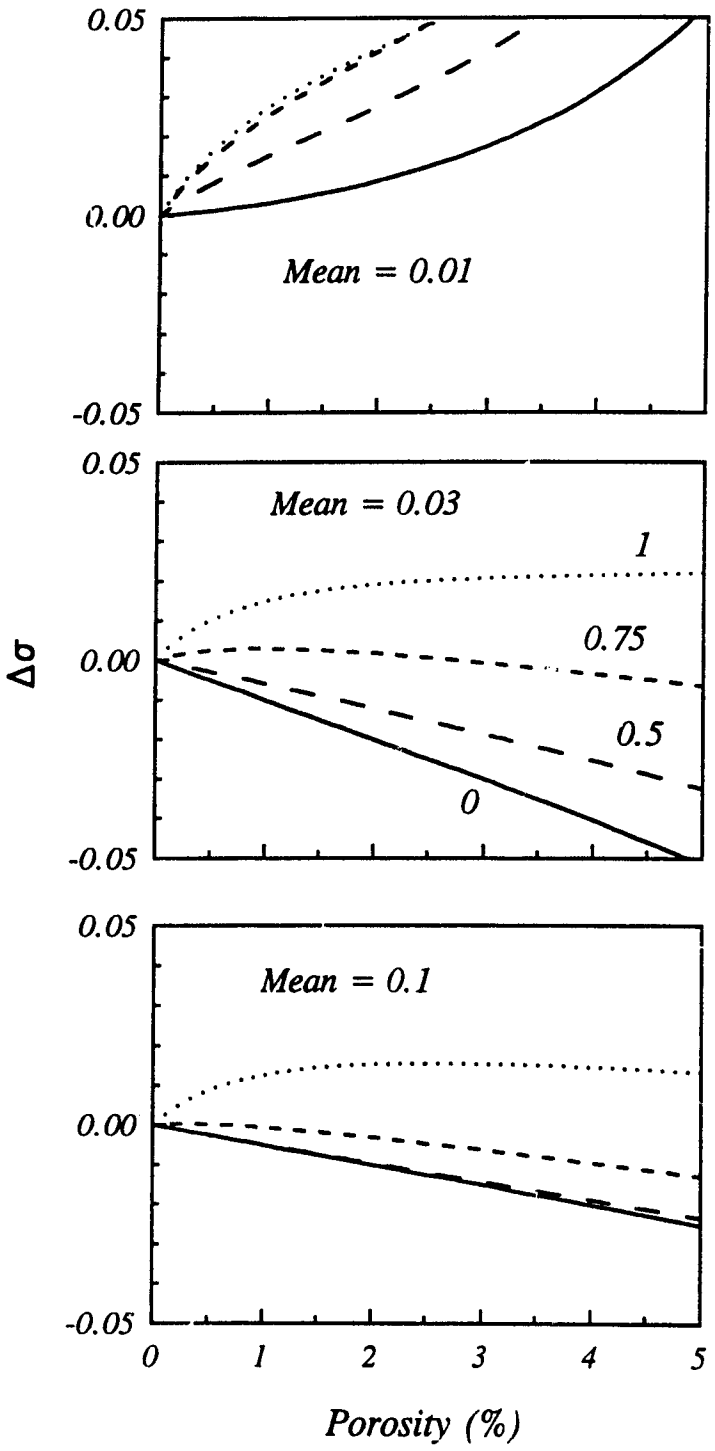

Figure 8 Poisson's ratio-Porosity relations for distributed pore aspect ratios. The numbers refer to the lognormal standard deviations as in Figure 5.

ii. Modelling of elastic properties for equilibrium pore geometries

Pore models have been developed using the program ANSYS (Swanson Analysis Systems, 1989), a package commonly used for mechanical engineering applications. ANSYS uses a matrix displacement method of analysis based upon a finite-element idealization of the model. The displacement method consists of approximating the solution by interpolating a function from the boundaries to the interior of the elements. The function has to satisfy the governing equations (Hooke's Law and Equation of Continuity in this case) and the pre-defined boundary-conditions. Pre-defined elements are chosen depending on the problem to be solved. The main advantage of using ANSYS is the ease of defining the system and the boundary conditions for calculations.

The study is limited to a two-dimensional case, since it is unlikely that a three-dimensional model would change the results by an amount larger that the accuracy obtained from seismic surveys, especially for the deep crust. The pore shapes of Cheadle (1989) have been discretised using two-dimensional fluid elements, and have been surrounded by two-dimensional solid elements (Figure 9). Both types of elements have been given realistic parameters of elastic moduli and density. The elastic moduli have been calculated using

$$\mu = \rho V_s^2$$

$$\lambda = \rho \left(V_p^2 - 2V_s^2 \right)$$

$$K = \lambda + \frac{2}{3}\mu$$

where V_s shear velocity
V_p compressional velocity
μ shear modulus
ρ density
λ Lamé's constant
K bulk modulus

The parameters obtained are shown in Table 2. The elements are then divided by ANSYS using an automatic griding procedure, with a higher density of grid points at edges and boundaries: there are 48 nodes on either side of the boundary between each grain pocket and the matrix, 4 nodes inside each pocket, and 20 nodes on either side of the channel-matrix boundaries.

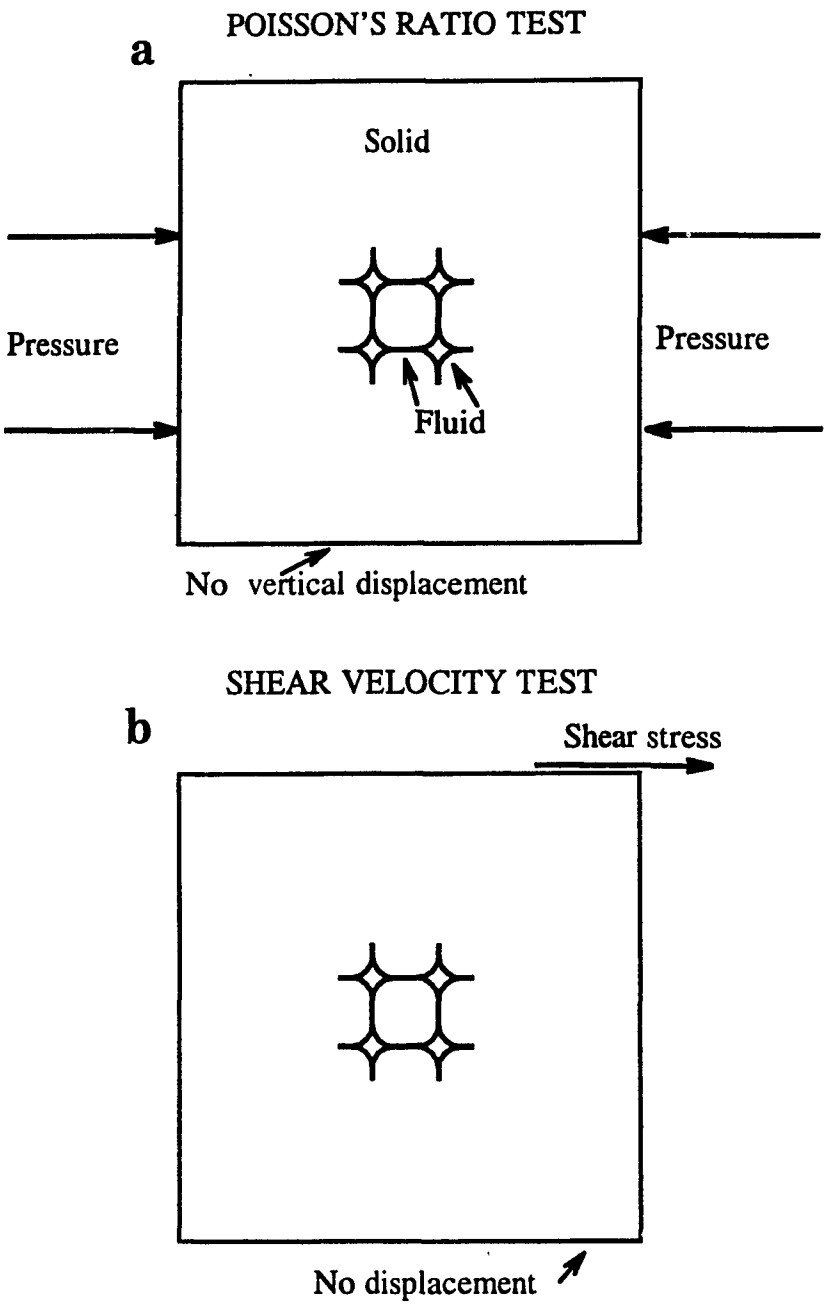

Figure 9 Equilibrium pore geometry model: (a) for calculation of Poisson's ratio, showing the pore configuration and the appropriate boundary conditions. (b) for calculating the shear modulus.

Table 2 Parameters for equilibrium pore geometry models

	Matrix	Fluid
V_p (m/s)	7200	1500
V_s (m/s)	4200	0
Shear Modulus μ (Pa)	$5.3\ 10^{10}$	0
Lamé's Constant λ (Pa)	$4.9\ 10^{10}$	$2.3\ 10^{9}$
Bulk Modulus K (Pa)	$8.5\ 10^{10}$	$2.3\ 10^{9}$
Density (kg/m^3)	3000	1000

The resulting porous rock models have then been analyzed to study the effects of uniaxial pressure (for Poisson's Ratio, Figure 9a) and shear stress (for the shear modulus, Figure 9b). Appropriate boundary conditions have been applied: no displacement through the lower horizontal axis for the Poisson's Ratio test (Figure 9a), and no horizontal and vertical displacements at the lower horizontal axis for the shear modulus test (Figure 9b). Knowledge of both Poisson's Ratio and shear modulus enable us to obtain both V_s and V_p, and comparison of the results with ellipsoidal pore models predictions gives an effective pore aspect ratio.

Numerical models of the deformation of rocks with equilibrium pores have been calculated for a few values of porosity. A special attention has been to porosity values less than 3%, because porosities in the deep crust are expected to be low.

Poisson's Ratio for each case has been calculated using the ratio of vertical displacement (strain) to the horizontal displacement. These values are output by ANSYS after each iteration. The solution converges rapidly. In all cases one iteration was sufficient, subsequent iterations giving very similar solutions.

The variation in Poisson's Ratio ($\Delta\sigma$) increases with porosity (Figure 10), with a second-order fit to the data of with a correlation coefficient (r) of 0.92. This suggests that the equilibrium pore geometries have a quite low effective aspect ratio. This in

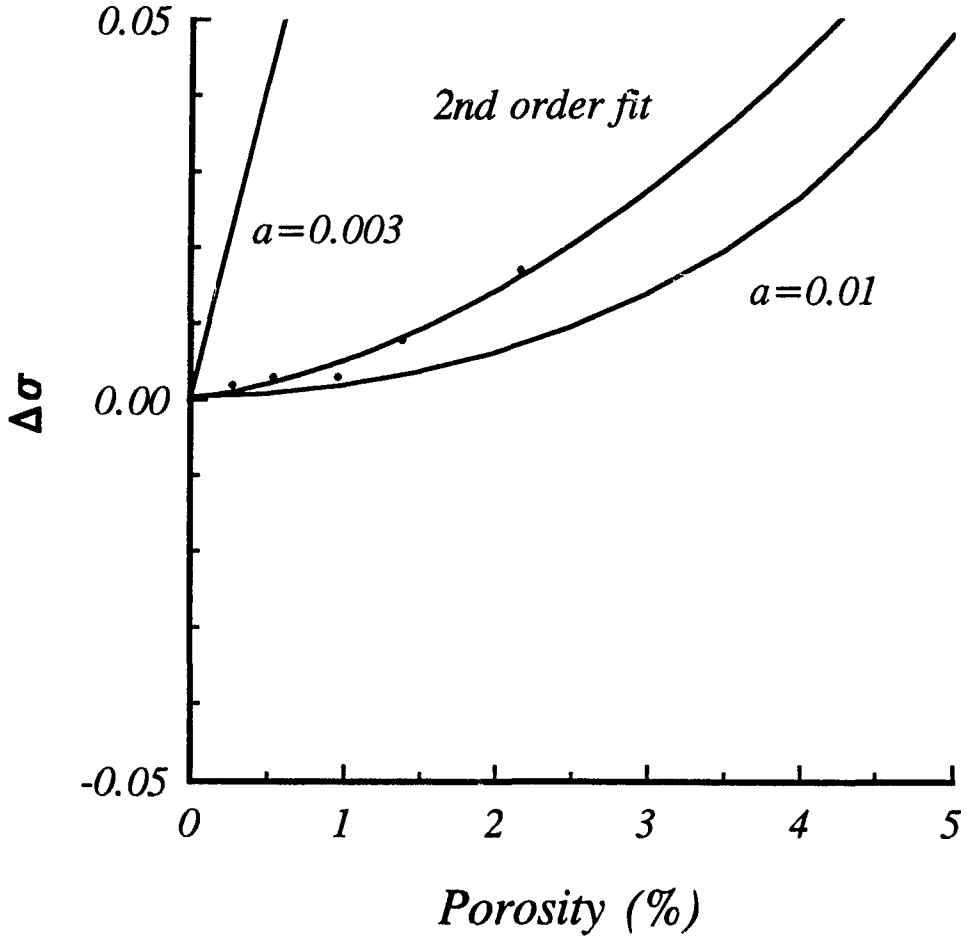

Figure 10 Poisson's Ratio-Porosity relations obtained from equilibrium pore geometry models (Figure 9a). Ellipsoidal pore models are shown for comparison.

agreement with the electrical resistivity models for which it will be shown that the small grain-boundary channels have much more influence on the physical properties than the larger volume grain-corner pockets (see next section). By comparison with the ellipsoidal pore models, the equilibrium pore geometries have effective aspect ratios slightly lower than 0.01 (see Figure 10).

The horizontal displacement at the top of the model volume caused by horizontal shear stress has been used to determine the shear modulus. Displacements have been obtained for the same porosity values used for determining Poisson's ratio. The conversion to shear velocity is not as straightforward however. V_s is defined as:

$$V_s = (\mu/\rho)^{1/2}$$

where μ Shear modulus (i.e. Shear stress/Shear strain)

ρ Density.

Since the applied shear stress is the same for all porosity models, the normalized shear modulus is inversely proportional to the normalized shear strain. All parameters (shear strain, shear stress, density, V_s) have been normalized to their values for dry rock.

Figure 11 shows the main results of this analysis: (a) the normalized shear modulus and (b) the resulting V_s vs porosity relation. V_s vs porosity relations for ellipsoidal pores of aspect ratio 0.01 and 0.03 are shown for comparison. A first-order regression line has been fit to the data ($r=0.88$). As for the Poisson's ratio situation, these results show that the narrow grain-boundary channels have more influence on the elastic properties of a rock than the grain-corner pockets. The effective pore aspect ratio is slightly higher than 0.01.

Once V_s and Poisson's ratio (σ) are known, the compressional wave velocity (V_p) can be obtained from

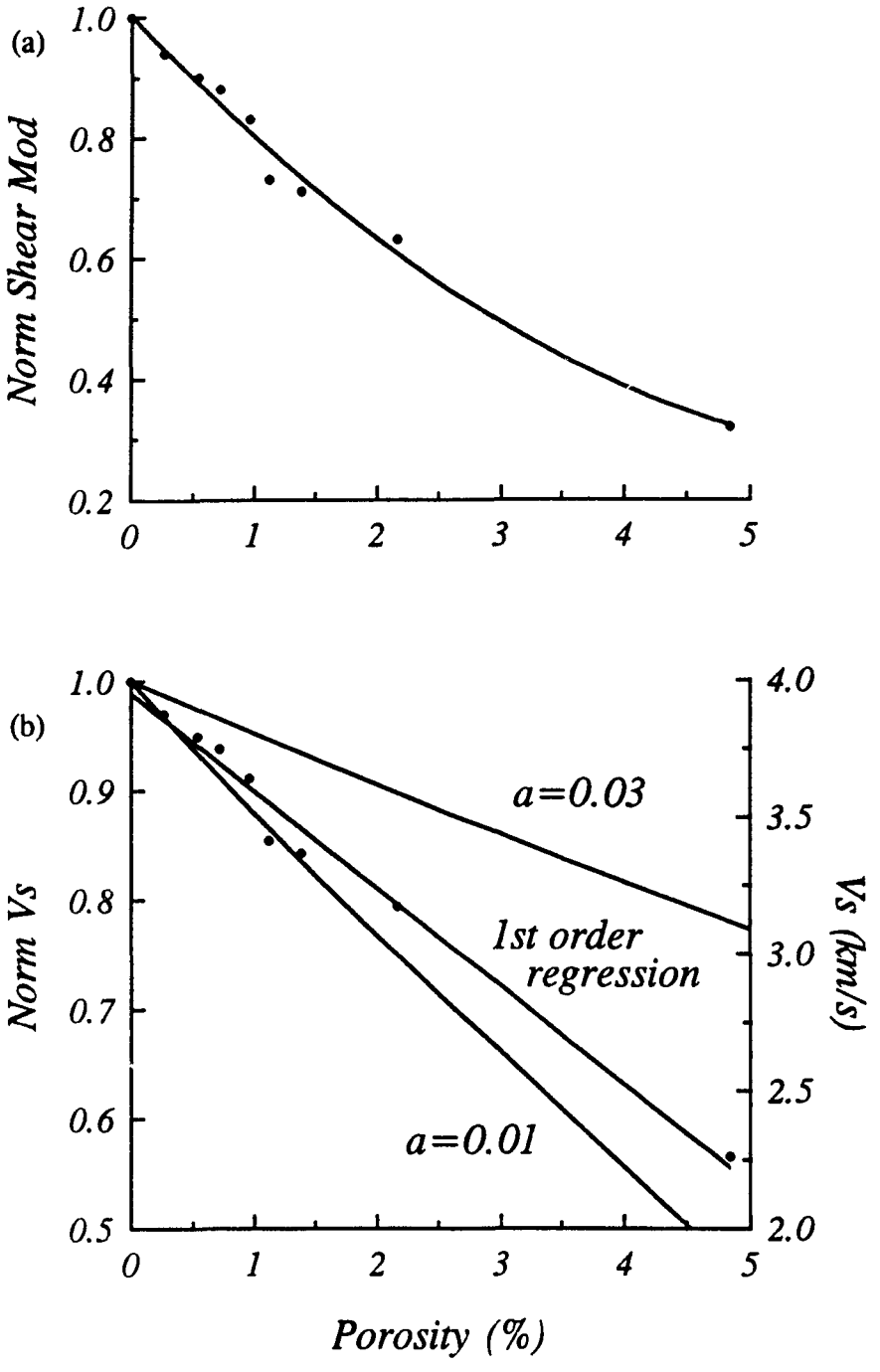

Figure 11 Normalized shear modulus (a) and normalized and true shear velocity (b) vs porosity obtained from equilibrium pore geometry models (Figure 9b). Ellipsoidal pore models are shown for comparison.

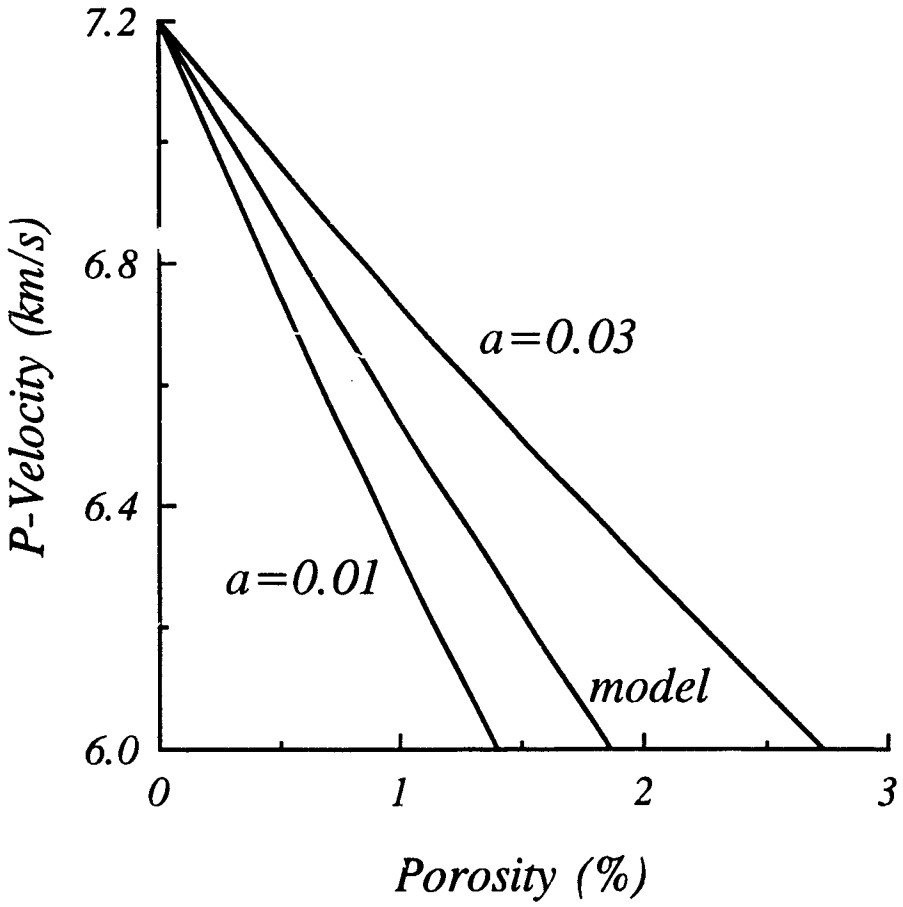

Figure 12 Velocity-porosity relation for equilibrium pore geometry model, using results from Figures 10 and 11b. Equilibrium pore geometries have very low effective pore aspect ratio.

$$V_p = V_s \sqrt{\frac{1-\sigma}{0.5-\sigma}}$$

The resulting V_p-porosity profile is shown in Figure 12. The effective pore aspect ratio is again slightly larger than 0.01, indicating that indeed the grain-boundary channels have a large influence on the elastic properties: the velocity is reduced by 10% for a porosity of about 1.5%. Therefore, very small porosities are required to obtain the velocities reported in the compilation, with a zero-porosity value of 7.2 km/s.

iii. Effects of porosity on electrical properties of rocks

Although other conduction mechanisms such as graphite cannot be excluded (Frost et al., 1989; Chapter VI), the low resistivity of the deep crust has been assumed to be the result of saline fluid porosity. In this fluid porosity model, the electrical resistivity of a rock is primarily controlled by the fluid porosity, the resistivity of the pore fluid, and the pore geometry. The resistivity of the matrix (10^4-10^5 ohm m; Kariya and Shankland, 1983) bears an insignificant influence. Figure 13 shows the influence of porosity on electrical resistivity for various geometries including the empirical relation of Archie (modified by Hermance, 1979):

$$\rho = \frac{\rho_f \rho_s}{\rho_f + (\rho_s - \rho_f)\ \phi^m}$$

where

ρ	porous rock resistivity
ρ_s, ρ_f	matrix and pore fluid resistivity
ϕ	porosity
m	Archie exponent

In Figure 13, the pore fluid is seawater salinity (0.5M NaCl), and in Figure 14, it is a 5M NaCl brine, a fluid that also could be present in the deep crust. Archie's Law with pore tortuosity exponents between 1.5 and 2.5 fit many laboratory measurements on crystalline rocks (e.g. Brace et al., 1965), while an exponent of 1.2 approximates closely

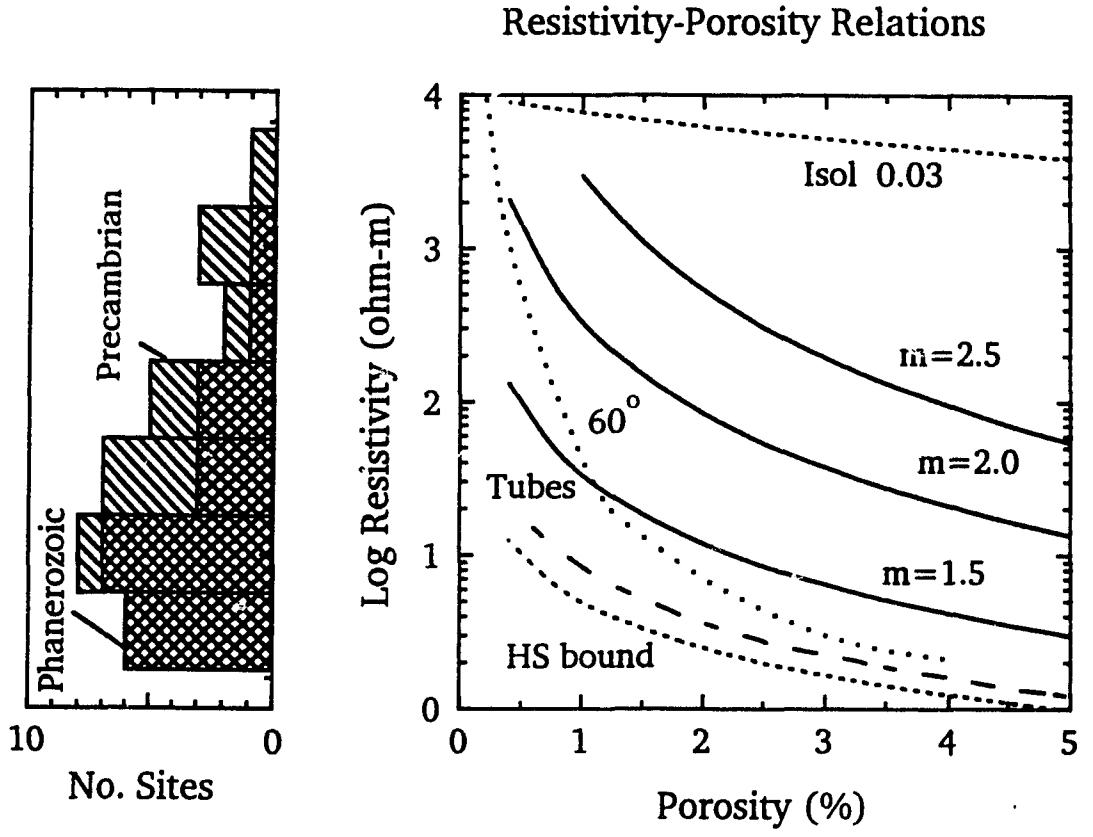

Figure 13 Resistivity-Porosity relations for 0.5M NaCl pore fluid. Fluid configurations used are: isolated ellipsoids, Archie's Law (exponent m), tubes, the lower Hashin-Shtrikman bound and 60° dihedral angle equilibrium pores. To the left, a histogram of lower crustal resistivity layers from the compilation in Table 3.

the theoretical behaviour of very well interconnected, tubular porosity. Unlike the elastic case, ellipsoidal pores are a poor representation for the effect of porosity on resistivity in the lower crust, since the critical factor is the degree of pore interconnection. Equilibrium pore geometries may be a more appropriate approximation at temperatures above about 400°C because mafic rocks are ductile under these conditions (Hyndman and Shearer, 1989), but the electrical behaviour of such geometries is computationally difficult: numerical solutions would be required. It can however be approximated by an abrupt resistivity variation arising from a transition from pinch-off (isolated porosity) to pore interconnection below about 1% porosity (Cheadle, 1989; Hyndman and Shearer, 1989). The actual pinch-off porosity depends on the dihedral or fluid-grain wetting angle of the equilibrium pores (von Bargen and Waff, 1986). Equilibrium pore geometries will be discussed more thoroughly in Chapter V. The approximation used here consists of the resistivity-porosity relation for isolated pores up to the pinch-off porosity value. The relation for tubes is then used for larger porosity, as the equilibrium pore geometries form a network of grain-boundary channels similar in shape to the tubular porosity model of Grant and West (1965). A histogram of electrical resistivities from the compilation of lower crustal layers is shown to the left in Figure 13, to illustrate what porosities are inferred for different pore geometries.

iv. Velocity-Resistivity relations

If both velocity variations and resistivity variations in the deep crust are primarily associated with porosity, there should be a relation between velocity and resistivity. Theoretical relations between velocity and resistivity (Figure 15) can be obtained from the velocity-porosity relations (Figure 4) and from the resistivity-porosity (Figure 13) already calculated. Again, the fundamental assumption is that both electrical resistivity and seismic velocity are controlled mainly by porosity. The effects of variations in composition and in pore geometry are assumed to be second order. These model relations will be compared with data from approximately coincident magnetotelluric and seismic refraction results in the next chapter.

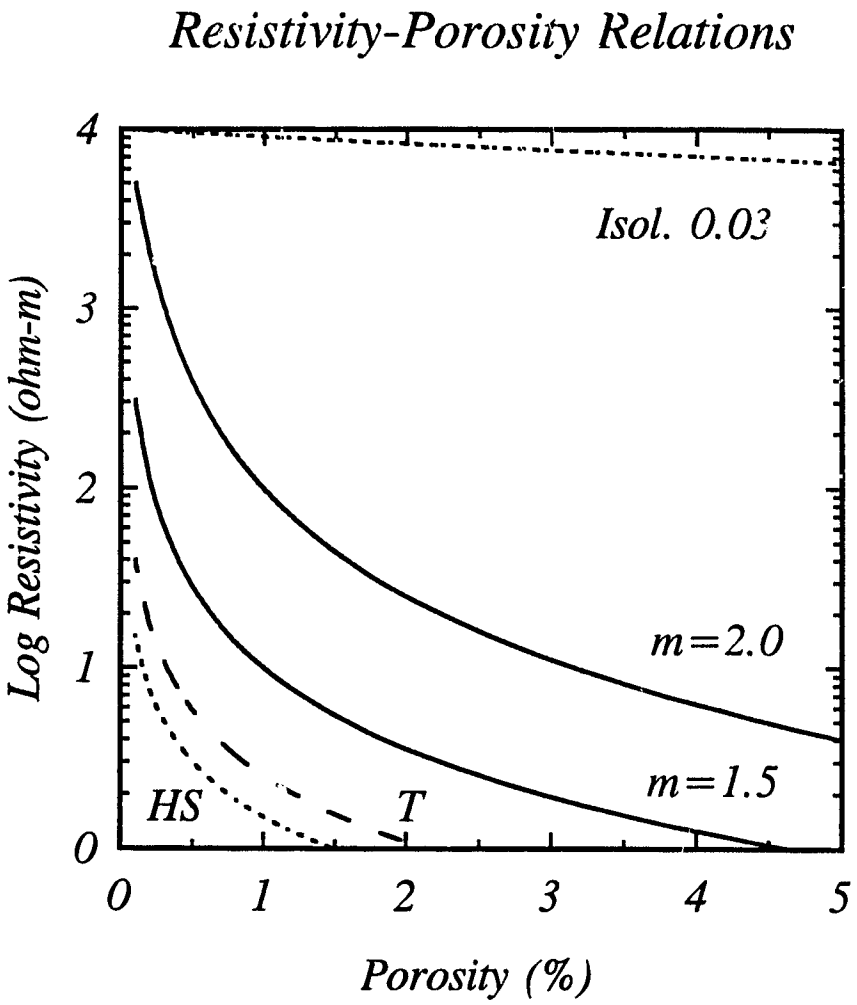

Figure 14 Resistivity-Porosity relations for 5M NaCl pore fluid. Same conventions as in Figure 13.

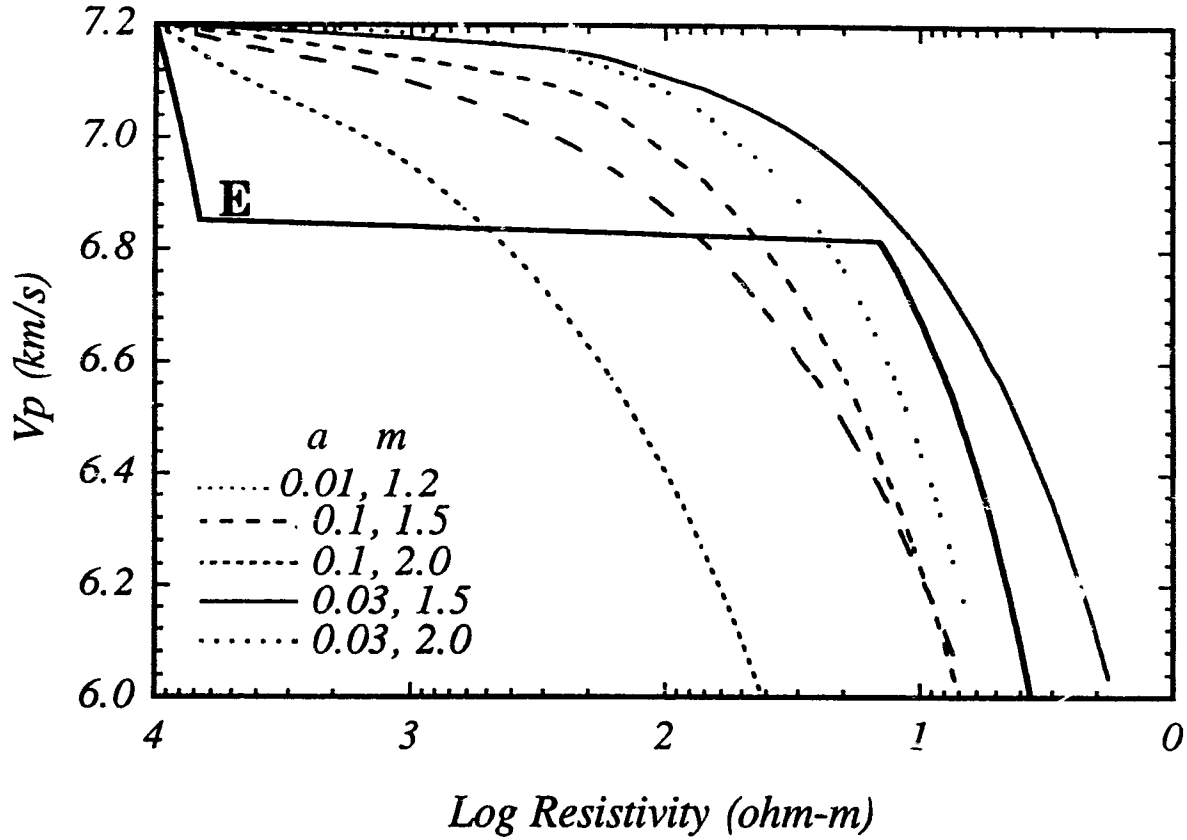

Figure 15 Velocity-Resistivity relations for selected pairs of pore aspect ratio (a) and Archie's Law exponent (m). The thicker solid line (E) represents a discontinuous model analogous to equilibrium pore geometries, using the velocity-porosity relation of Figure 12, and the resistivity-porosity relation for equilibrium pores with a 60° dihedral angle. The relation shows a sharp change because of the transition from isolated to interconnected porosity.

CHAPTER III GLOBAL COMPILATION OF DEEP GEOPHYSICAL DATA

i. Data sources and selection criteria

To test the validity of the velocity-resistivity relations obtained above, a compilation of approximately coincident velocities from seismic refraction surveys and resistivities from magnetotelluric and deep-probing controlled-source electromagnetic surveys is presented here, as well as some associated data on seismic reflection and heat flow (Table 3). The number of reflection studies reported is small, because of the coincidence requirement. There is a large number of coincident reflection and refraction studies (e.g. Mooney and Brocher, 1987), but since the least equivocal evidence for deep crustal fluids is the low electrical resistivity, the emphasis was put on magnetotelluric studies. The refraction and magnetotelluric survey pairs were required to be within the same tectonic unit, usually separated by less than 100 kilometres. The layers reported here were also required to be in the lower half of the crust, to justify the earlier assumption of a predominantly mafic composition.

Results from a wide range of tectonic environments have been included. To study whether the tectonic regime has an effect on lower crustal physical properties, the sites have been divided according to the most recent (< 300 Ma) tectonic deformation type in Table 3 as being stable, compressional, or extensional. It is however difficult to determine what recent event was the most influential in determining the structure of the present crust in some areas. For example, the Cordillera of western Canada-northwest United States has undergone compression in the Mesozoic, transcurrent dislocation in the Cretaceous-Paleocene, extension in the Eocene, and is under compression by subduction again today. The sites have also been divided according to age (most recent orogenic or thermotectonic event) to establish if there is any difference in inferred porosity with geologic age.

The electrical resistivity data have been restricted mainly to broad frequency band magnetotelluric soundings with modern forms of data inversion or modelling. A few controlled source surveys have also been included. Data from geomagnetic depth sounding and from narrow-band magnetotelluric surveys have been excluded, the former

because of their poor vertical resolution for both depth and resistivity, and the latter because they provide little information on either the deep crust (if only shorter periods are used) or the near-surface (if longer periods are used).

There are two serious difficulties in obtaining resistivities over depth ranges that correspond to velocity layers. The first is that magnetotelluric surveys only resolve well layer conductance or thickness/resistivity (in one-dimension inversions), rather than resistivity alone (e.g., Edwards et al., 1981). This problem has been dealt with in part by a normalization scheme based on the lower crustal layers being 10 km thick (approximately the data average). Applying this additional assumption as a constraint gives somewhat less scatter in the velocity-resistivity plot. The second important problem is the static shift (e.g. Jiracek, 1990), caused by local near-surface galvanic effects, resulting in a shift of the whole resistivity-depth profile. A more thorough discussion of static shift effects is presented in Chapter IV. At only a few localities have detailed static shift corrections been made.

Resistivity anisotropy is another important problem. The current flow and thus the resistivity sensed in magnetotelluric surveys is approximately horizontal at the earth's surface, but in some of the surveys in the compilation, the apparent resistivity curves for the E- (electric field parallel to most conductive direction - strike) and B- (magnetic field parallel to strike) polarizations are quite different, especially at longer periods. These discrepancies may be caused either by the larger scale geological structure, or by small grain-scale anisotropy, for example in the pore geometry. In many cases, inversion of both E- and B-polarizations gave similar results for the lower crust. In cases where the results greatly differed, the E-polarization inversion has usually been presented, because the investigators judged that it provided the best resistivity average. In many instances only the E-polarization has been inverted by the original investigators. The polarization used is indicated in Table 3.

For seismic refraction velocities, the most serious problem is that low-velocity layers in the deep crust have undoubtedly been missed in older interpretations that were based only on first-arrivals, since such layers often generate only secondary arrivals. Thus, only velocity data that have been obtained through amplitude synthetic modelling

of first and secondary arrivals have been used in the compilation. This minimizes the possibility that lower crustal layers that do not produce first arrivals are missed in the interpretation (see Hyndman and Klemperer, 1989). Refraction velocities refer primarily to horizontal propagation, and anisotropy in different horizontal directions are frequently observed in surveys that include more than one direction, as with magnetotelluric surveys, although the effect is usually small. In most of the surveys presented here, only one direction of propagation is available. Typical uncertainties for deep crustal refraction velocities when primary and secondary arrivals are analyzed are about 0.1 km/s. If intermediate layers are missed, the uncertainties can be much larger.

Lower crustal seismic reflectivity has not been correlated with velocity and resistivity in detail in this study. In some areas, there may be a depth correlation between high reflectivity and low resistivity; examples of coincidence in which the depth of the conductive layers are defined by controlled source electromagnetic surveys are given in Connerey et al. (1980) and Haak and Hutton (1986). An example of low-resistivity from magnetotelluric data and high seismic reflectivity in the lower crust for a restricted area in the southern Canadian Cordillera will be presented in the next chapter. Where seismic reflection surveys have defined bands of lower crustal reflectors in the areas of the velocity-resistivity data, the depth range of the bands has been given by the authors for comparison with the resistivity and velocity data depths (Table 3). Reflector band depths and thicknesses given only in two-way reflection time have been converted to depth using the seismic refraction velocities.

The depths to the top of velocity layers cannot be readily tested against the other parameters, because the effect of porosity on velocity is superimposed on a progression with depth to more high velocity mafic rocks. It is not practical to try to separate these effects.

The correlation between the tops of conductive layers and reflective bands with temperature at depth has also been investigated. It has been shown by Ádám (1978), Shankland and Ander (1983), and by Klemperer (1986) respectively that both conductive and reflective layers appear to be influenced by the geothermal regime. The temperatures ranges given in the compilation here are from either published temperature

inversions when available, or from published heat flow results converted into temperatures at depth using the generalized continental geotherms of Chapman (1986). There is a considerable uncertainty in inverting heat flow data, especially when the surface heat production is not known. Heat flow measurements having typical uncertainties around 10%, deep crustal temperature uncertainties are about 50°C (Lewis et al., 1992).

Table 3. Compilation of lower crustal resistivity, velocity and inferred temperatures

Locality	Z (km)	Tec	ρ (Ω m)	ρ_{10} (Ω m)	Pol	V_p (km/s)	T° range (°C)	Ref.int. (km)	References
				PRECAMBRIAN AREAS					
1. Charlevoix	22-30	S	30-70	62	E	6.9	225-300		Kurtz (1982), Lyons (1980)
	30-40		70-120	100		7.1	300-		
2. Laurentides	20-30	S	12-30	20	E	6.8	200-300		Kurtz (1982), Berry & Fuchs (1973)
	30-40		30-70	50		7.0	300-		
3. Wisconsin	12-40	S	10-100	28	B	6.5	150-		Dowling (1970)
4. Timmins	22-30	S	270	250	-	6.6-6.8	200-250		Duncan et al. (1980), Boland & Ellis (1989), Misener et al. (1951)
5. Kapuskasing	20-30	S	150	150		6.6-7.0	200-300		Maréschal et al. (1989), Boland & Ellis (1989)
	30-40		1000	1000		7.0-7.4	300-		
6. Kaapval, South Africa	25-40	S	10	6.7	-	6.6-7.0	450-600		Van Zijl (1977), Bloch et al. (1969), Gupta (1989)
7. Indian Shield (Choutuppal)	16-25	S	35	39		6.5	200-300		Sastry et al. (1990), Kaila et al. (1979), Gupta (1989)
	25-40		5200	3467		6.8	300-500		

8. Smaland-Varmland, Sweden	10-80	S	500-10^4	125	B	6.5-7.4	200-1000	19-25	Rasmussen et al. (1987), Clowes et al. (1987), Eriksson & Malmqvist (1979), Dahl-Jensen et al. (1987)
9. Norrland, Sweden	15-35	S	20-80	30	B	6.75-7.15	200-325		Rasmussen et al. (1987), Hirschleber et al (1975), Eriksson & Malmqvist (1979)
10. Norbotten, Sweden	25-50	S	50-200	40	EB	6.9	300-500		Jones et al. (1983), Luosto & Korhonen (1986), Eriksson & Malmqvist (1979)
11. Baltic Shield	35-50	S	18-36	20	B	6.5-6.9	380-450		Jones et al. (1983), Hirschleber et al. (1975), Čermak & Hurtig (1979)
PHANEROZOIC AREAS									
12. Appalachians	20-25	C	10-30	40	-	6.7	350-400		Connerey et al. (1981), Luetgert et al. (1987), Lachenbruch & Sass (1977)
13. Georgia	15-22 22-35	C	10 2000	14 1538	-	6.05 6.05-6.7	250-350 350-550		Thompson et al. (1983), Kean & Long (1980), Lachenbruch & Sass (1977), Cook & Oliver (1981)
Rio Grande Rift									
-14. Santa Fe	13-22 22-30	E	1-10 50-100	5.5 100	EB	6.09-6.15 6.62-6.72	400-450 450-650	15-28	Hermance & Pedersen (1980), Sinno et al. (1986), Lachenbruch & Sass (1977), Brown et al. (1980)
-15. El Paso	25-35	E	10	10	EB	6.62-6.72	550-700		same as above

16. Basin and Range	22-36	E	1-10	3.8	-	6.7	500-750	23-30	Lienert & Bennett (1977), PASSCAL (1988), Lachenbruch & Sass (1977), Klemperer et al. (1986)
17. Newberry Volcano	15-30	C	1-20	6.7	EB	6.5	450-800		Fitterman et al. (1988), Catchings & Mooney (1988), Blackwell et al. (1989)
18. Cascades	20-25 30-40	C	2-20 1200-3000	20 2000	B	6.5-6.8 7.0-7.1	600-800 900-1100		Stanley (1984), Leaver et al. (1986),
Canadian Cordillera									
-19. Pemberton	20-30	C	50-200	100	B	6.5	450-650		Dragert et al. (1980), Berry & Forsyth (1975), Lewis (pers. comm.)
-20. Valhalla	20-30	E	1-10	5	EB	6.2	450-650	16-23	Jones et al. (1988), Cumming et al. (1979), Lewis (pers. comm.), Cook et al
21. 'E' reflector Vancouver Island	25-35	C	10-60	30	EB	6.35	400-600	25-35	Kurtz et al. (1990), Drew & Clowes (1990), Lewis et al. (1988)
22. Caledonides, Scotland	20-40	C	100-300	100	EB	6.6	225-350	16-32	Hutton (1980), Bamford et al. (1978), Čermak and Hurtig (1979), Brewer et al. (1983)
23. So. Uplands, Scotland	20-33	C	30-100	46	EB	6.3-6.6	400-600	19-28	Hutton (1980), Barton & Wood (1984), Bloomer et al. (1979), Brewer et al. (1983)
24. Rheingraben	32-35	E	5-20	33	EB	6.25	750-800	14-28	Schmucker (1988), Zucca (1984), Bram (1979), Fuchs et al. (1987)

25. Black Forest	12-15	E	5	17	E	5.8-6.0	275-325	14-26	Tezkan (1988), Gajewski & Prodehl (1987), Bram (1979), Lüschen et al. (1987)
	15-35		1000	500		6.6-6.8	325-650		
26. Rhen. Massif	5-18	E	5	17	EB	6.2	300-350	14-22	Volbers et al. (1990), Giese et al. (1990), Bram (1979), DEKORP Research Group (1990)
	18-30		300	250		5.9	350-500		
27. Lhasa Block	25-30	C	1-10	10	EB	6.5			Pham et al. (1986), Sapin et al. (1985)
28. Yarlung Zangbo River	30-60	C	100-500	100	EB	6.5-6.8	500-750		Pham et al. (1986), Hirn et al. (1984), Jaupart et al. (1985)
29. Yubei Basin	25-30	E	5-13	16		6.4-6.6	350-400		Prof. Liu Guodong (personal communication)
30. Ordos Block	30-38	?	12-20	20		6.5-6.6	350-400		same as above
31. Tangshan	22-28	C	3-5	5		6.0-6.4	400-500		same as above
32. Haicheng	15-20	?	4-6	10		6.1	350-400		same as above
	20-30		10^4	10^4		6.9-7.0	450-550		

Depths given are to the top and bottom of the resistivity layer; Tec, type of latest tectonic activity: S, stable shield, C, compression, E, extension; ρ, resistivity of the layer as reported by the original investigators; ρ_{10}, resistivity for a 10 km-thick equivalent layer; Pol., E- or B-polarization used for inversion, -, not applicable, controlled-source survey; V_p, velocity from seismic refraction profiling; Ref. int., reflection interval for a lower crustal reflective layer (see calculation method in text); references are in order: resistivity, velocity, heat flow and reflectivity.

ii. Relation of porosity with geological age

Figure 16 presents theoretical relations between resistivity and velocity, along with the values obtained from the compilation (Table 3). Although the experimental data have considerable scatter, there is a systematic trend of decreasing resistivity with decreasing velocity. The two data types (velocity and observed resistivity) have a correlation coefficient of 0.68. It is remarkable, considering the limitations of the geophysical techniques and the assumptions made, that the results are not more scattered. The Phanerozoic areas are seen in general to have lower electrical resistivities and seismic velocities (see also the histograms of Figures 4 and 13), indicating that if porosity is indeed the main factor controlling these physical properties, the deep continental crust in Phanerozoic areas has a higher average porosity than that of Precambrian shields. The fluid argument is also reinforced by the geochemical evidence from xenoliths showing that the lower crust in Precambrian areas is less mafic (i.e. should have lower velocity) than in Phanerozoic areas (Griffin and O'Reilly, 1987). The opposite is observed. This can best be reconciled with porosity in the deep crust, with loss of free water with time such as through recurring metamorphic events or by retrograde metamorphism associated with cooling.

iii. Shear wave constraints

The correlations presented in Figure 16 support the presence of fluids in the deep crust, but they also show that many pore geometries (i.e. aspect ratio/Archie exponent combinations) can satisfy the experimental results. When shear-wave data are available, Poisson's ratio can provide an additional constraint on the pore geometry.

Three techniques have been used to obtain Poisson's ratio in the lower crust: seismic refraction, seismic reflection and earthquake studies (Table 4). The measurement uncertainty is at least ± 0.02 and the values of observed Poisson's ratio vary substantially. There are a few values at ~ 0.32, but the largest number are in the range 0.25-0.28 (Figure 17). The latter values can be explained by: (1) rocks with a zero-porosity Poisson's ratio near the preferred value at 0.29 for lower crustal rocks (see Chapter II), having a few percent porosity with pores of aspect ratio 0.03 to 0.1 that

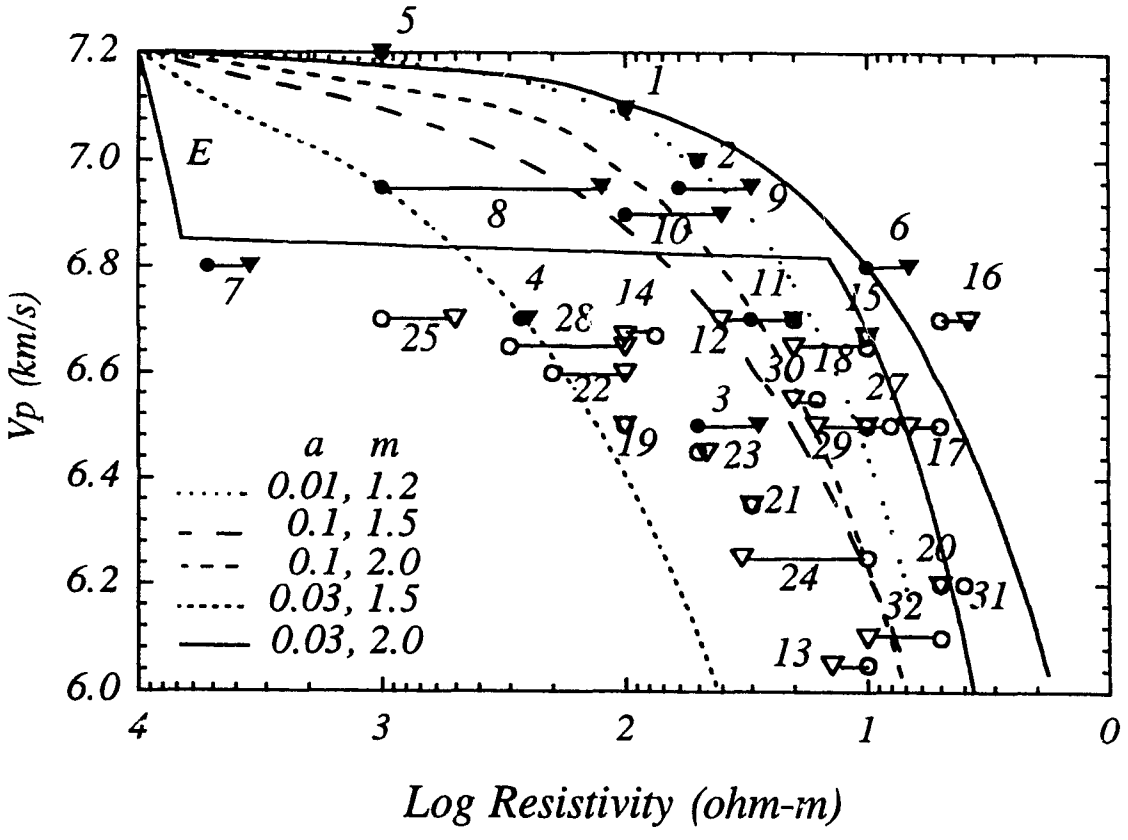

Figure 16 Velocity-Resistivity relations and values from the compilation in Table 2. Closed symbols denote Precambrian and open symbols Phanerozoic areas. Circles denote resistivity as reported by the original investigators, triangles resistivities for a 10 km thick layer of same conductance. The lines represent the same velocity-resistivity relations as in Figure 15.

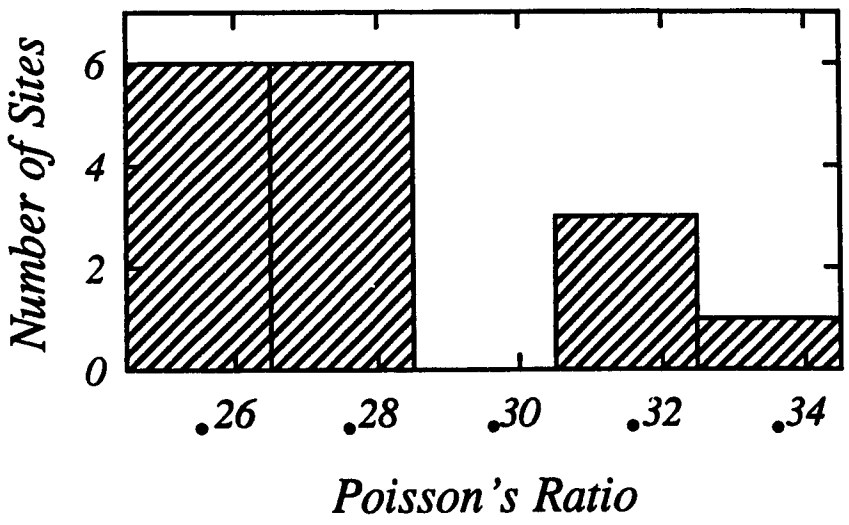

Figure 17 Poisson's ratio values from the compilation (Table 4)

slightly reduces Poisson's ratio, or (2) rocks with a lower zero-porosity Poisson's ratio (0.26-0.28) and thick pores (aspect ratio >0.1) that have little effect on Poisson's ratio. There is clearly a need for more laboratory measurements of Poisson's ratio, especially as a function of porosity, to help resolve the uncertainty in deep crustal pore geometry.

Table 4. Lower crustal Poisson's Ratio

Locality	Depth	σ	References
Seismic refraction studies			
Lewisian, Scotland	20-30	0.23-0.27	Assumpção & Bamford (1978)
Black Forest, Germany	15-25	0.27-0.28	Holbrook et al. (1988)
Arizona Transition Zone	20-30	0.25-0.29	Goodwin & McCarthy (1990)
Ordos Block, China	20-40	0.24-0.25	Liu Guodong (pers. comm.)
Jordan	20-30	0.29-0.32	El-Isa et al. (1987)
Seismic reflection studies			
Weardale, U.K.	20-30	0.29-0.32	Ward & Warner (1991)
Earthquake studies			
- P to S conversion			
Vancouver Island	25-35	0.29-0.32	Cassidy & Ellis (1991)
- Surface wave inversion			
Napa Region, California	15-22	0.25-0.26	Levander & Kovach (1990)
Diablo Range, California	15-30	0.27-0.28	Levander & Kovach (1990)
Snake River Plain, Idaho	20-41	0.30-0.32	Greensfelder & Kovach (1982)
Rio Grande Rift	20-32	0.27	Sinno & Keller (1986)
Wellington, New Zealand	15-25	0.23-0.27	Robinson (1983)
South Africa	25-40	0.25-0.29	Bloch et al. (1969)
Iranian Plateau	15-43	0.24	Asudeh (1982)
S.E. China	30-40	0.24-0.25	Wier (1982)
- Tomographic inversion			
Southern Peru	20-40	0.26-0.30	Cunningham et al. (1986)

CHAPTER IV DETAILED INTERPRETATION: INTERMONTANE BELT, BRITISH COLUMBIA

The global compilations presented above support the presence of aqueous fluids in the deep crust in most regions. However, very few of the studies reported in the previous chapter have been optimal for correlation. The LITHOPROBE South Cordillera Transect provides an opportunity to jointly interpret coincident high-quality deep crustal geophysical data; in addition to the primary program of reflection seismic lines, there have been extensive coincident magnetotelluric and seismic refraction surveys. This chapter deals with the joint analysis of LITHOPROBE magnetotelluric and reflection data for Line 10, in the Intermontane Belt, British Columbia (Figure 18). Geothermal and seismic refraction data from the same area will also be integrated to this study.

i. Magnetotelluric survey

The magnetotelluric (MT) survey is an important component of the LITHOPROBE South Cordillera transect. Wide-band MT data were acquired in 1989 by Phoenix Geophysics Ltd at 80 stations. The MT stations were approximately coincident with the multichannel seismic lines (Figure 19) acquired a year earlier and discussed in the next section. Initial interpretations of the MT survey have been presented by Jones et al. (1992).

MT data for each station contain measurements of all three components of the magnetic field, and the horizontal components of the electric field. The former were measured with high-sensitivity iron cored induction coils and the latter with lead-lead chloride (Pb-PbCl) electrodes. Recording sessions lasted typically two days, but on occasion up to five days, depending on signal strength, and data were recorded over six decades from 2.7 ms (384 Hz) to 1820 s (A.G. Jones, personal communication).

The general relation between the horizontal components of the electric and magnetic fields is given by (see Kaufman and Keller 1981):

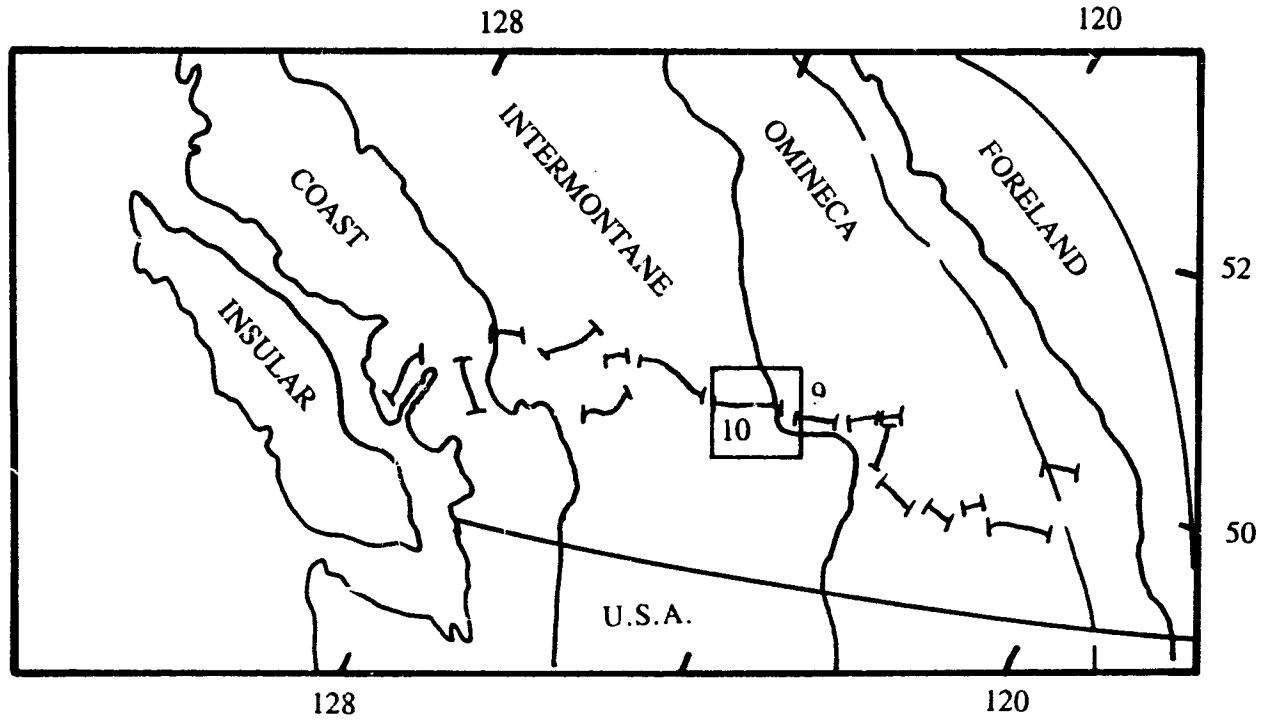

Figure 18 General map of the Cordillera and location of LITHOPROBE Line 88-10. The major morphological belts are identified in upper case letters.

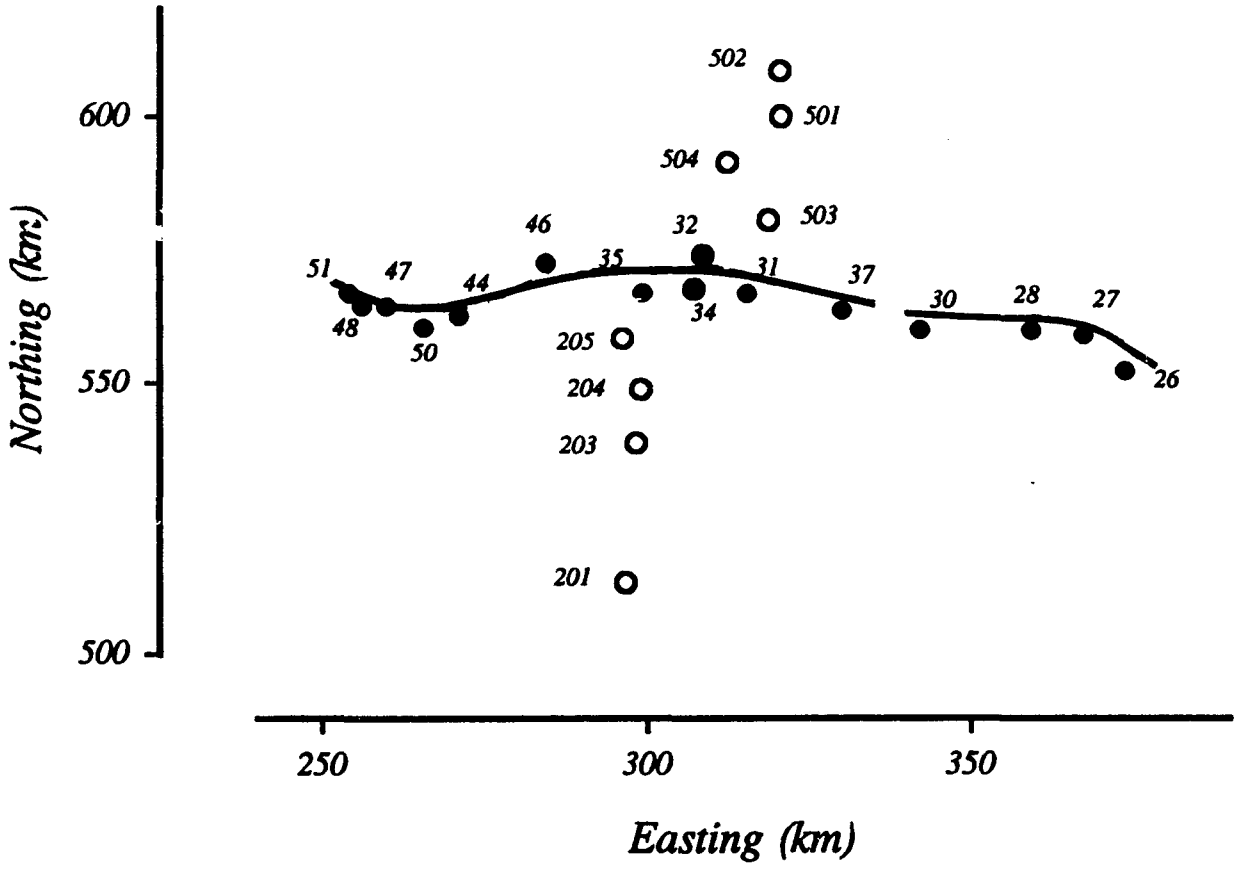

Figure 19 Detail of LITHOPROBE Line 88-10 and the western part of Line 88-9, and locations of the magnetotelluric stations. Numbers refer to stations used in the interpretation. Solid (hollow) circles represent the East-West (North-South) profile. Stations 32 and 34 have been used in both profiles.

$$\begin{bmatrix} E_x \\ E_y \end{bmatrix} = \begin{bmatrix} Z_{xx} & Z_{xy} \\ Z_{yx} & Z_{yy} \end{bmatrix} \begin{bmatrix} H_x \\ H_y \end{bmatrix}$$

where Z_{xx}, Z_{xy}, ... are the elements of the complex impedance tensor. For a one- or even two-dimensional distribution of conductivity, in the strike coordinate frame, the off-diagonal elements are very large compared to the diagonal elements. The skew of the impedance tensor

$$\frac{Z_{xx} + Z_{yy}}{Z_{xy} - Z_{yx}}$$

is a useful parameter allowing the appraisal of the dimensionality of the conductivity structure. For the data analyzed below, the skew values range between 0.01 and 0.40, with most values being below 0.10 (Figure 20). These low skew values indicate that the local structure is not distorted greatly by near-surface three-dimensional effects.

If the electric fields are measured in mV/km and the magnetic fields in gammas (1 A/m = 1257 gammas), the complex impedances can then be converted into apparent resistivity (ρ_a) and phase (ϕ):

$$\rho_{a\,xy} = 0.2\ T\ |Z_{xy}|^2$$
$$\phi_{xy} = \arctan\ [\mathrm{Im}(Z_{xy}) / \mathrm{Re}(Z_{xy})]$$

where T is the period in seconds. Note that both of these parameters are function of period. It is in this form that the MT data will be presented throughout this section.

The study area is in the central Intermontane Belt, along LITHOPROBE seismic line 88-10. In addition to the MT survey directly coincident with the seismic line (EW profile; Figure 19), another MT transect crossing it has been acquired (profile NS) and will also be presented here. It is of interest to establish if there are any important changes in the electrical structure in a direction perpendicular to strike. Since strike is very close to a north-south direction, the E-polarization has been assumed as being north-south, the B-polarization, east-west. The very small skew values at short periods

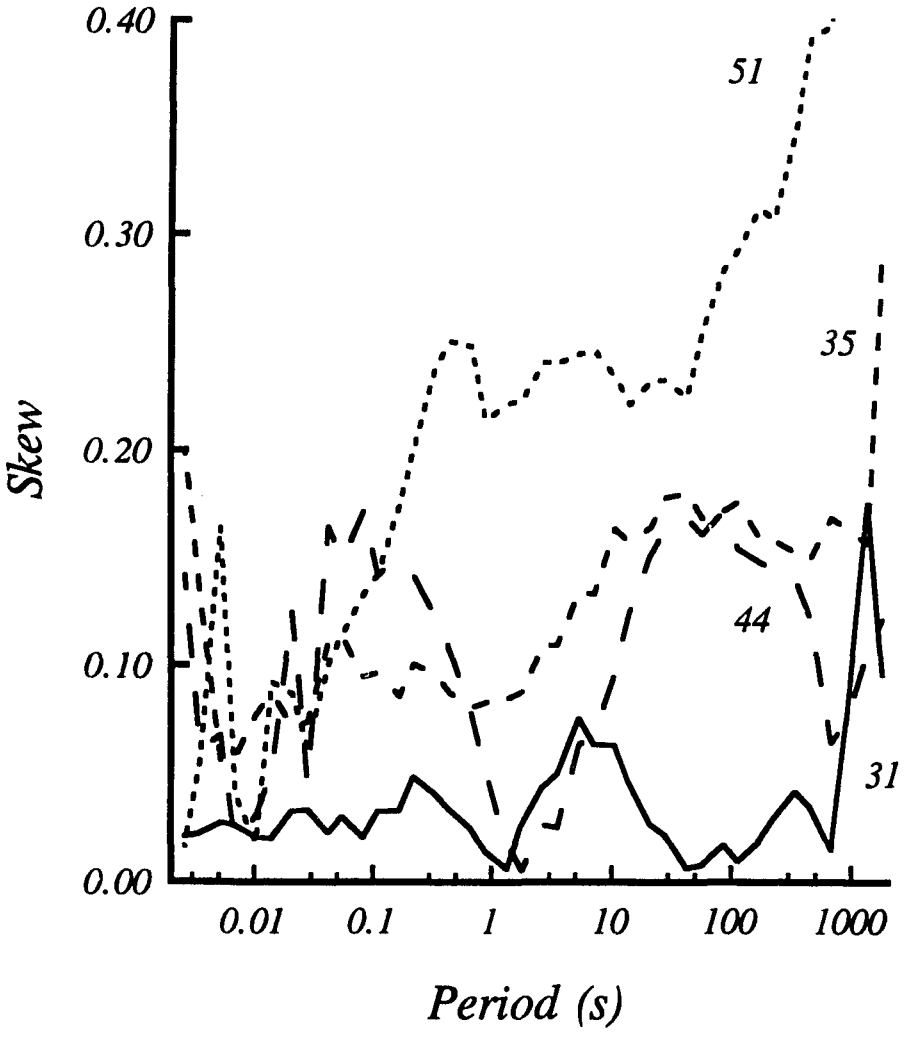

Figure 20 Skew for selected stations. The very low skew values indicate that the directions chosen are clearly along and perpendicular to strike

strongly support this assumption.

The apparent resistivity and phase curves for stations from both the East-West and North-South profiles are shown in Figures 21 and 22. The most important feature is the remarkable consistency of the phase curves (bottom of Figures 21 and 22), compared to the apparent resistivity curves, especially at longer periods. Such consistency indicates that at great depths the electrical resistivity is similar for all stations. In addition, the E- and B-polarization phases at most stations being $\sim 180^{\circ}$ apart indicates that this deep resistivity is close to one-dimensional, i.e. the deeper part of the section is layered.

On the other hand, the apparent resistivity curves are widely separated (top of Figures 21 and 22), even at long periods. This contrast between the behaviour of the apparent resistivity and the phase curves indicates the presence of static shift (for a review see Jiracek 1990). Static shift is caused by near-surface galvanic effects that produce secondary electromagnetic fields. As these fields are recorded by the MT apparatus, the apparent resistivities are increased (or decreased) by a constant factor. The phase curves are not affected by static shift, since they involve a ratio of impedances, but the apparent resistivity curves are shifted by a constant factor. Static shift is increasingly recognized as one of the most important problems in electromagnetic sounding of the earth. Many workers have investigated this problem in the last few years (e.g. Jones, 1988; Sternberg et al., 1988; Berdichevsky et al., 1989). The reader is referred to these papers for more information.

The approach used here for static shift corrections is based on the work of Berdichevsky et al. (1989):

- The phase curves being approximately coincident at long periods implies that the apparent resistivity curves for E-polarization should also be coincident. For this study, one the longest periods, 910.2, 1365 or 1820 s, have been adjusted to 80, 70, and 50 ohm m respectively, depending on the longest period with a small error (difference between max and average less than 20%). These periods correspond to depths of 50 km or more, i.e. well under the crust. The resistivity values at these periods have been chosen because they are representative of the behaviour of a majority of stations. It

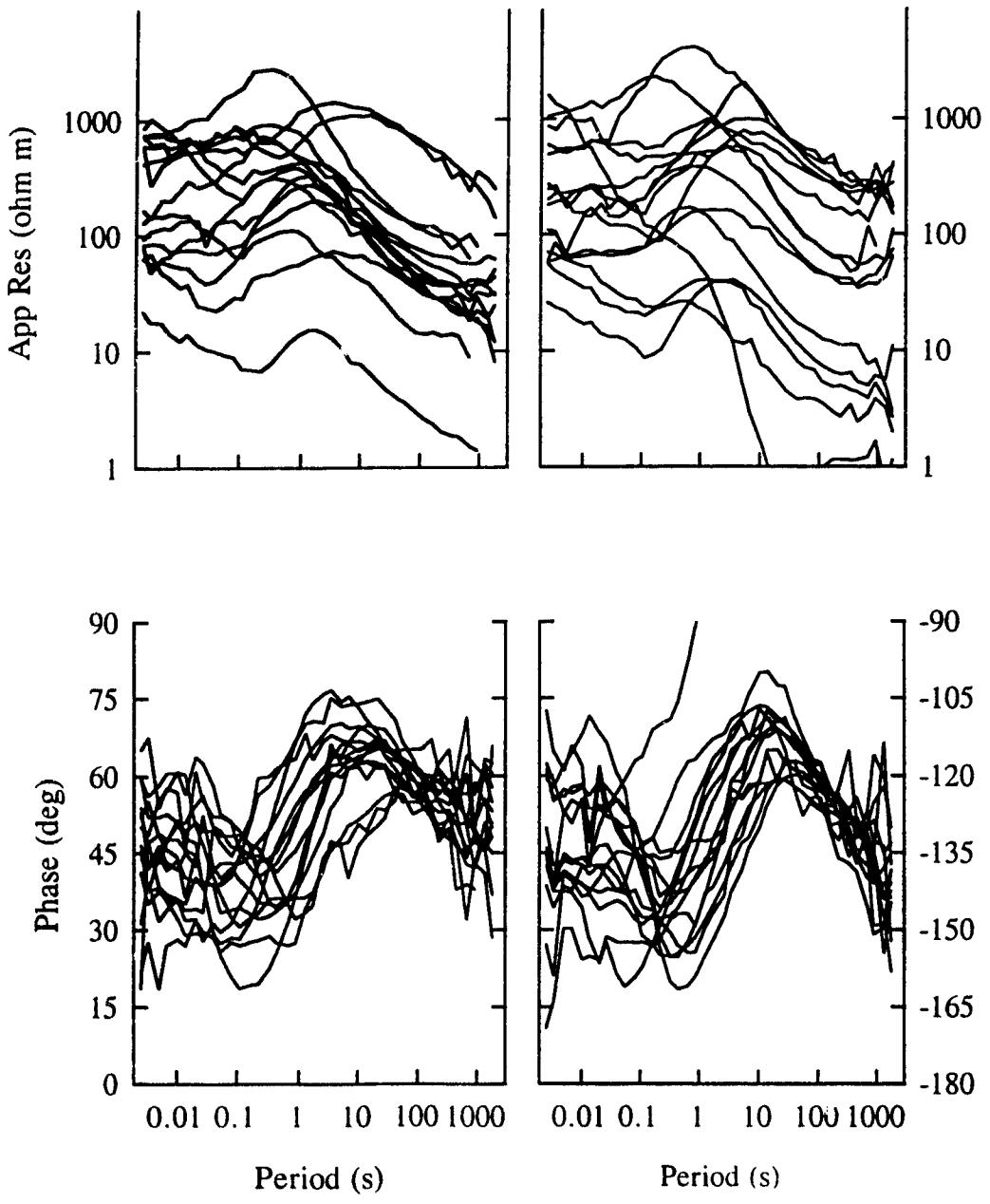

Figure 21 Raw MT data, East-West profile: top, apparent resistivity; bottom, phase; left, E-polarization; right, B-polarization.

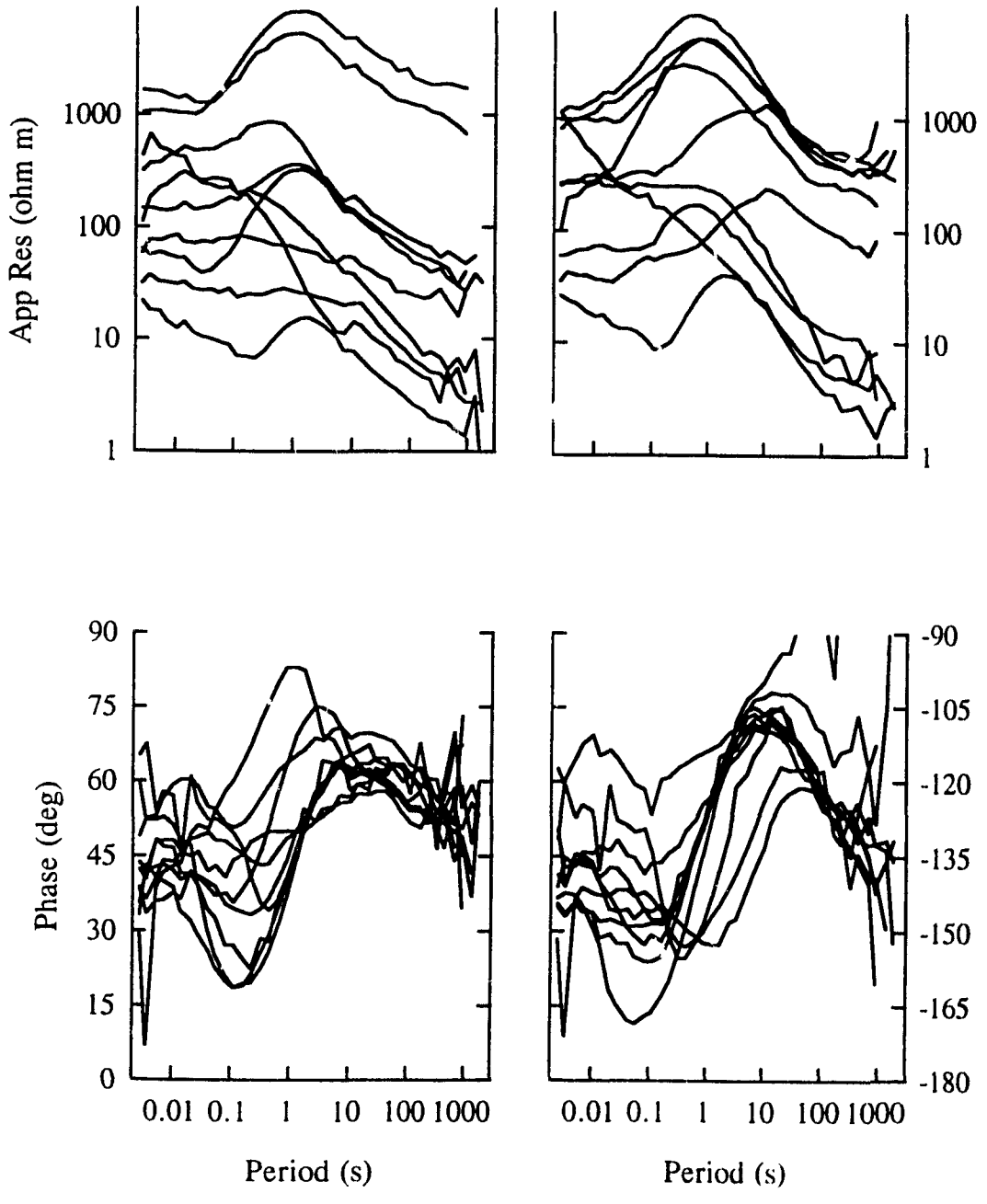

Figure 22 Raw MT data, North-South profile. Same conventions as Figure 21.

should be noted that the resistivity should really be adjusted at a particular depth, rather than at a particular period, but this would require determining the period that corresponds to that depth for each station, and adjust the resistivity-depth profile accordingly. The correcting factor was then applied to all the other values. Changing this correction factor does not affect significantly the dimensions of the layers obtained by inverting the data, but it strongly affects both the resistivity values and the depth to the top of the layers.

- Once the E-polarization curves have been corrected, their respective B-polarization curves were shifted so that at very short periods both E- and B-pol coincide. This adjustment is justified by the fact that at short periods a very small part of the earth is sampled and hence it should be devoid of any large-scale anisotropy.

The MT data have been inverted using a two-step approach: first the data for each station have been inverted separately to obtain a series of adjacent one-dimensional resistivity-depth profiles. The one-dimensional inversion technique of Weaver and Agarwal (1992) has been used. This routine gives the minimum number of discrete layers, each of constant resistivity, that have an acceptable fit to the data. In this routine, a simple Niblett-Bostick inversion of the E-polarization data is first calculated. This initial profile is then used to construct models with increasing numbers of layers until the addition of an extra layer does not improve the fit to the data significantly.

The second step is a two-dimensional inversion of the data. The technique of Weaver & Agarwal (personal communication) has been used: it is based on an iterative scheme for minimising the misfit of 2D forward models (forward method described in Poll et al. 1989). The adjacent one-dimensional models obtained earlier are used as a starting model for the 2D inversion. A smaller numbers of sites and frequencies had to be selected to make the computations manageable. The inversion technique minimises both the vertical and horizontal structures of the resistivity, and hence requires a very large number of calculations, even with a small number of model parameters.

The major advantage of using this two-dimensional modelling is that it takes into account both E- and B-polarizations in the inversion. Inversion of only E-polarization data resolves well only the depth and the resistivity-depth product of the resistivity layers, while the inversion of only B-polarization data resolves well their horizontal

extent and the thin resistive layers (A.K. Agarwal, personal communication). Using both E- and B-polarization in the inversion allows for a much better evaluation of the resistivity structure over a large area. Using only averages (e.g. Berdichevsky and Dmitriev, 1976) in the inversions, while often a useful approximation (especially when E- and B-polarization data are not too different), gives resistivity-depth inversions of intermediate resolution that are biased both in depth and resistivity. The averaged phases are however useful for identifying conductive structures at depth.

ii. East-West profile

A spatial distribution of the E-polarization phases is shown in Figure 23. The vertical scale used is the period, since it is analogous to depth. There is some variation in the short period phases (indicating of near-surface variations in resistivity), but the long-period phases are high ($> 60°$) across the whole profile. This is a reliable indication of the presence of a low-resistivity layer at mid- to lower crustal depths, since phase curves are not affected by static shift. It is however impossible to get a resistivity value with the phase data alone: inversion of apparent resistivity curves will be required.

Figure 24 shows a series of one-dimensional inversions of the data with no static shift corrections for this profile. The structure obtained shows high conductivity usually in the deep crust, but does not provide useful resolution. Very high-resistivity (10000 ohm m) layers juxtapose very low-resistivity (0.1 ohm m) layers. The undesirable effects of static shift are obvious in this case: corrections are required to obtain a meaningful resistivity structure.

The apparent resistivity curves corrected for static shift are shown in Figure 25. The phase curves, which are not corrected, are not shown again (shown in Figure 21). The E-polarization curves are now quite consistent at long periods, just as expected from the phase curves in Figure 21b. The near-surface two-dimensionality remains however: there is still over an order of magnitude of scatter at short periods, indicating that the near-surface resistivity indeed varies. This in turn supports the argument for the presence of static shift. At intermediate ($10s < T < 100s$) and longer ($T > 100s$) periods, the E-polarization curves show little variation (half an order of magnitude), indicating

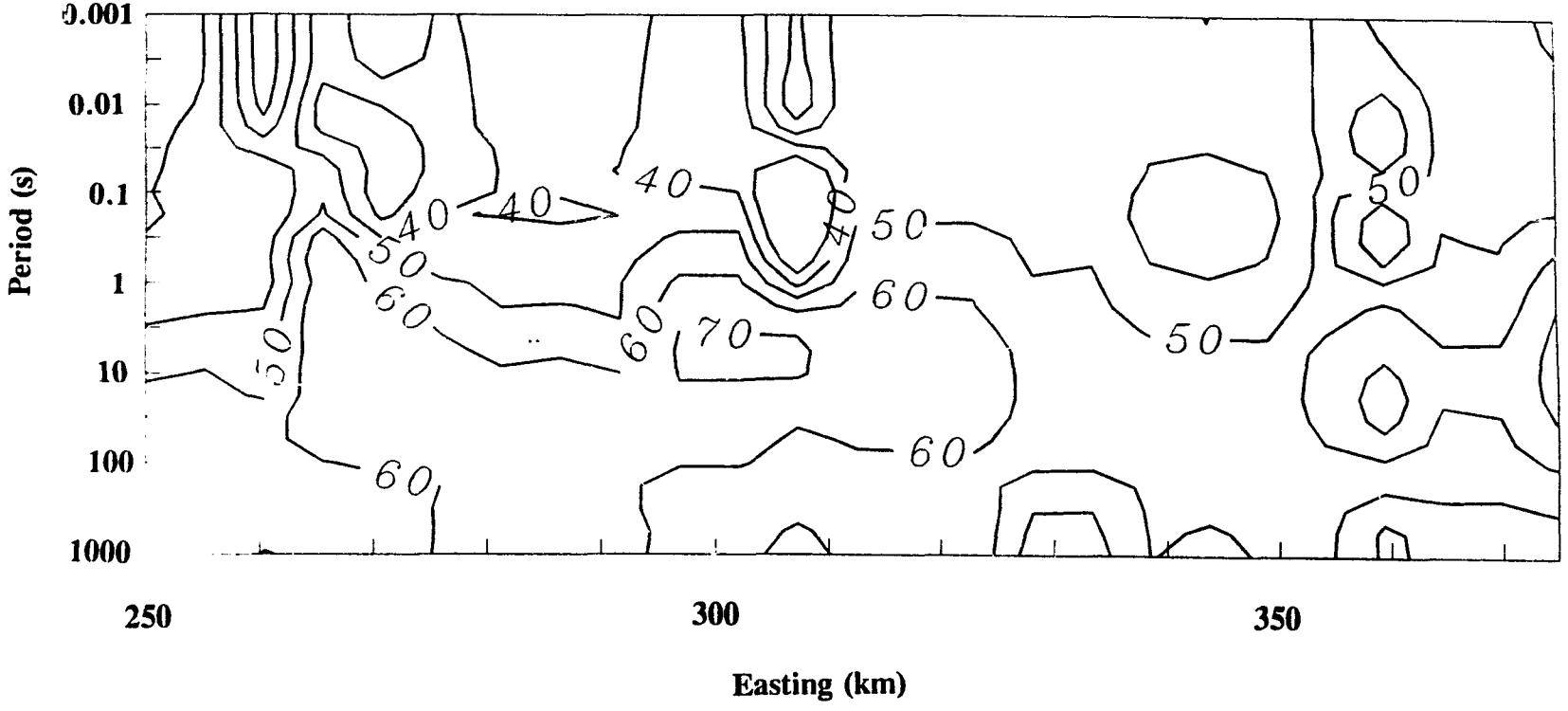

Figure 23 E-polarization phase pseudosection, East-West profile. The high phases observed at periods longer than 10 s are indicating a low-resistivity layer at mid- to lower crustal depths.

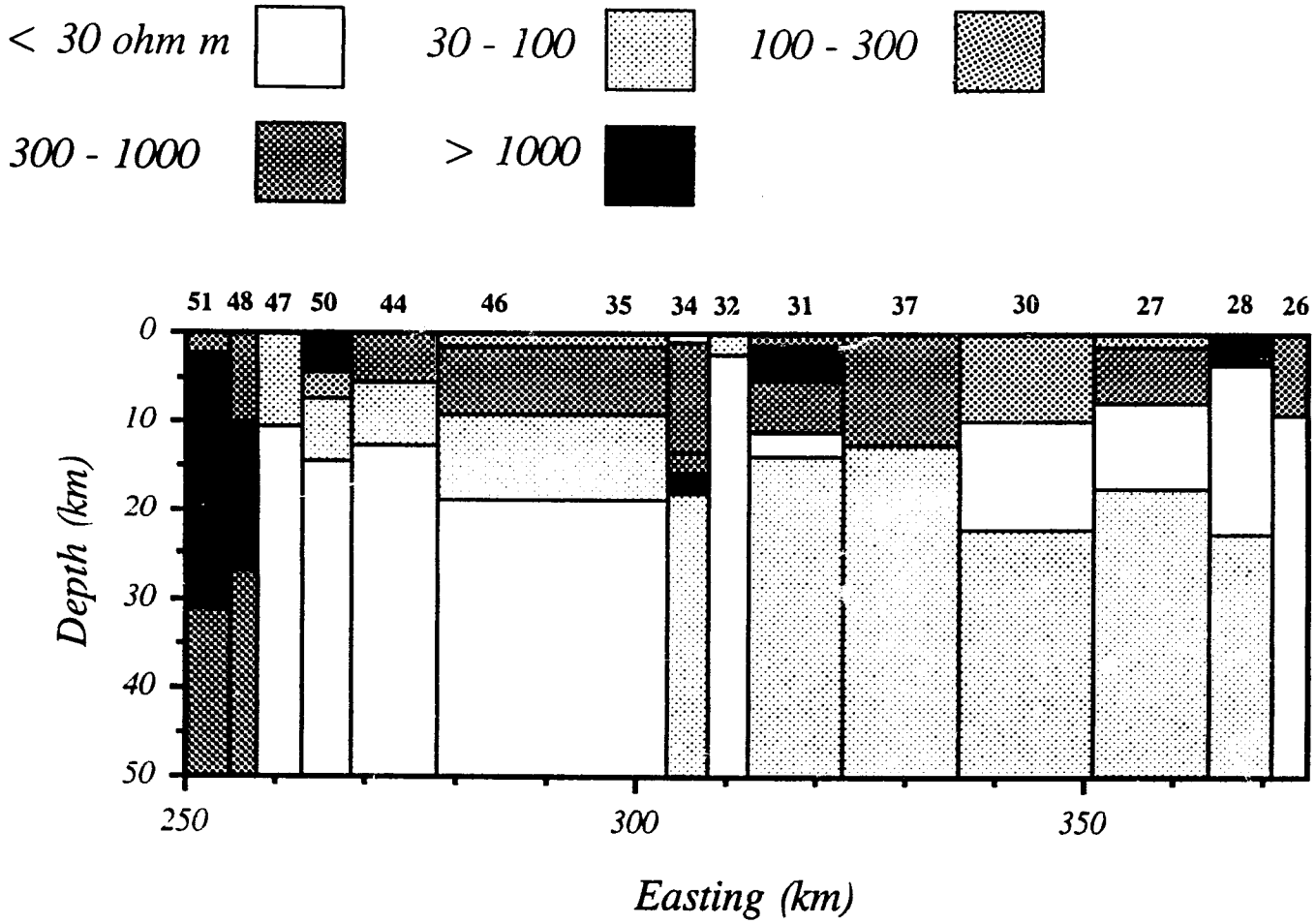

Figure 24 One-dimensional inversion of raw data, East-West profile. The shading key is the same for all other resistivity structures. Numbers refer to magnetotelluric stations. No vertical exaggeration.

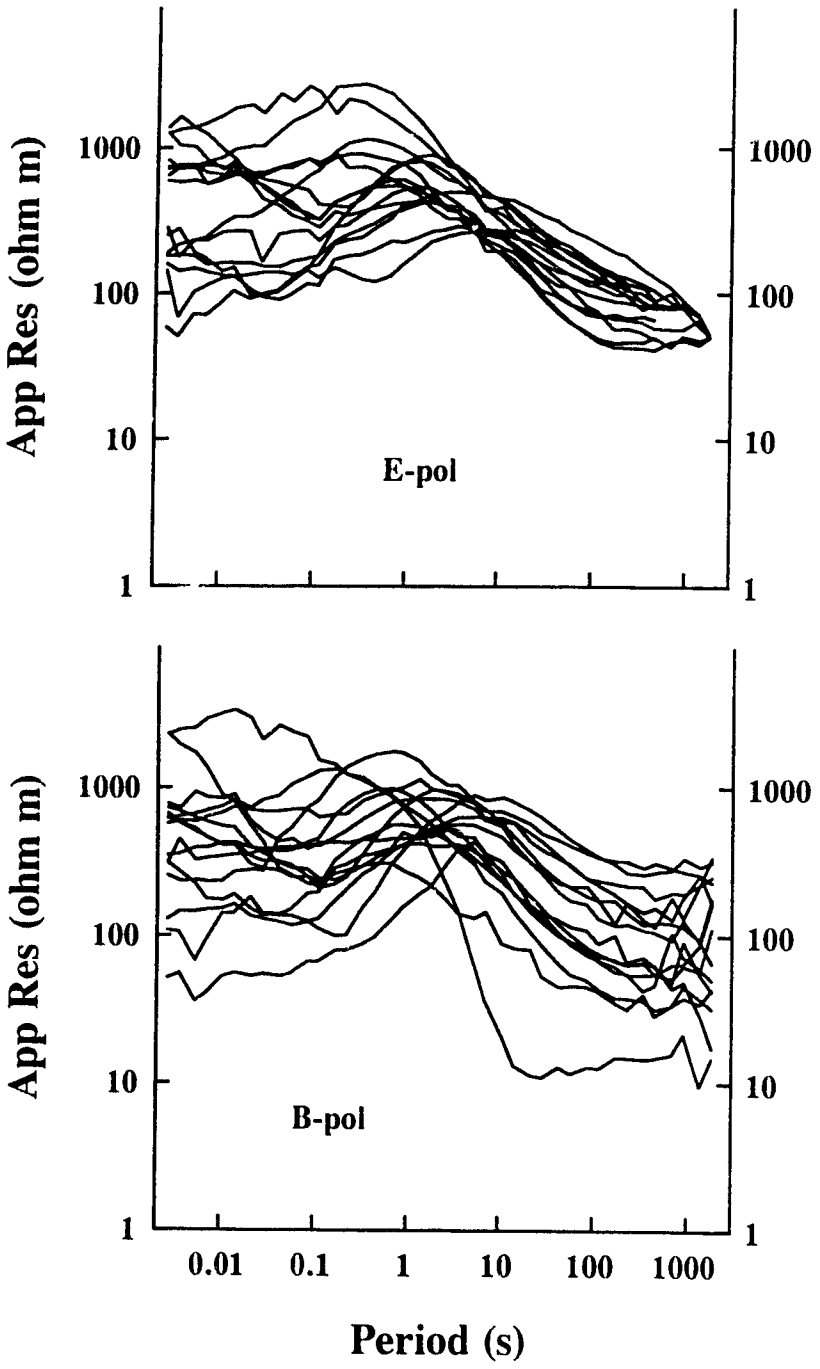

Figure 25 East-West profile data corrected for static shift

that the mid- to deep crust has a fairly consistent value of resistivity in the east-west direction.

One-dimensional inversions of the corrected data are shown in Figure 26, for the E-Polarization data. It can be seen that the near-surface resistivity values show large scatter, probably mainly dependent upon whether the stations are on conductive sedimentary cover or resistive igneous plutons. The most important feature is the decrease in resistivity at mid- to lower crustal depths (15 to 28 km at the top of the low-resistivity layer) for all stations. This is in agreement with what has been observed in most MT surveys in Phanerozoic terrains (e.g. Haak and Hutton 1986; Hyndman & Shearer 1989). The resistivity in these layers ranges from 30 to 60 ohm m, similar to the 'Canadian Cordilleran Regional Conductor' (Caner et al, 1971) and the 'Mainland Conductor' reported in Kurtz et al. (1990).

The series of one-dimensional inversions was used as a starting model for a two-dimensional inversion. For the 2-D inversion, the number of stations had to be reduced from fifteen to eight and the number of periods used had to be reduced from twenty to six to reduce the number of unknowns. Since the emphasis of this study is in the middle to deep crust, periods ranging from 5 to 455 seconds have been chosen. Choosing shorter periods would greatly increase the computing time, since the two-dimensional forward model has to design a very close-spaced grid, increasing dramatically the number of parameters to be calculated. The inversion routine was implemented on the Sun SparcServer 470 at the Pacific Geoscience Centre: it takes about one hour in batch mode to calculate five iterations.

The final two-dimensional inversion model after 800 iterations is shown in Figure 28: it is much simpler than the starting model, and fits the data much better (original misfit: 0.265, final misfit: 0.057). The misfit is obtained by (Weaver and Agarwal, 1992):

$$\epsilon^2 = \frac{(\epsilon_\rho)_E^2 + (\epsilon_\phi)_E^2 + (\epsilon_\rho)_B^2 + (\epsilon_\phi)_B^2}{4}$$

where:

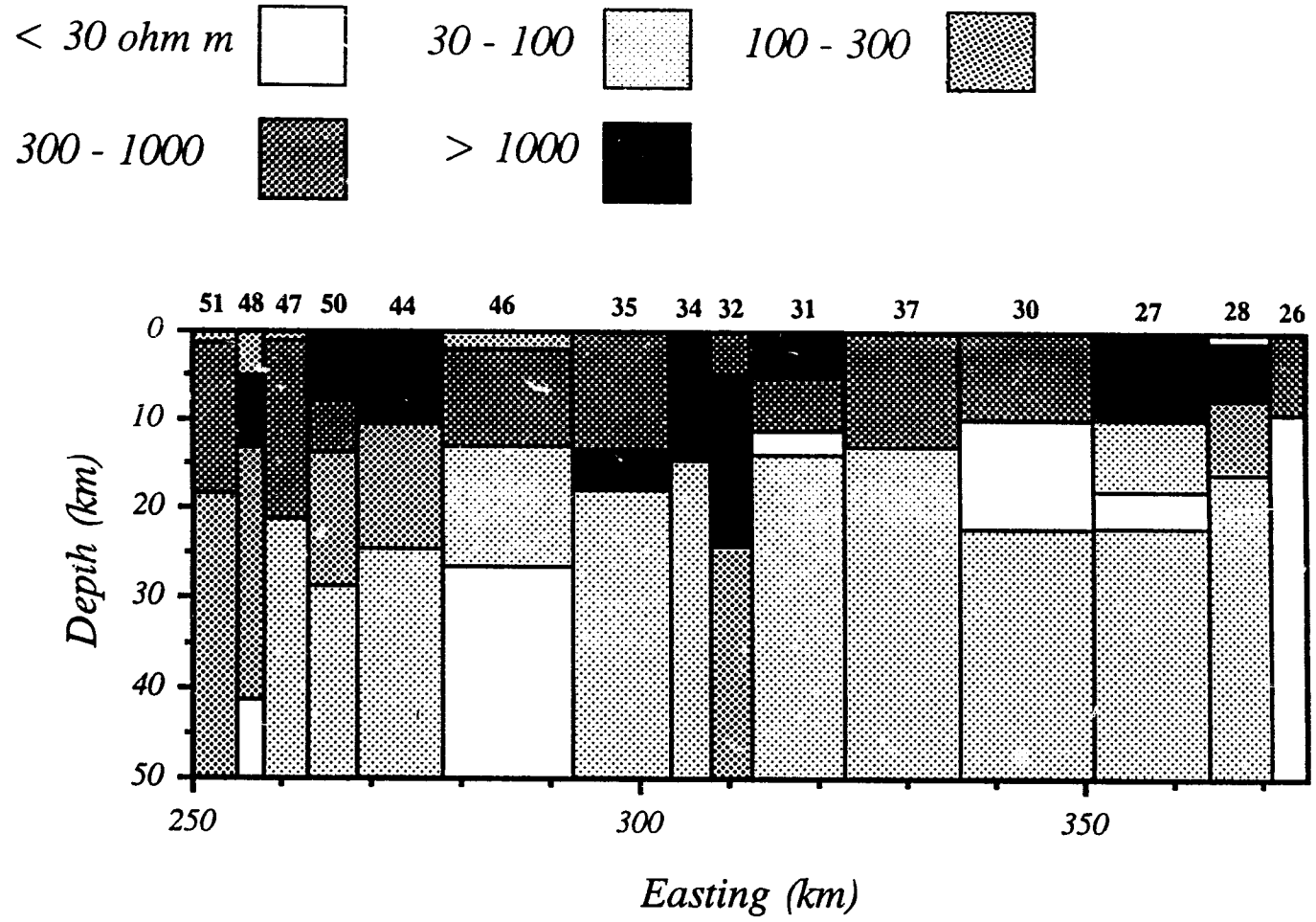

Figure 26 One-dimensional inversion of E-polarization data, East-West profile. Data have been corrected for static shift. Note the general decrease in resistivity below 10 to 20 km depths.

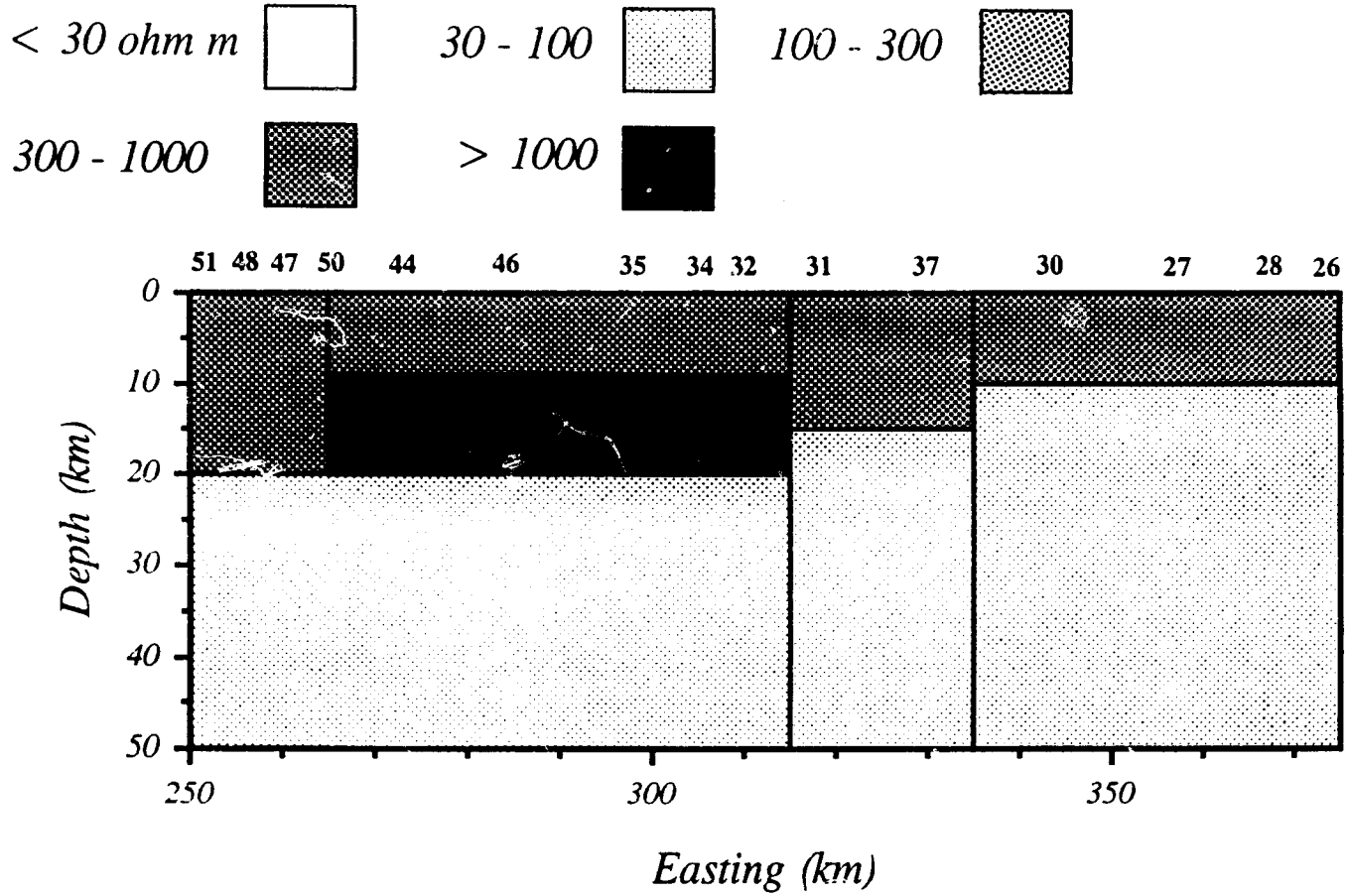

Figure 27 Two-dimensional model after 800 iterations, East-West profile. The two-dimensional inversion method of Weaver and Agarwal has been used. Note the simplicity of the resistivity structure. This result will be compared with seismic reflection and geothermal data.

$$(\epsilon_\rho)_E^2 = \frac{1}{KN} \sum_{k=1}^{K} \sum_{n=1}^{N} (0.5 \log \frac{\rho_E^m}{\rho_E^c})^2 \qquad 60$$

$$(\epsilon_\phi)_E^2 = \frac{1}{KN} \sum_{k=1}^{K} \sum_{n=1}^{N} (\phi_E^m - \phi_E^c)$$

m (c) : measured (calculated) values

K (N) : number of sites (periods)

The lower crustal low-resistivity layer is still present and is better defined: its top is at 20 km depth to the west and 15 km to the east for the Intermontane Belt, and 10 km depth for the western part of the Omineca Belt. This variation is expected, as the eastmost section of Line 10 and the western part of Line 09 are at the edge of the Omineca Belt, where heat flow is higher than in the central Intermontane Belt (see below).

To get a better picture of the relative accuracy of the two-dimensional model, modelled and observed apparent resistivities and phases are shown in Figure 28 for 5 sites. The modelled values were output from a two-dimensional forward modelling program (Poll et al., 1989). The match between the modelled and the observed values is excellent at all stations for the E-polarization apparent resistivities and phases. There is not such a good fit with the B-polarization apparent resistivities: this might be cause by using a starting model based only on E-pol data, thus biasing the model towards the E-pol curves. This bias is especially obvious at station 26, where the E- and B-pol apparent resistivity curves are quite separated. This mismatch might also indicate an improper distortion correction: perhaps there are three-dimensional effects present in this area that cannot be corrected by the static shift procedure used for this work.

Jones et al. (1992) present an interpretation of the same data, but it is based on the phase values of the effective impedance of Berdichevsky and Dmitriev (1976)

$$\sqrt{Z_{xx}Z_{yy} - Z_{xy}Z_{yx}}$$

They argue that these values are the least affected by near-surface 3D inhomogeneities, since the galvanic effects are opposite for opposite directions, i.e. the effective impedance should cancel out these effects. They have corrected for static shift by fitting

the apparent resistivity curves at a period of 10 s to a low-order polynomial, based on the regional distribution of the apparent resistivity curves. This method was preferred because it gave the most stable image on a regional scale (Jones et al., 1992), but it should be noted that this corresponds to fixing the resistivity at mid-crustal depths, hence making the deep crustal interpretation heavily dependent upon the static shift corrections. It should be emphasized here that the work of Jones et al. addresses problems of a larger, regional scale covering many orogenic belts, while the results presented in the thesis are focused on a very local scale.

The main results of Jones at al. (1992) of relevance to this thesis are the 60°-65° phase values at 10 s in the Intermontane Belt. Modelling of E-polarization data yielded a corresponding ~150 ohm m layer in the mid to lower crust. The lower crustal resistivity reported by Jones et al. (1992) is half and order of magnitude higher than reported here (~50 ohm m). This discrepancy can be explained by the different methods used for static shift corrections. In this thesis they were based on adjusting the apparent resistivity curves at periods corresponding to depths well blow the crust, independently of any regional structure, since it was assumed that the upper mantle has an homogeneous resistivity distribution. The depth to the top of the low-resistivity layer to the east of the East-West profile is similar to the depth to the conducting layer in the Omineca Belt of Jones et al. (1992).

Another MT survey, simultaneous to the Lithoprobe MT survey, was conducted further north by the University of Alberta group under the direction of D.I. Gough (Majorowicz and Gough, 1991). The period range is smaller than the Lithoprobe survey: 7.6 ms (130 Hz) to 62.5 s, and hence provides less information on the lower crustal resistivity. One-dimensional inversion of determinant apparent resistivity and phase for one site (908) in the Intermontane Belt shows a 10 ohm m layer from 10 km depth, but the lack of long-period data prevents a better definition of this lower crustal conducting layer.

iii. North-South profile

The E-polarization phase pseudosection for the North-South profile is shown in

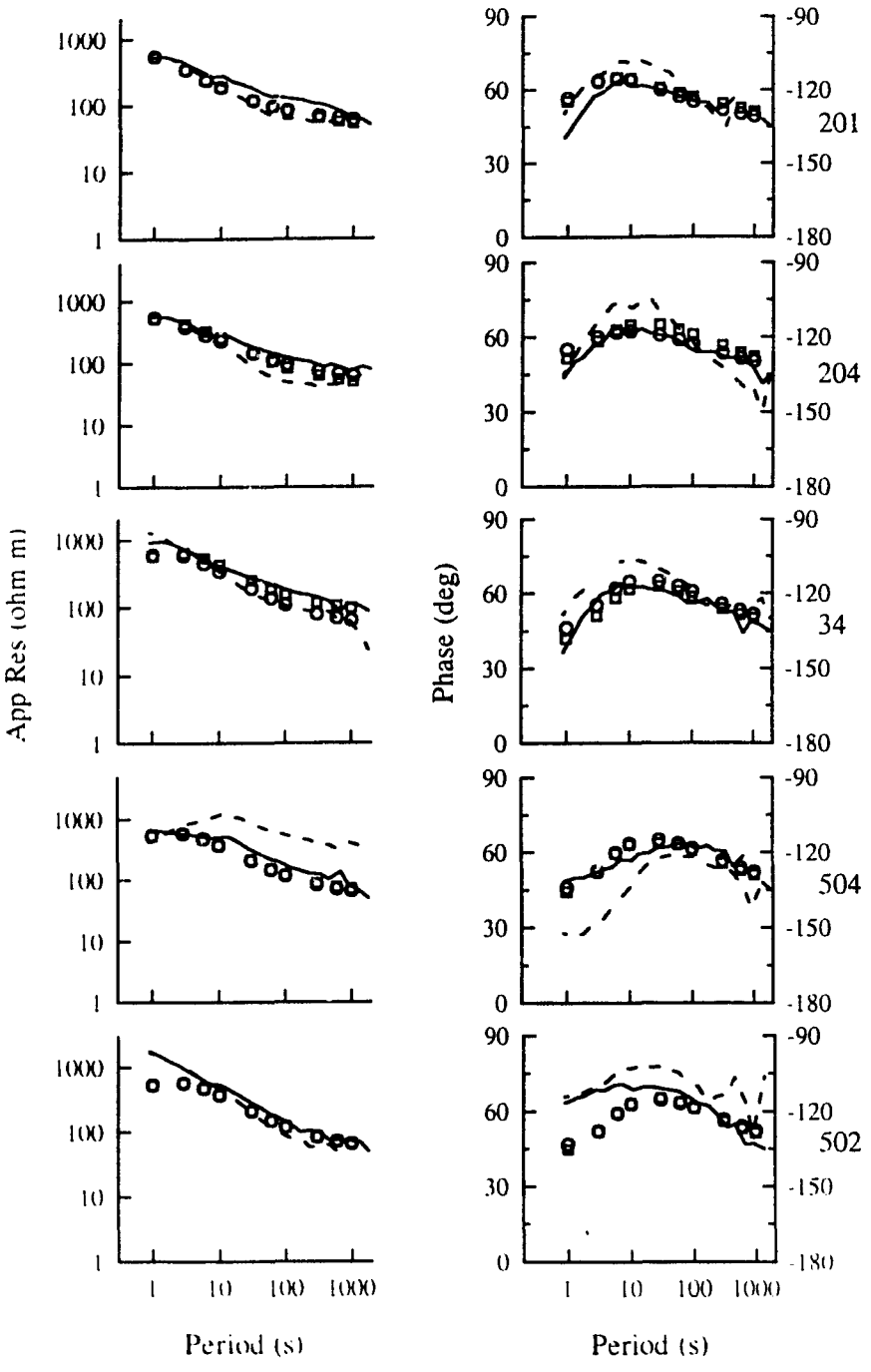

Figure 28 Comparison between apparent resistivity and phase (circles, E-pol, squares, B-pol) with observed data (solid lines E-pol, dashed B-pol)

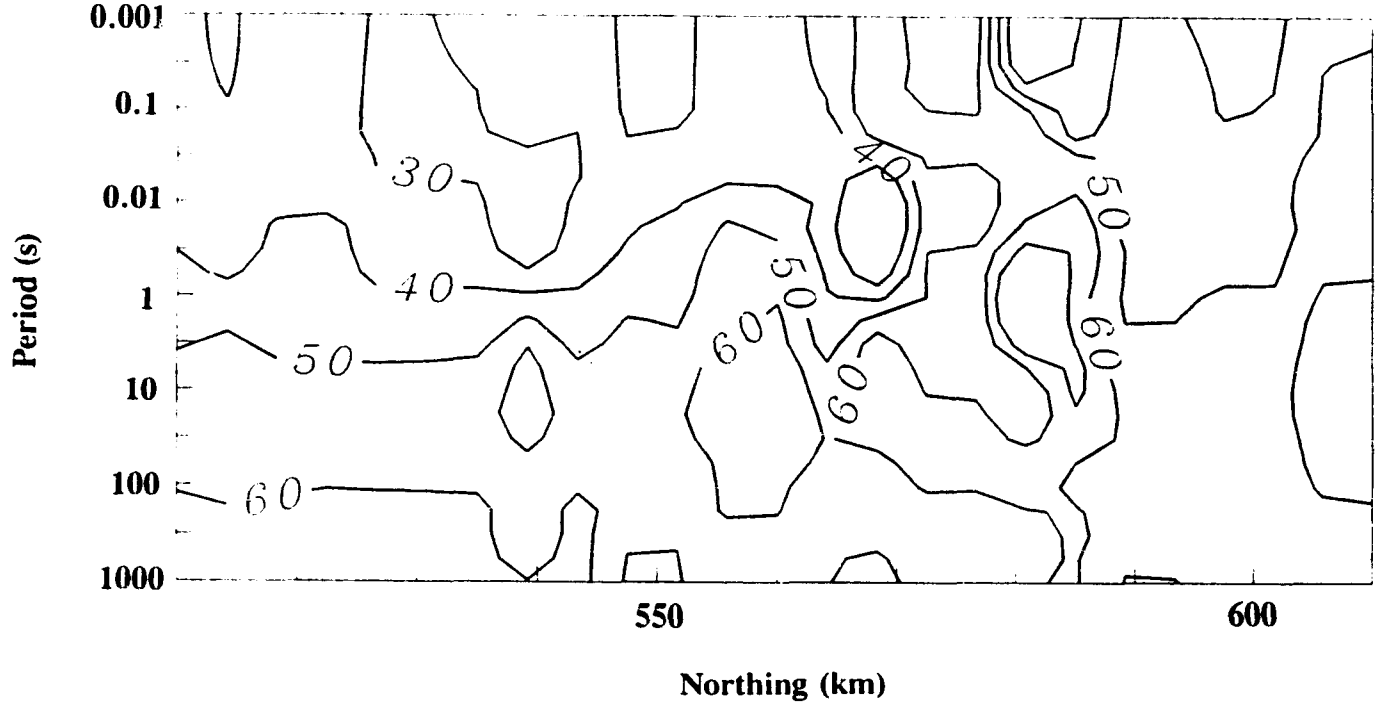

Figure 29 E-polarization phase pseudosection, North-South profile. High phases are again observed at periods larger than 10 s: the mid- to lower crust has low resistivity.

Figure 29. There is again great variation in the near-surface phases, but at periods of 10 seconds and longer, the phases are 60° and higher, indicating that the mid to lower crust has low resistivity. Apparent resistivity inversions will however be required to determine the resistivity at depth.

As for the East-West profile, data from the North-South profile are also strongly affected by static shift. Figure 30 shows the result of one-dimensional inversions of the original MT data. Very little meaningful information can be obtained from this section, and static shift corrections have to be made, the same way as for the East-West profile.

The new data corrected for static shift are shown in Figure 31 and results from a one-dimensional inversion of the E-polarization apparent resistivity and phases are shown in Figure 32. The most important feature is, as for the East-West profile, a low-resistivity layer in the lower crust. Depths to the top of this layer vary from 18 to 30 km. A preferred model for the East-West profile is shown in Figure 33. It was constrained to match the East-West profile where the two profiles intersect, and represents a compromise between simplicity and goodness of fit.

Modelled apparent resistivities and phases from the preferred model are shown in Figure 34, together with observed data from 5 stations. The fit between the E-polarization apparent resistivity and phase data is very good, but as in the previous case, there is still a discrepancy for the B-polarization curves at station 504. Again, there could be improper distortion corrections applied at that station, since the match is quite good at the other stations.

iv. Multichannel seismic processing and interpretation

As part of the LITHOPROBE Southern Cordillera Transect, multichannel reflection data were acquired in 1988 by Sonix Inc. of Calgary. Initial processing on these data was done by Western Geophysical Ltd., and their geological interpretation have been presented by Cook et al. (1991, 1992).

The processing previously carried out was designed to emphasize structural discontinuities through the use of AGC (automatic gain control) and migration and

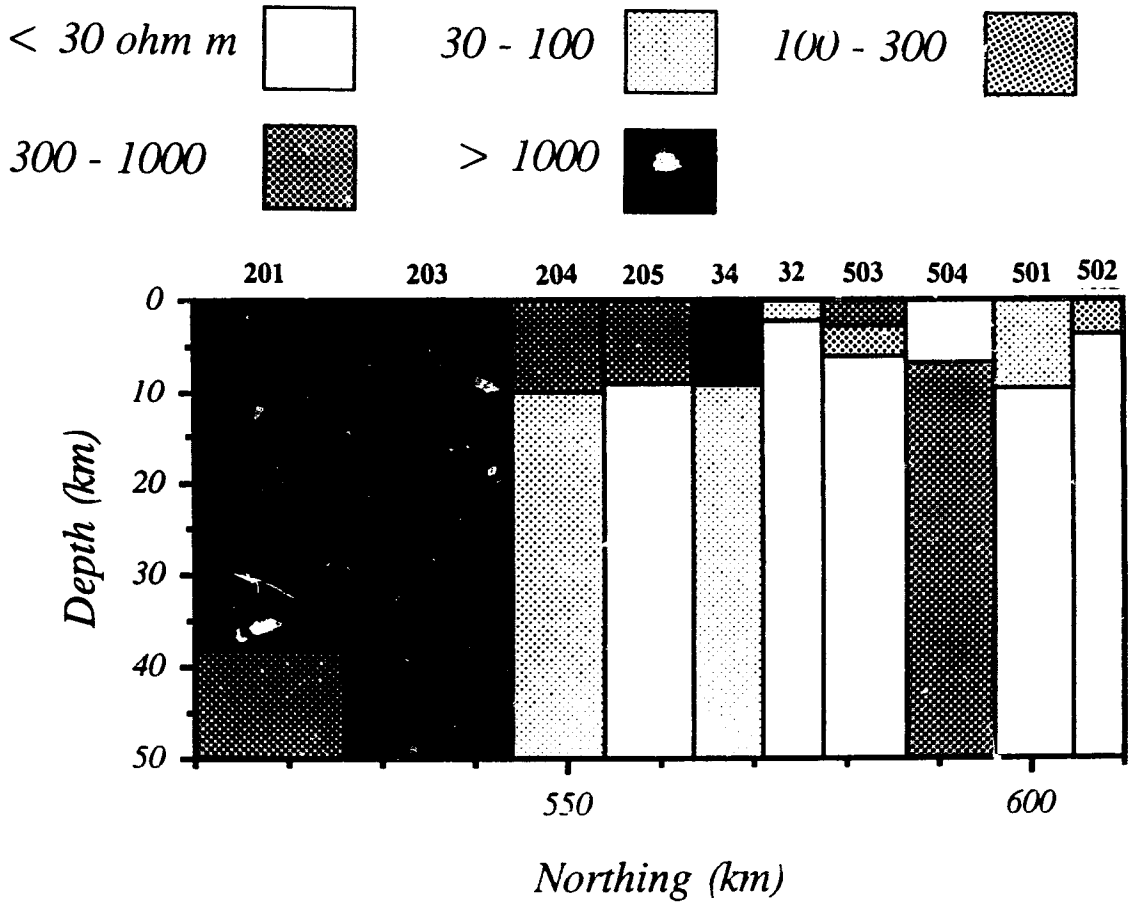

Figure 30 One-dimensional inversion of raw data, North-South profile.

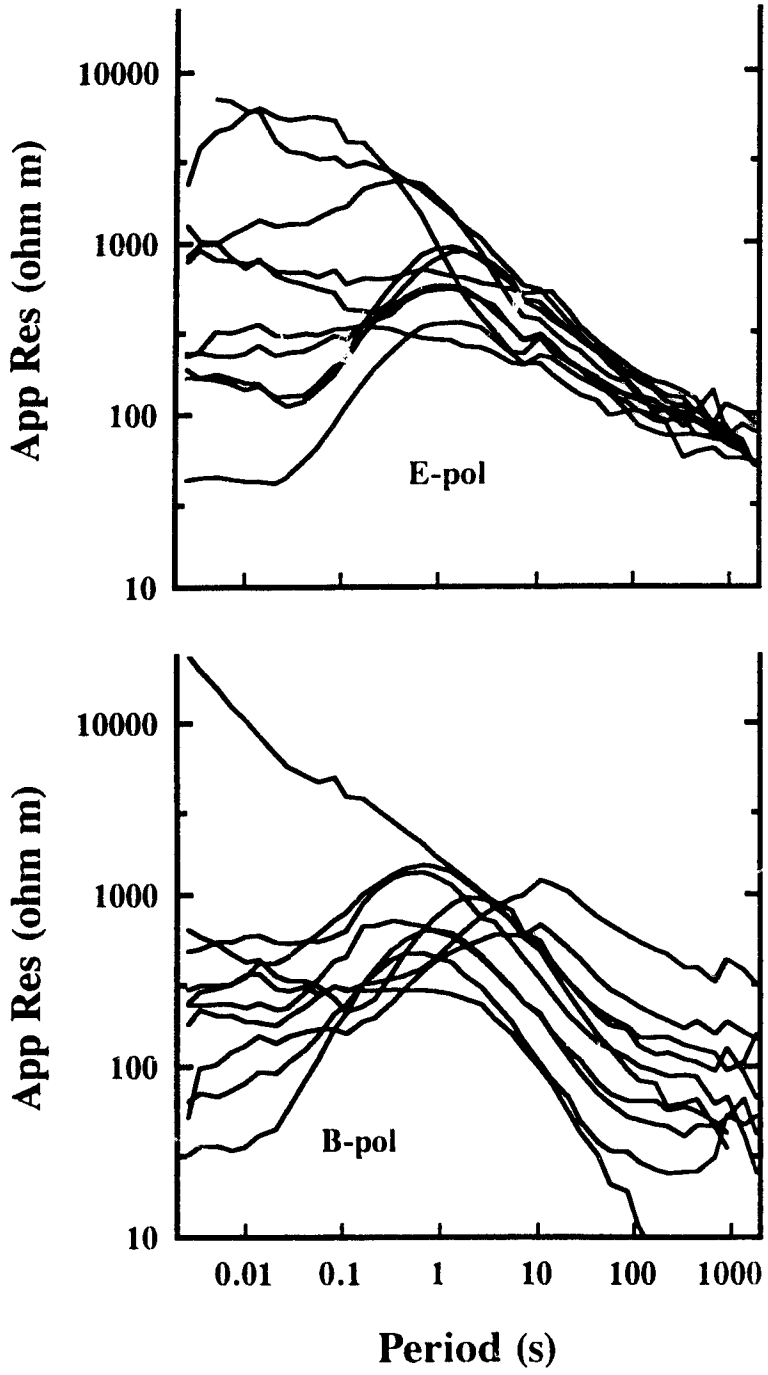

Figure 31 North-South profile data corrected for static shift

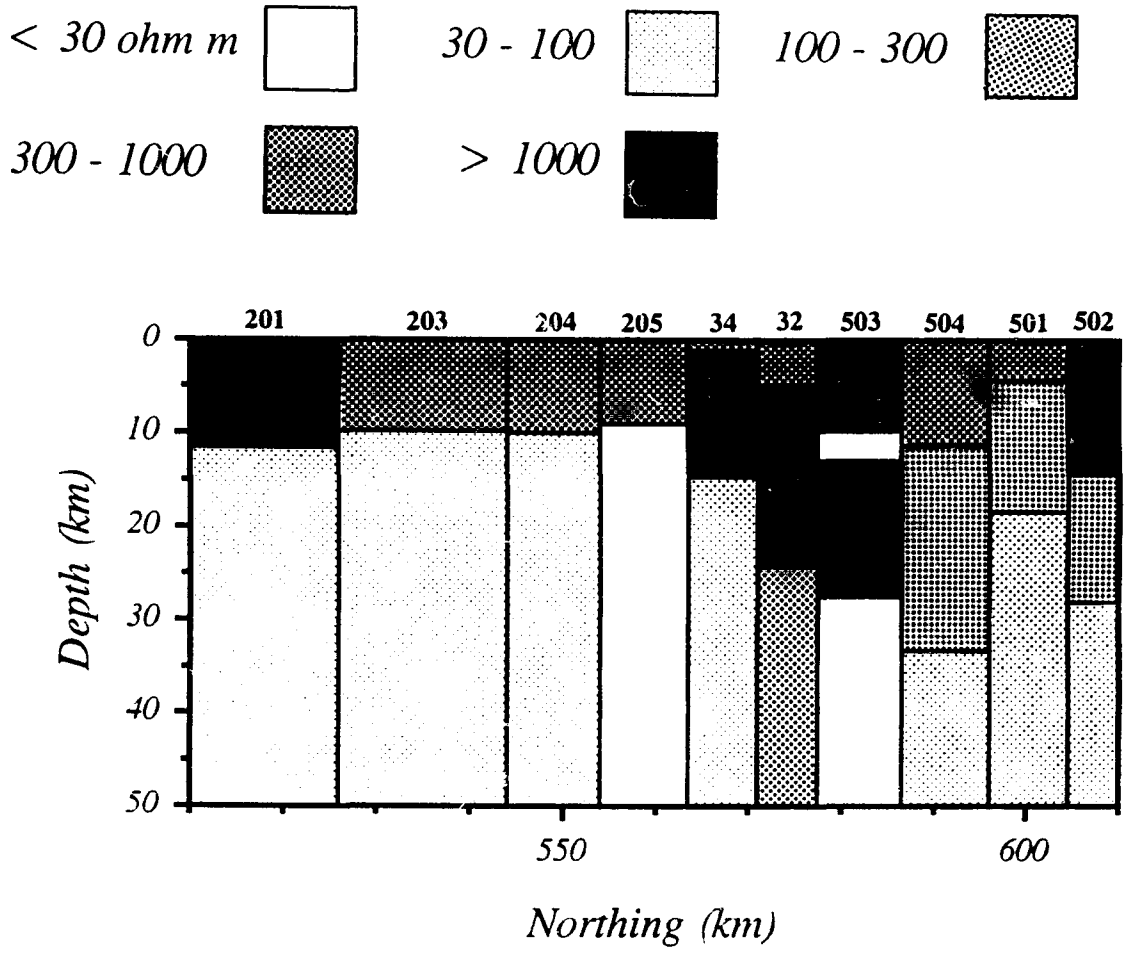

Figure 32 One-dimensional inversion of E-polarization data, North-South profile. Data have been corrected for static shift. Note the general decrease in resistivity below 10 to 15 km depths.

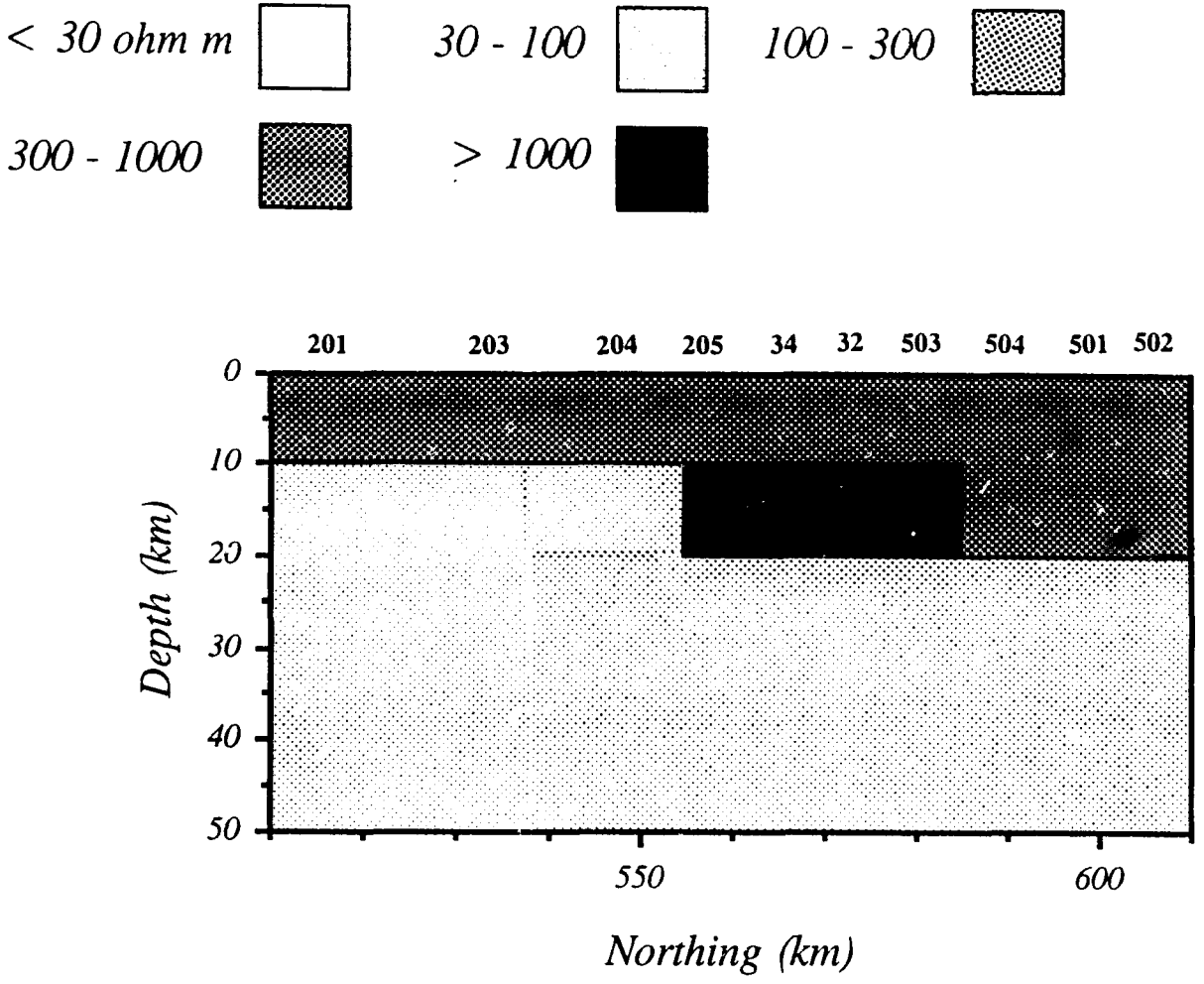

Figure 33 Preferred model, North-South profile.

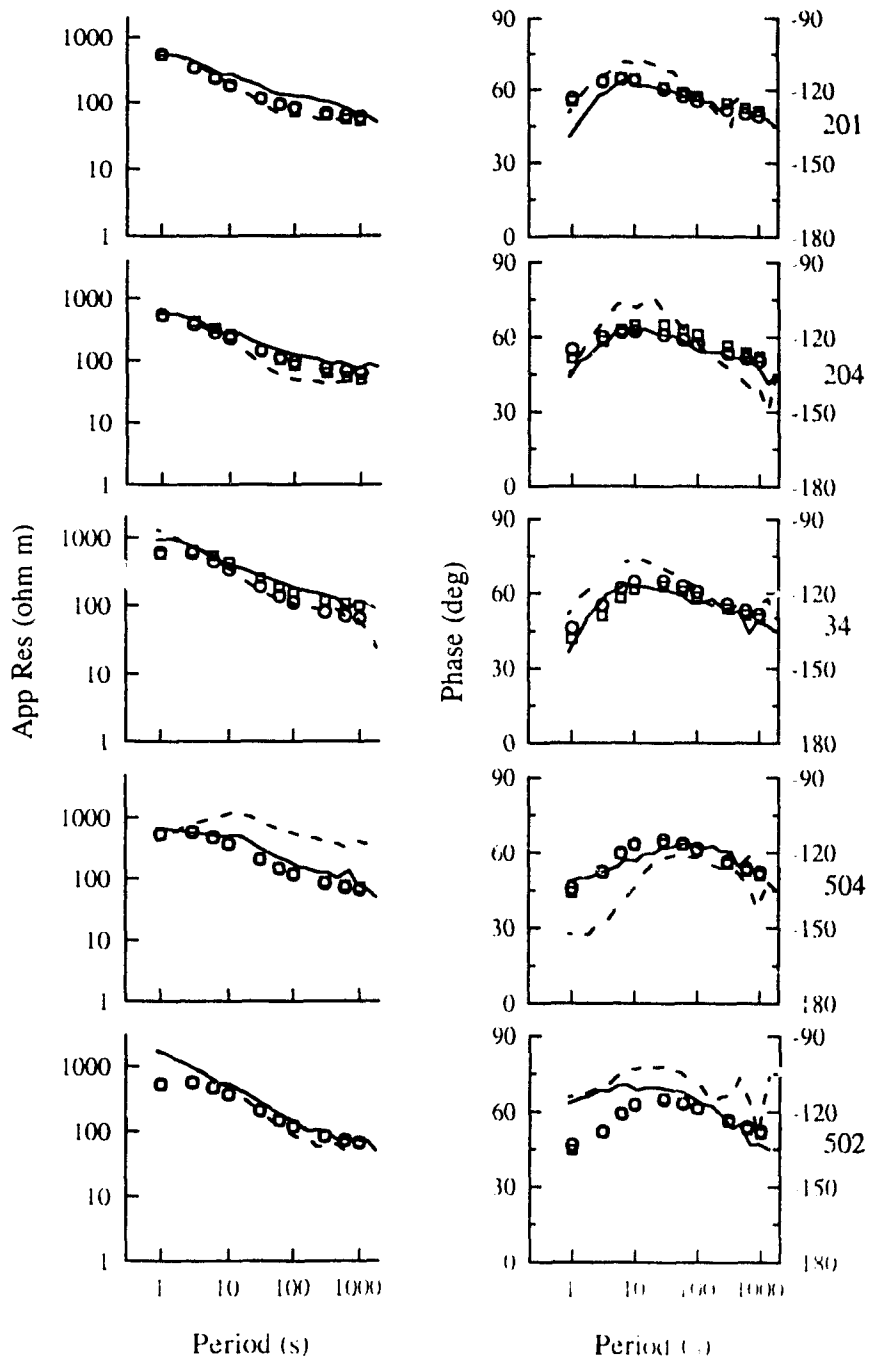

Figure 34 Comparison between modelled apparent resistivity and phase (circles E-pol, squares B-Pol) with observed data (solid lines E-pol, dashed B-Pol).

coherency techniques (Cook et al. 1991). The sections do not provide much information on the true reflectivity amplitudes. AGC will enhance small reflectors that would otherwise be missed, but it obliterates any information on the relative strengths of reflectors or reflection bands from different AGC windows. In order to study the true-amplitude characteristics of the reflectors, original data from Line 88-10 have been re-processed at the LITHOPROBE Seismic Facility in Calgary, using the CYBER/DISCO system for pre-stack processing, and the ITA/INSIGHT system for post-stack processing.

The original data for the new analysis consisted of true-amplitude common-depth point (CDP) gathers of 18 seconds length. The so-called "true-amplitudes" have been corrected for geometric spreading by a factor of $tV^2_{rms}(t)$, where t is the traveltime and $V_{rms}(t)$ is the root-mean-square velocity to traveltime t. These velocities were determined by Western Geophysical. After normal moveout corrections using the RMS velocity values, each CDP gather was stacked into one trace. No pre stack mute corrections have been applied here because far-offset large-amplitude shear-wave arrivals have no effect on the deep-crustal reflectivity, and there are no major sources of multiples since near-offset first arrivals are weak. The traces were then truncated to 12.5 seconds, about one second below the Moho.

Throughout the new processing sequence (bold type in Table 5), the data were kept as close as possible to true amplitude: trace balancing was necessary because of the large discrepancies in amplitude between traces associated with vibrator and geophone ground coupling. After stack, all traces have been energy-balanced over the whole 12.5 second range. This ensures that all traces have equal weight before further processing. To reduce the effect of incoherent noise, a coherency/semblance filter (Milkereit and Spencer, 1989) has been applied to the whole section: coherency is calculated for many slowness, or dip, values (31 here) in a trace window (21 traces here), and the maximum coherency value is kept. Incoherent noise is greatly reduced. The number of dips used is quite small because the main focus is to emphasize flat-lying reflectors: there is thus a potential for the removal of coherent dipping events. However, comparison with sections processed for structural interpretation using a larger range of dips (see Cook et al., 1991) indicates that the main west-dipping events in the east of the section have

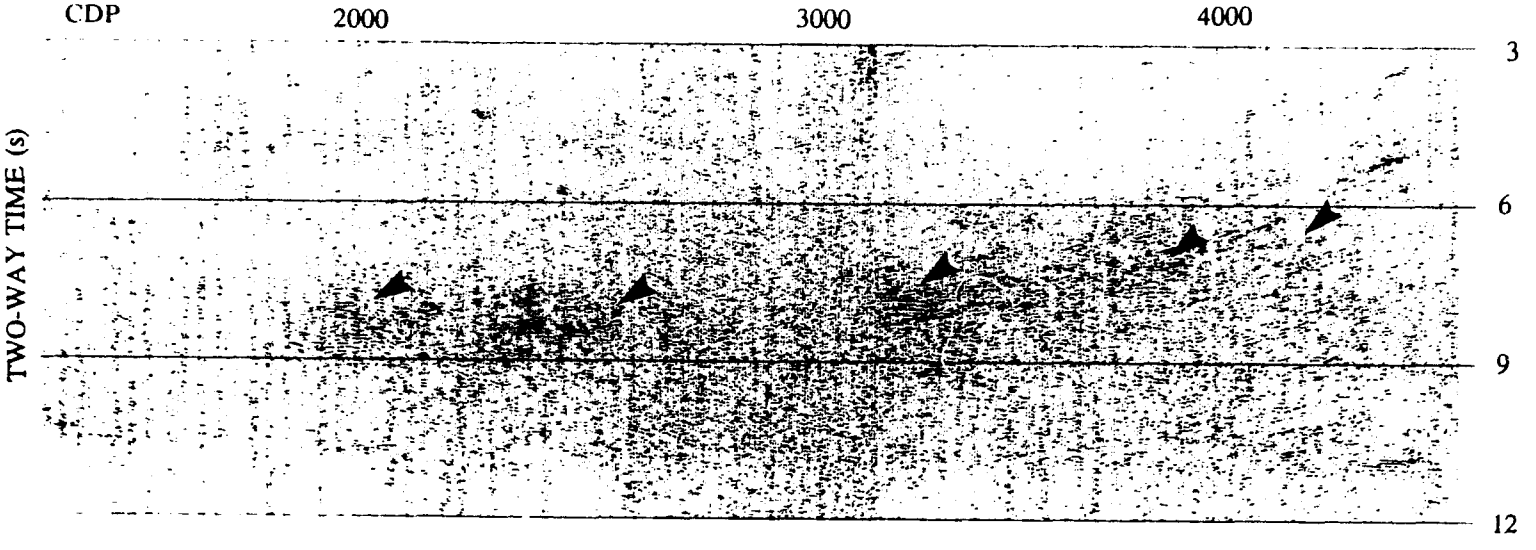

Figure 35 Stack section of LITHOPROBE Line 88-10. Only data from 3.0 to 12.0 two-way time are displayed. Processing steps are described in text. Arrows refer to tops of reflecting bands.

survived the process. The number of traces used here requires coherency over distances of at least 400 m. The resulting section is shown in Figure 35.

Table 5 Seismic acquisition and processing parameters

Recording	
Source	4 Vibroseis Units 20 000 kg each
Source Interval	100 m
Receiver Group Interval	50 m
Geophone Array	12 geophones (10 Hz) over 50 m 240 Channels 8300 m Maximum Spread
Sweeps per location	8 sweeps, 14 s length
Sweep Frequency Range	10 - 56 Hz
CDP Coverage	60-fold
Correlated Record Length	18.0 s
Sample Rate	4 ms
Processing	
Demultiplex	
Crooked Line Geometry Corrections	
Amplitude Recovery	
CDP Gather	60-fold usually
Deconvolution	Spiking
Trace Edits	
Elevation Statics	Datum Plane 1000 m Replacement Velocity 5000 m/s
Automatic Gain Control	1.0 s window
Velocities Picked by Western Geophysical	
Normal Moveout Corrections	
Automatic Gain Control	1.0 s window

Energy Balancing	12.5 s window over the whole section
Coherency (Semblance) Filter	Milkereit and Spencer (1989) method 31 equally-spaced dips (slownesses) 21-trace window maximum slowness 0.5 ms/m or about 56° dip
Migration	

Regular type, done by Sonix or Western Geophysical; Bold type, done by the author; Underlined, as presented in Cook et al. (1991, 1992). The coherency filter method and the parameters used here are different from those reported in Cook et al. (1991, 1992).

The final step was to determine the reflectivity characteristics of the crust underneath Line 88-10. The method used is the energy histogram technique of Bittner and Wever (1991): it consists of summing the squares of the individual trace values for a range of traces and a time window (superstack). There are many advantages in using this technique: first, it provides a quick, objective evaluation of the reflectivity, compared to other methods such as line-drawing, which is rather time-consuming and very subjective, second it reduces the effects of small-scale diffractors and other geological noise, since they can be made only a small part of each time-trace window. Windows of 500 traces by 0.5 second have been used, since we are only interested in the gross reflectivity features of the crust.

The results of this energy histogram technique applied to LITHOPROBE Line 88-10 are shown in Figure 36. Each histogram represents the energy distribution of reflectivity with two-way time for a group of 500 CDPs. For display, each histogram has been normalised to its highest value. The overall reflectivity is strongly enhanced from 8.0 s twt to 10.0 s twt in the west (~25 to 32 km depth), and from 7.0 to 11.0 s (~22 to 35 km) at the eastmost part of the line. This is as expected if the depth to the top of the reflective layer follows the general pattern of heat flow increase to the east in this area.

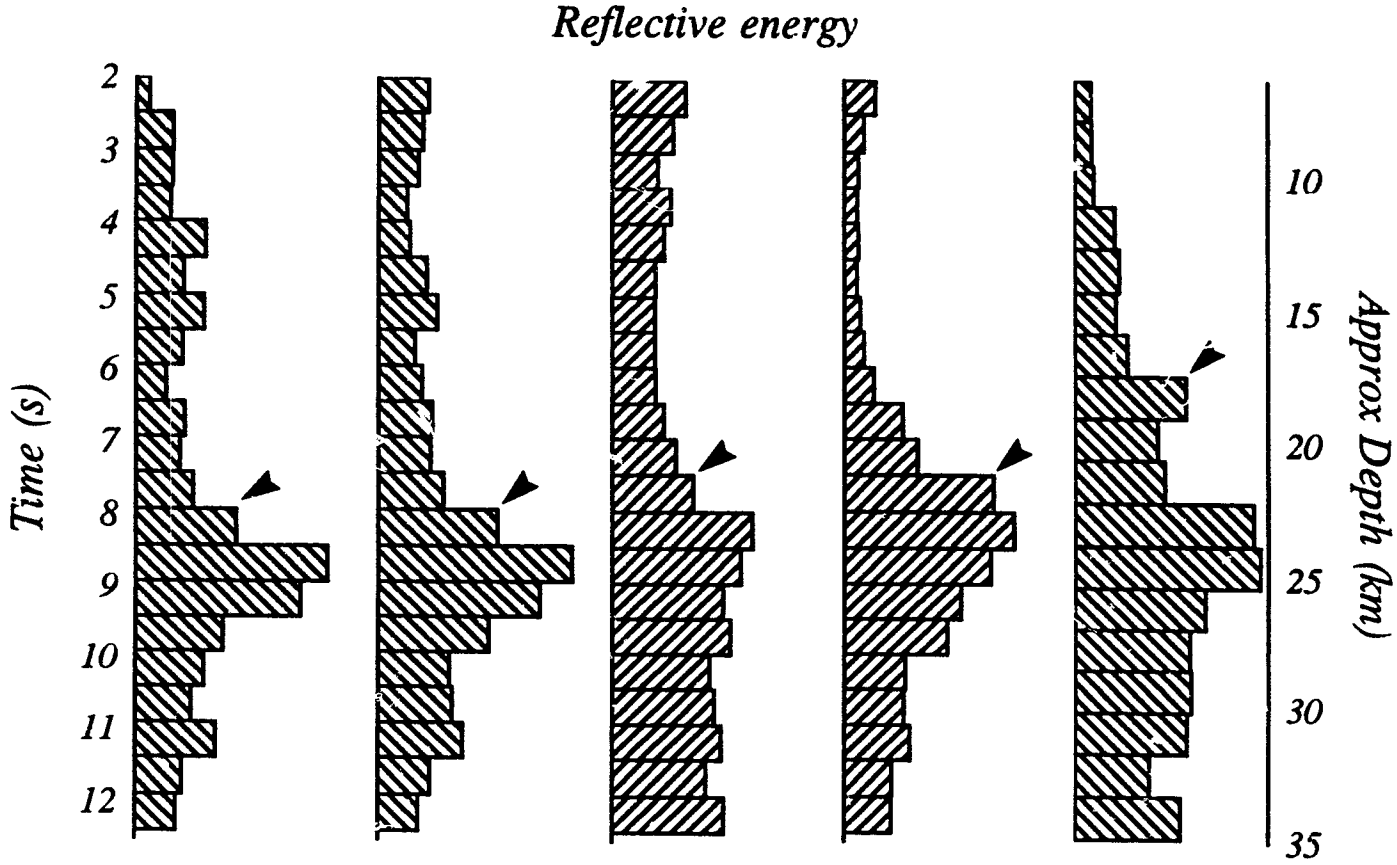

Figure 36 Reflectivity energy histograms for Line 88-10. Arrows refer to the same bands as in Figure 34.

Cook et al. (1991, 1992) have presented structural interpretations of the reflection data from the Lithoprobe South Cordillera transect. They interpret the west-dipping events in the east of line 88-10 as being the Okanagan Valley Fault that listrically merges into the lower crustal reflecting bands at about 7.0s (~CDP 3600). The small east-dipping events at the west end of line 88-10 are interpreted as the Quilchena Creek Fault that bounds the east side of the Nicola Horst (Cook et al., 1992). The lower crustal reflectors have been presented as not horizontal but rather gently dipping to the west, and have been interpreted as continuations of the Foreland-Omineca Belts for the upper part ($7 < t < 9$s), and underlying autochthonous North America for the lower part ($9 < t < 11$s).

Small-scale analysis of the true-amplitude section (Figure 35) shows that while some of the lower crustal reflectors appear to dip gently, the dips are not systematic, some being to the east, some to the west. However a great majority of these reflectors are flat over the distances resolved by the semblance filter. Therefore, it is argued here that the presence of lower crustal reflectors is not caused by structural changes, although reflector details may be affected by structure. The major division within the lower crustal reflecting band of Cook et al (1991) is certainly not obvious in Figure 35.

v. Deep crustal temperatures

The heat flow data used for this analysis have been taken from the compilation of Lewis et al. (1992). Geothermal measurements have usually been made in boreholes drilled for mining exploration purposes. Samples of near-surface rocks have been collected at most sites, and heat production has been determined using gamma-ray spectrometry (Lewis et al., 1992). Lewis (1991) obtained a linear heat flow-heat production relationship, and concluded that the Canadian Cordillera, excluding the Insular and Coast Belts, is a single heat flow province, i.e. the heat flow at depth is the same across it: variations in surface heat flow are caused primarily by local changes in upper crustal heat production.

There is very little thermal data available immediately around line 88-10. Lewis (1991) reports an average heat flow of 72.6 mW/m^2 (standard deviation 6.0) for 17 measurements in the Intermontane Belt. The relatively small scatter suggests that there

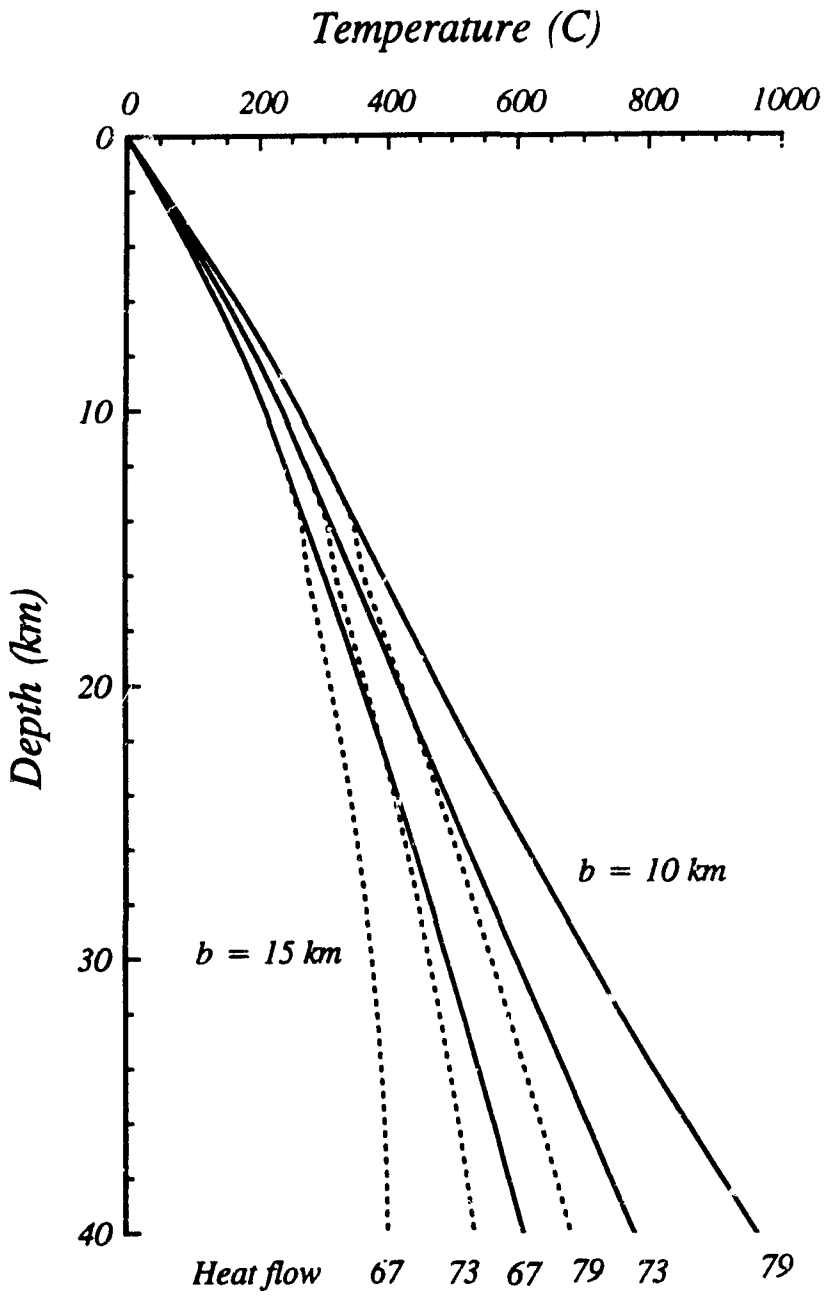

Figure 37 Temperature profile from one-dimensional inversion of heat flow data. Solid curves are for a 10-km thick heat producing layer, dashed curves for a 15 km-thick layer.

is little horizontal variation in heat flow or heat production. Temperature distributions with depth have been calculated using the mean +/- standard deviation as bounds. I also used different values of thickness for the heat producing layer. Other parameters as well as the temperatures profiles are shown in Figure 37. A few combinations of reasonable heat production and thickness of heat producing layers are displayed. The heat production may increase at depths of a few km in the Intermontane Belt, since there are some high heat-producing Eocene plutonic rocks (e.g. Coryell), just to the east in the Omineca Belt that might be covered by their equivalent volcanics in the Intermontane (e.g. Marron). There is a possibility therefore that the heat-producing layer is unusually thick close to the Intermontane-Omineca boundary. A thicker heat-producing layer causes the geotherms to be shifted towards greater depths, but might represent a more geologically realistic picture of the temperatures in the Intermontane Belt.

vi. Refraction velocity data

Also as part of the Lithoprobe South Cordillera transect, seismic refraction lines with close station spacing (SCoRe) were shot in 1989 and 1990. Line 1 in the Intermontane Belt (Zelt et al., 1992) is of relevance to this thesis. Since it does not coincide with reflection line 88-10 and is in fact perpendicular to it, caution must be exerted in correlating these two types of data.

SCoRE line 1 is shot along strike in the Intermontane Belt, and a comprehensive interpretation is presented in Zelt et al. (1992). The most important features relevant to this thesis are the three distinct velocity layers from the middle crust to the Moho: a 6.2 km/s layer in the middle crust down to 22 km depth, a 6.5-6.8 km/s layer from 22 to 30 km depths, and a 2 km thick high-velocity (7.5 km/s) transition zone in the lowermost crust. These layers are very well constrained by strong intracrustal reflectors, indicating important variations in elastic properties between the layers. The top of the intermediate layer corresponds very well to the top of the enhanced reflectivity and of the low-resistivity layer found for line 88-10. The velocity is also lower than expected, if the rocks there are mafic and if they are similar in composition to those in the high-velocity layer at the bottom of the crust. It is worth noting that the refraction analysis of Zelt et

al. (1992) does not separate the lower crust into the same two layers as Cook et al. (1992).

Zelt et al. (1992) suggest fluids as a possible explanation for the strong reflectors at the base of the mid-crustal layer. However this layer does not correspond to the zone of low-resistivity, which is deeper. It is still possible that fluids are present, but the degree of interconnection would have to be very low. From the thermal data the mid-crustal layer is above the brittle-ductile transition temperature (see Chapter V). As stated above, there is considerable uncertainty when inverting heat flow data, so it is possible that this mid-crustal layer corresponds to a ductile régime. It is argued here that because of the agreement between reflectivity, conductivity and velocity, the temperature profile presented earlier is more representative, since it shows the layer of inferred porosity below the brittle-ductile transition, but there is no support for this argument from the heat flow data per se.

vii. Joint interpretation of geophysical data

A composite section of reflectivity, temperatures, resistivity and velocity for Lithoprobe Line 88-10 is shown in Figure 38. The boundaries of interest for this study are the 450°C isotherm, the approximate depth of the brittle-ductile transition, and the 750°C isotherm, where granulite facies conditions are reached (see Marquis & Hyndman, 1992). There is a very good agreement among the reflective, conductive and lower velocity layers with their tops at 450°. A lower bound for the conducting layer cannot be obtained because of the limitations of the inversion of MT data.

Such closeness between the reflectivity and low-resistivity layers, as well as their near coincidence with critical geotherms argue in favour of having a same origin. It is argued here that lower crustal fluids can explain both the higher reflectivity and the low resistivity.

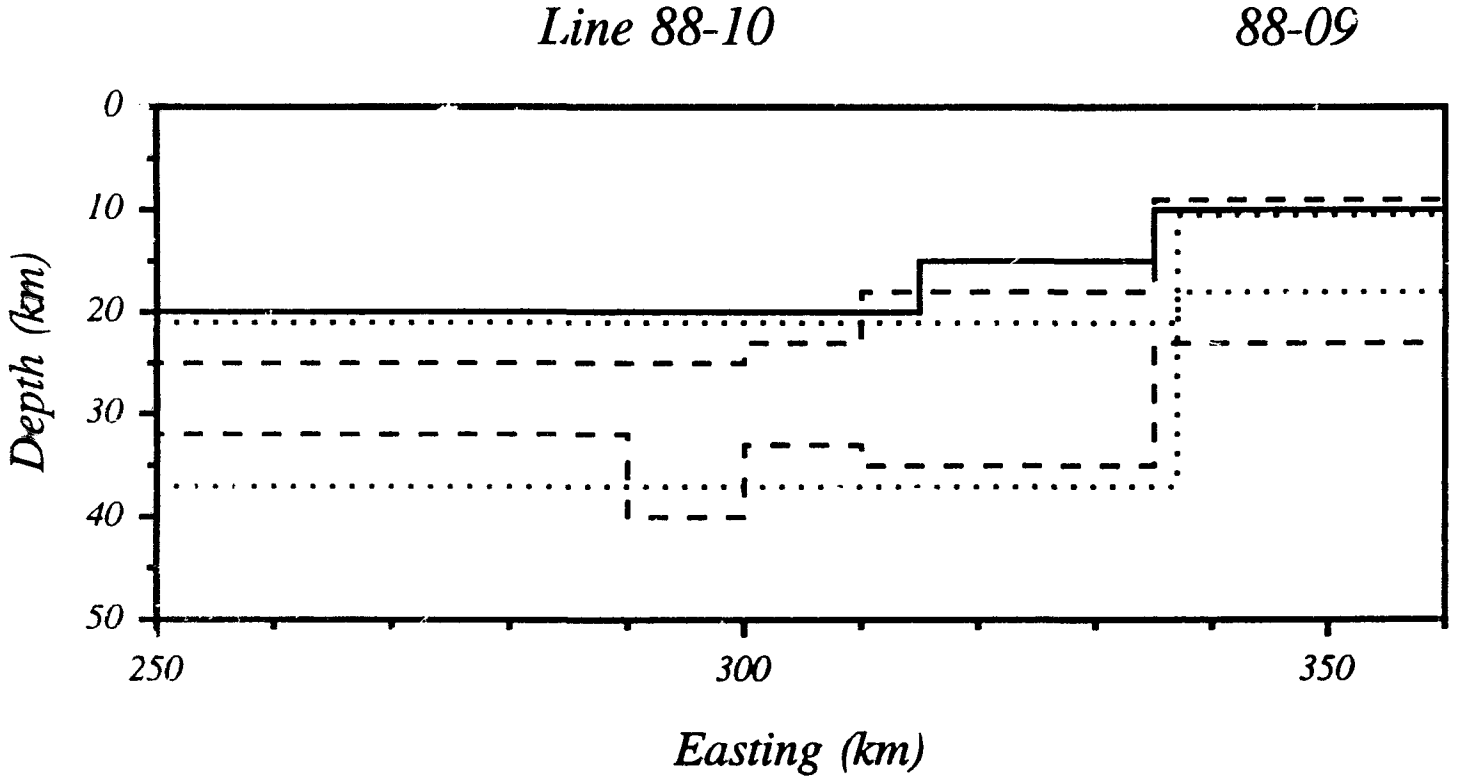

Figure 38 Enhanced reflectivity (dashed lines) and low-resistivity (solid lines) bands for LITHOPROBE Line 88-10 and the western section of Line 88-09. Dotted lines correspond to the 450° and 750°C isotherms.

CHAPTER V. CONDITIONS FOR TRAPPING FLUIDS AT DEPTH

The conclusions of the previous two chapters support the presence of fluids in the deepest crust. However, the question of how substantial amounts of fluids can be trapped at depth for geologically significant periods of time has not been addressed. One important constraint on possible trapping mechanisms may be provided by the thermal conditions at which the interconnected porosity is inferred to be present (e.g., Hyndman and Shearer, 1989). For example, the required horizontally interconnected porosity may be associated with temperatures high enough for equilibrium minimum energy pore geometries (e.g., von Bargen and Waff, 1986; see section ii), for the rheology allowing regional horizontal shearing that aligns pores horizontally, or for a particular range of metamorphic conditions.

i. Temperatures at the top of the conductive and reflective layers

To investigate this question further, histograms of the temperatures of the tops of the lower crustal conductive and reflective layers from the compilation (Table 3) have been plotted (Figure 39). As stated previously, the refraction velocity data are not included since effects on velocity associated with porosity variations are superimposed on a general increase in velocity with depth associated with an inferred change from mostly intermediate to mostly mafic compositions. A clear pattern is observed for the low-resistivity layers: their tops are mostly at temperatures in the interval 350-450°C (Figure 39 a). This temperature limit has been previously observed by Ádám (1987) in a more general compilation of resistivity data.

For comparison with the resistivity data, temperature conditions of the reflecting bands at the sites of the compilation (Figure 39 b) have also been estimated. The average temperature to the top is about 400°C, similar to that found by Klemperer (1987). This temperature limit correspondence provides support for the hypothesis that the observed reflectivity and low resistivity might have a common cause, perhaps associated with crustal rheology or with the metamorphic conditions.

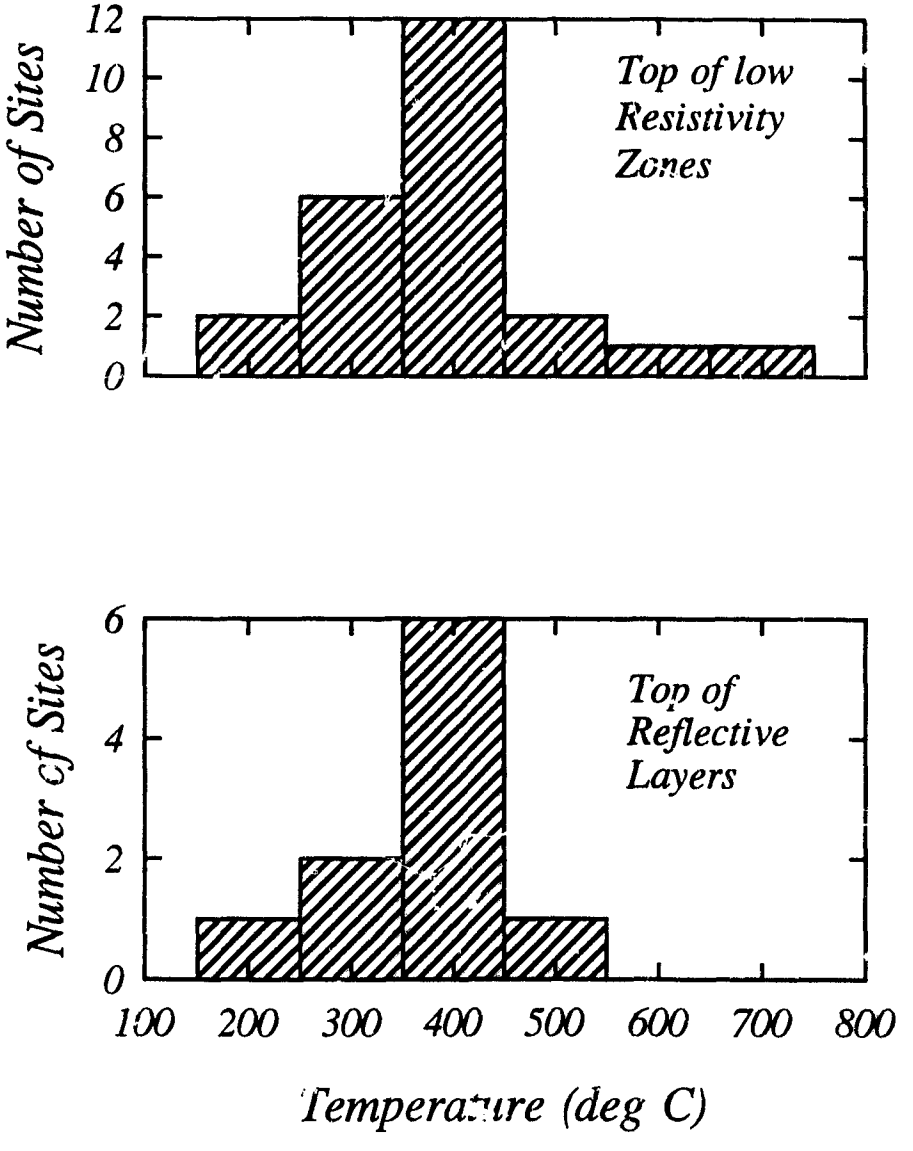

Figure 39 Histogram of temperatures of conductive and reflective zones, from compilation in Table 3.

ii. Pressure conditions and physical properties in the ductile crust

A fundamental concept that may often be incorrectly applied is the effective pressure at depth and its effect on the physical properties of rocks. It has usually been assumed that the high-confining pressure (i.e. hydrostatic pore pressure) measurements of physical properties (for velocity, see Christensen, 1979, 1982) are directly applicable to the lower crust. This assumption however may not be valid when the lower crust is ductile.

In the upper brittle crust where the pores are interconnected to the surface, the effective pressure is approximately the difference between lithostatic (column of rock) and hydrostatic (column of water) pressure (Figure 40a). The porosity, particularly that in thinner cracks, is progressively closed by the increase in effective pressure with depth, and both velocity and electrical resistivity increase. A general velocity-effective pressure curve for a mafic rock in which the pore pressure is maintained at a low value is shown in Figure 40b. The velocity increases rapidly at first, as very thin pores that contribute the most in reducing velocity are closed (arrows under the curve). The resistivity-effective pressure relation is qualitatively similar.

Deeper than the brittle-ductile transition at approximately 400-450°C, the very weak matrix grains can no longer support a differential pressure for geologically long times and hence the pore pressure must approach lithostatic. The effective pressure then decreases to near zero (see Figure 40a). The grain boundary configuration should relax and particularly the thinner pores may remain open resulting in a low velocity and low resistivity. The actual pore configuration may then be controlled by the equilibrium minimum energy configuration. In laboratory samples, some of the thin cracks that are closed with increasing effective pressure were generated when the rocks were exhumed at the surface or by the sample collection process. However, much of the porosity should be original such that low effective pressure laboratory velocities (corrected to in situ temperatures) may best correspond to those in the lower crust, where the effective

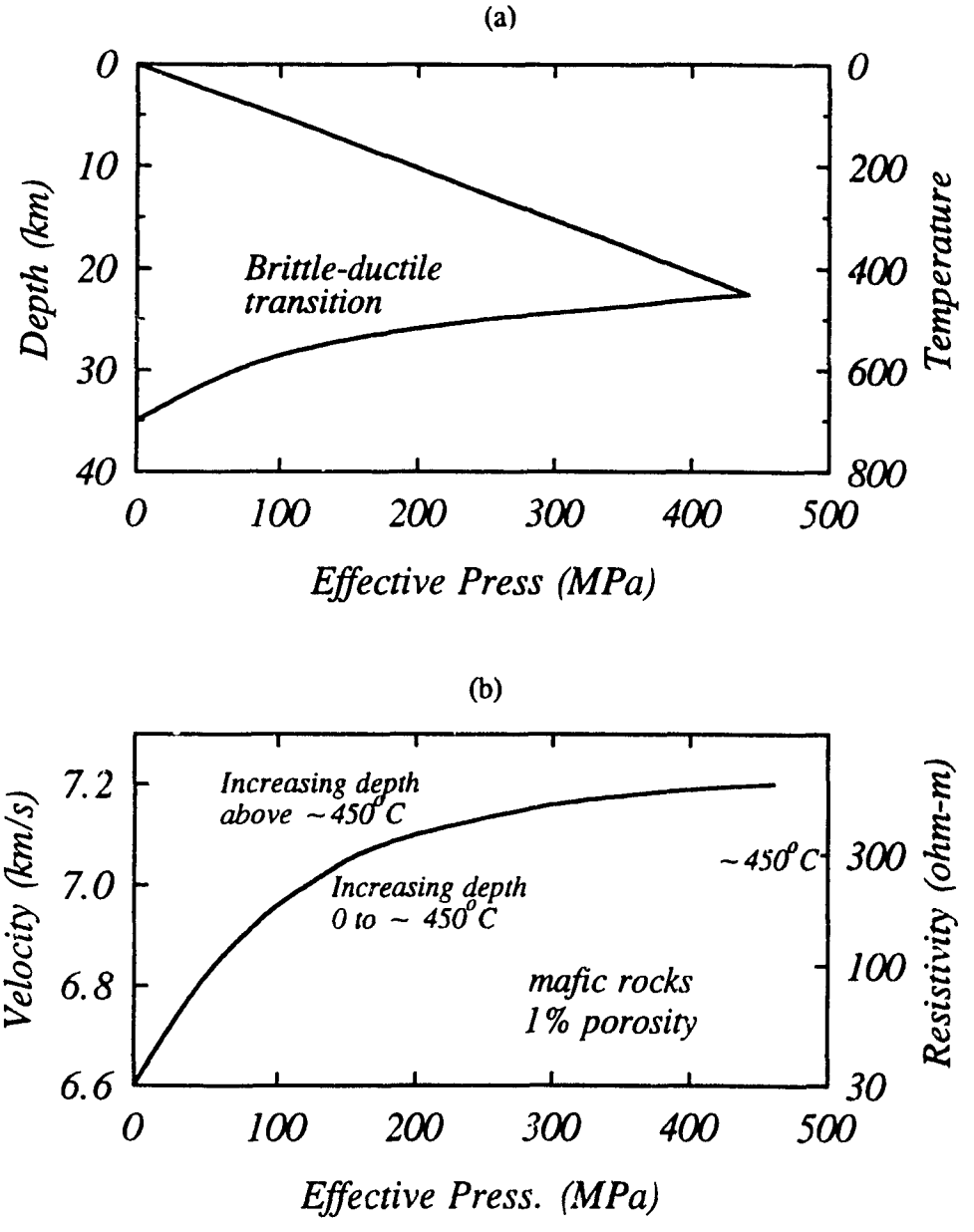

Figure 40 Effective pressure-depth profile and its effect on physical properties. A 20° C/km temperature gradient is assumed. Detailed explanations in text.

pressure is also low.

Even if temperatures around 450°C seem the most favourable environment for porous layers in the deep crust, the compilation in Table 3 shows that there are also some low-resistivity layers in the lower crust at lower estimated temperatures, mostly in Precambrian areas (e.g. Kapuskasing, Maréschal et al., 1989); these might be caused by a solid conduction mechanism, such as interconnected graphite (see Chapter VII). It is noted that these colder low-resistivity layers do not generally coincide with low velocities or with strong reflecting bands; they also usually have velocities of 7.0 km/s or higher, and hence, if this model is correct, should have little or no porosity.

Temperature may also limit the base of the low-resistivity (i.e. porous) layers. At temperatures above about 700-750°C present granulite metamorphic facies conditions are reached. At such high temperatures, CO_2 is the dominant fluid phase as indicated by fluid inclusions and inferred from chemical equilibria with granulite mineralogy (Newton, 1989). CO_2 has no significant effect on the electrical resistivity (see Chapter VII). Granulites probably have no free water and are resistive (e.g. Wannamaker, 1986), thus free aqueous fluids may be restricted to above this depth. The ~700-750°C isotherm may provide a lower boundary to the low-resistivity porous layers.

iii. Equilibrium pore geometries

As stated above, at high temperatures, a porous system will tend to textural equilibrium pore geometries (von Bargen and Waff, 1986). These geometries are controlled mostly by the relative surface tensions between the matrix and the pore fluid at grain boundaries. The grains will deform to the minimum energy configuration. The mineral grains will also tend to dissolve in the fluid where the surface energy is high and to exsolve where it is low. The important parameter is the dihedral, or wetting, angle, defined by

$$\theta = 2 \cos^{-1} (\gamma_{ss}/2\gamma_{sl})$$

where γ_{ss} is the solid-solid interfacial tension and γ_{sl} is the solid-fluid surface tension.

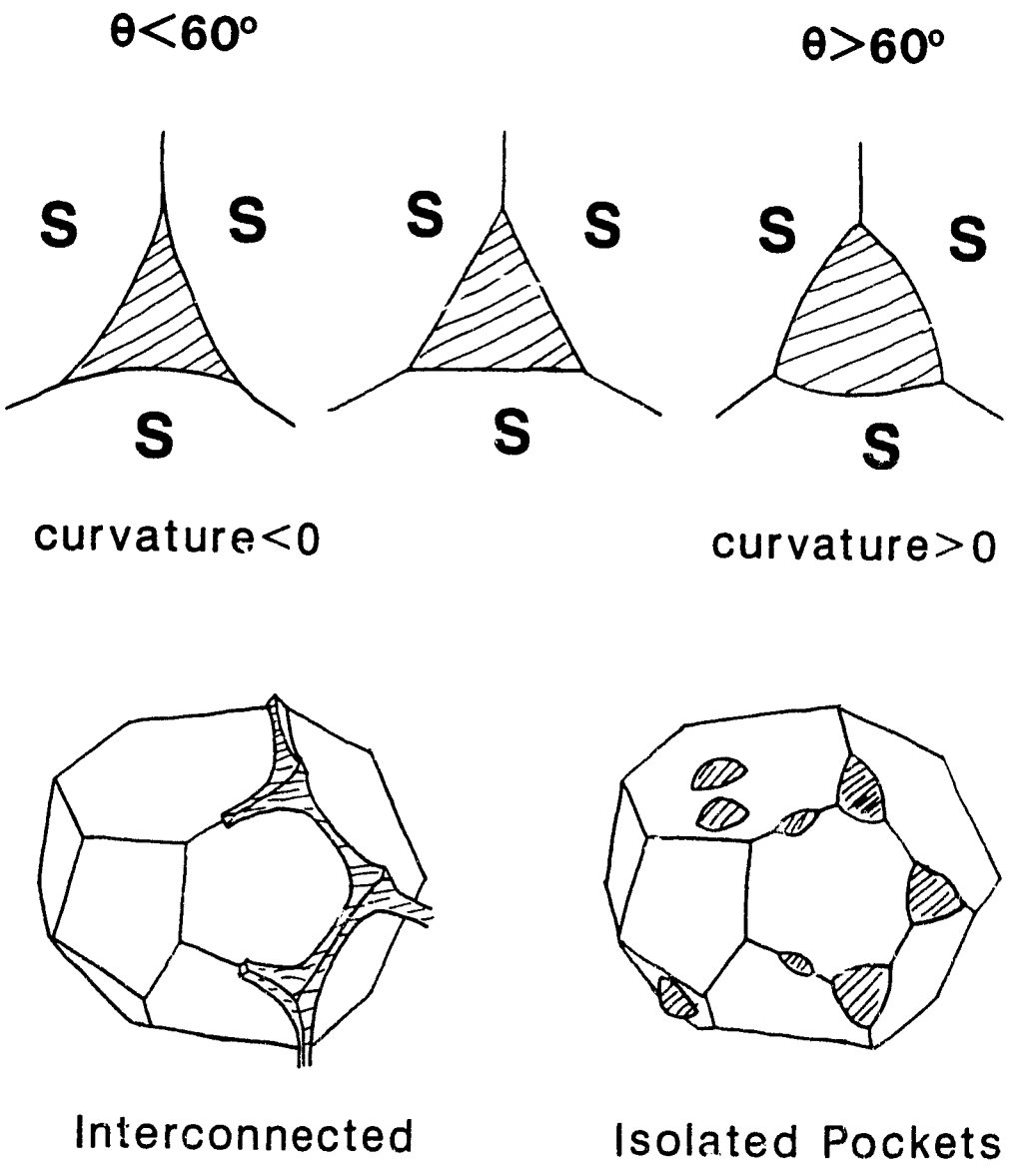

Figure 41 Equilibrium pore geometries, from von Bargen and Waff (1986). The important parameters are the dihedral angle and the sign of the curvature, indicating whether the fluid phase is interconnected

This angle and the porosity will determine whether or not the pore fluid is interconnected. Figure 41 shows the fluid-matrix configuration for a 1% porosity and two ranges of dihedral angle. If $\theta > 60°$ (the pinch-off angle for that value of porosity; von Bargen and Waff, 1986), the fluid will be gathered in pockets at grain corners, the mean curvature of the solid-fluid interface is positive, and the fluid is not interconnected. This implies that for such a configuration, the electrical resistivity will remain high. If $\theta < 60°$, the fluid forms pockets at grain corners joined by grain-boundary channels. This ensures interconnection and a substantial reduction in electrical resistivity.

There are very few measurements of dihedral angle for crystalline rocks. Theoretically the value of γ_{ss} should be in the same order of magnitude for most types of silicate rock, but γ_{si} is expected to vary with fluid composition, especially if liquid-gas mixtures are involved. There are three major published works on experimental measurements of the dihedral angle for several water-CO_2-NaCl systems: Watson and Brennan (1987) have measured dihedral angles for systems at P = 1 GPa (10 kb) and T = 950°-1150°C. They have found that the median dihedral angle values for pure water and a variety of rock types are about 60°, and that this angle increases up to 90° with increasing CO_2 concentration for several rock types. They have also found that adding substantial solutes decreases the angle to 40° for a quartz matrix, but this only had little effect for an olivine matrix. Despite the very high temperatures at which the experiment was performed, the authors claim their results are valid at any temperature higher than the brittle-ductile temperature.

Lee et al. (1991) have measured dihedral angles for water-CO_2-solute systems in Arkansas Novaculite at 200 MPa, 600°C, closer to actual conditions in the mid- to deep crust. They have found that pure water, pure CO_2 and a water-CO_2 fluid form isolated pockets at grain corners (median $\theta > 60°$). In all cases, the addition of either NaCl, $MgCl_2$, KCl, or $CaCl_2$ reduces θ to median values less than 60°, all the way down to 33° for a high concentration of NaCl, therefore ensuring fluid interconnection when solutes are present.

Laporte and Watson (1991) have studied quartz-water-CO_2-NaCl systems at pressures up to 1 GPa, and temperatures between 600 and 850°C. Only at extremely

high pressures (P ~ 1 GPa) can H_2O-rich, saline fluids form an interconnected network of grain boundary channels. All the other combinations gave median values of θ above 60°.

In summary:

(a) low salinity fluids may be partly isolated and partly interconnected (since some angles are larger than 60°, others are smaller), but most probably isolated at low porosity values. Pure CO_2 forms isolated pockets.

(b) High-CO_2 fluids most likely form isolated pockets at grain corners; therefore any subsequent graphite produced by the reduction of CO_2 should also be isolated. This will be discussed in more detail in Chapter VII.

(c) High salinity solutions are probably generally interconnected even at very low porosities, therefore significantly reducing the electrical resistivity.

However, if the pores are isotropic, such pore interconnection should also result in high permeability, and the fluid should migrate upwards rapidly. Reconciliation of high horizontal pore interconnection required for the low resistivity and the low vertical interconnection required to keep the fluids in the lower crust is discussed in section v.

iv. Retention of pore fluids at lower crustal depths

The retention of pore fluid in the lower crust for geologically long periods of time while maintaining sufficient pore interconnection for low electrical resistivity is an important difficulty to be resolved in the model (see Hyndman and Shearer, 1989; Warner, 1990 for opposite views on this problem). If porosity is substantial, so is the permeability (commonly proportional to the third power of the porosity; Blake-Cozeny-Karmann equation from Dullien, 1979). The fluids should therefore migrate up to the surface in relatively short times. To illustrate this point, let us look at the situation for a column of rock with a homogeneous, isotropic 1% porosity. The characteristic emptying time is defined by McKenzie (1984) as $\tau = \delta/W$, where δ is the compaction length and W the fluid migration velocity. These can in turn be obtained by

$$\delta = (K \nu / \mu)^{1/2}$$

$$W = K (1-\phi) \Delta\rho \, g / \mu$$

where K is the permeability ($\phi^3/10^9$), ϕ is the porosity, ν and μ are the matrix and fluid viscosities respectively, $\Delta\rho$ is the density difference between the fluid and the matrix, and g is the acceleration due to gravity. Using

$\phi = 0.01$ gives $K = 10^{-15}$ m^2

$\nu = 10^{18}$ Pa s and $\mu = 10^{-4}$ Pa s give $\delta = 3162$ m

$\Delta\rho = 2000$ kg/m^3 and $g = 9.8$ m/s^2 give $W = 2\ 10^{-7}$ m/s

$\tau = W/\delta = 1.6\ 10^{10}$ s

therefore $\tau \sim 500$ years. Hence the porosity at depth will be reduced by a factor of 1/e in about 500 years, a very short time indeed geologically speaking.

A variety of models have been proposed to keep substantial porosity at depths for long periods of time. Gavrilenko and Gueguen (1989, 1992) assume that the porosity is made of rough cracks with spherical asperities, the size of which is controlled by pressure solution. The resulting permeability then depends both on the crack closure rate (asperities growing larger will eventually close the cracks) and on the fracture density variation with depth. This fracture density decreases with time up to the point where the percolation threshold is reached, preventing any more fluid flow and producing a low-permeability zone in the middle to deep crust under which fluids can be trapped. However if fluids keep on being produced, for example by deep dehydration reactions, overpressures and hydrofracturing should eventually occur, releasing the trapped fluids (McKenzie, 1984).

Merzer and Klemperer (1992) have tried to get around this requirement of having fluids interconnected over a large scale by studying the electrical behaviour of isolated horizontally elongated groups of conducting lamellae within a highly resistive matrix. They have found that if the lamellae group separation is small, the effective resistivity of such a system is comparable to the ones commonly observed in magnetotelluric surveys. Their model requires a difference in lithology between the matrix of the porous lamellae and the rest of the crust, in order for the porosity to remain within the lamellae. The lamellae could correspond to those that produce the enhanced lower crustal reflectivity.

As pointed out earlier, two important associations with temperature are the

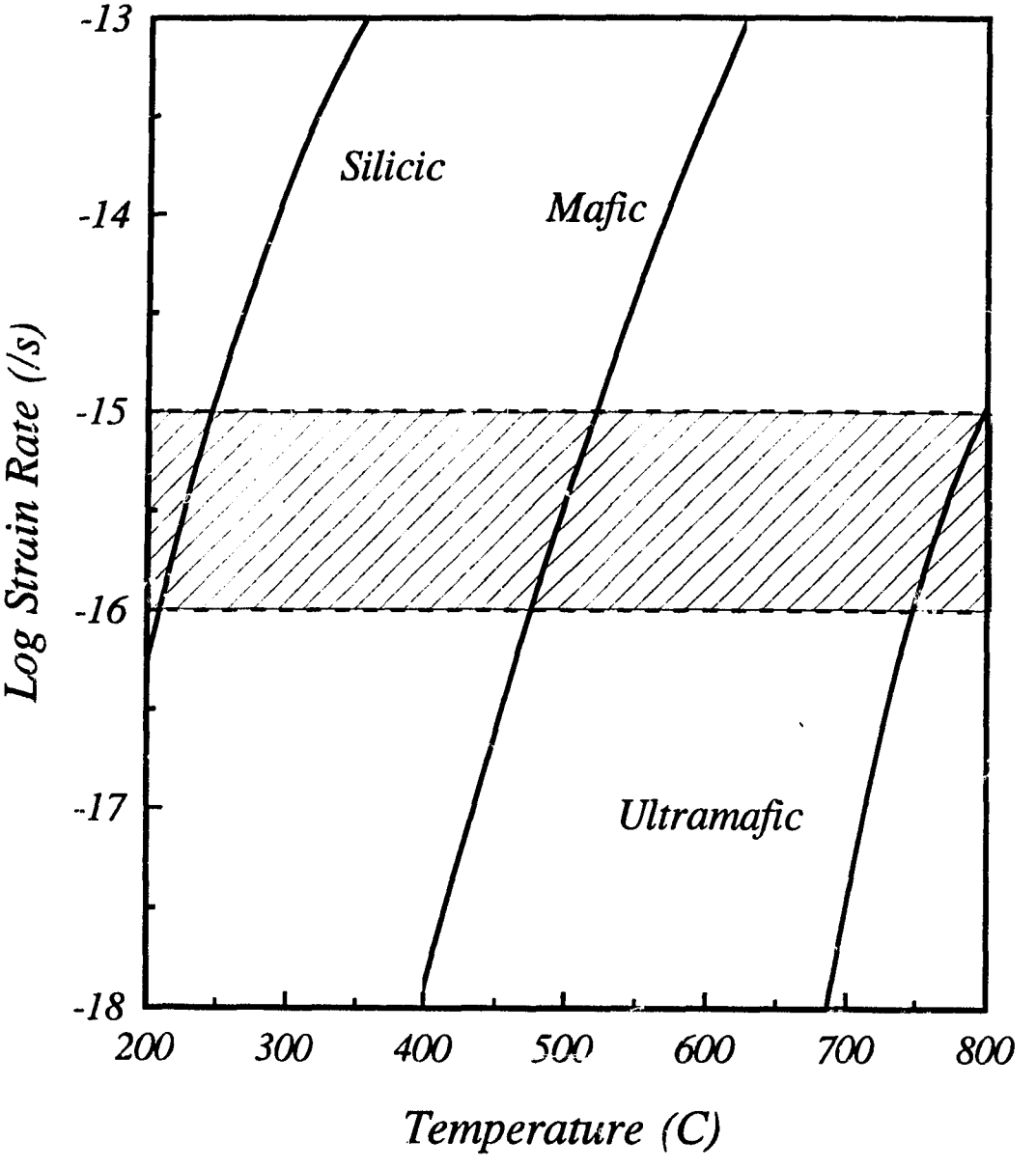

Figure 42 Strain-Kate temperature relations. The box represents realistic geological strain rates (from Kusznir and Park, 1986).

rheology of the crust at depth and metamorphic processes. An important result presented above is the large number of lower crustal low-resistivity and reflective layers that have their top near the 400-450°C isotherm, just below the brittle-ductile transition for most mafic rocks, although this also depends on the strain rate (e.g. Kusznir and Park, 1986; Figure 42) and on porosity. This change in the rheological regime of the crust might be a factor in producing impermeable layers.

The brittle-ductile transition is a fundamental phenomenon in geodynamics: it controls most tectonic processes and limits earthquakes. The transition is gradual rather than sharp (e.g. Ranalli, 1987). Nikolaevsky (1985) discusses the rheological layering within the earth's crust: the upper crust is a zone of brittle deformation with decreasing strength as depth (i.e. temperature) increases (up to ~300°C); the middle crust is a zone of "stick-slip" deformation, i.e. a mix of solid friction and intact rupture, with the former overtaking the latter with increasing temperature up to ~450°C, and acts as a transition zone; the lower crust is a zone of cataclastic flow.

Nikolaevsky (1985) correlates these three zones with fault geometry: faults are vertical near the surface and are increasingly inclined with depth, becoming horizontal at the top of the cataclastic lower crustal layer (listric faulting). The west-dipping events to the east of Line 88-10 (Figure 35) are an excellent example of this behaviour: the Okanagan Valley Fault (see also Cook et al., 1992) merges with the top of the reflective zone, located in the ductile, cataclastic lower crust.

Jones (1987) proposed the presence of a wet layer between the 400°C and 500°C isotherms. Its top is close to the greenschist-amphibolite dehydration reaction temperature, and its bottom is at a temperature above which rocks become too weak to sustain the differential pressures at the fluid-matrix boundary. The fluids are capped by precipitation of minerals in the upper part of the porous zone. The amount of fluid required to precipitate enough minerals to close the porosity is quite large, and hence a high porosity is required. An alternate possibility is having a very high passing fluid:rock ratio, but this will require a high permeability, i.e. also a high porosity. Such a high porosity at pressures exceeding lithostatic should cause hydrofracturing at the base of the brittle crust and should eventually escape to the surface. It seems unlikely that this

capping mechanism can be stable for geologically long times.

Another trapping mechanism dependent upon the brittle-ductile transition has been proposed by Bailey (1990). He computed characteristic emptying times for the crust (as done above), modifying McKenzie's (1984) equations to take into account the effects of temperature on matrix viscosity. His results show that a hot crust will empty rapidly (100 years), but that a cold crust can retain its fluids for tens of millions of years. The temperature interval from short to long trapping times corresponds to that for the transition to a ductile crust. Bailey also proposed that the fluid should mostly flow in the horizontal direction, since that is the direction of maximum stress. Again, there is the problem that even though the cold crust should retain its fluids for a long time, the underlying rocks should empty themselves rapidly, producing a layer of very high pressure fluid at the brittle-ductile transition. As with Jones's (1987) model, such a 'lake' in the middle of the crust is likely to be very short lived. The fluids should eventually migrate up to the surface.

v. Stress control of pore geometries

A model allowing both low vertical permeability and low horizontal resistivity involving horizontal-vertical anisotropy arising from the deformation of the pore space by small deviatoric (tectonic) stresses is proposed here. The effect of such stresses on equilibrium pore geometries that represent the minimum solid-fluid surface free energy will be discussed. The chemical potential of a fluid-matrix interface is obtained by (von Bargen and Waff, 1986):

$$\mu^s_j = \mu^o_j + V^s_j [\Delta p - 2\gamma_{sl}k + (1/4\mu) \sum \Delta p^2_i]$$

where $\Delta p_i = p_i - P$ principal pressure - mean pressure (lithostatic)
$\Delta p = p - P$ deviatoric stress - lithostatic
V^s_j partial molar volume of component j in solid at pressure P
k curvature
γ_{sl} solid-liquid surface tension

μ elastic shear modulus at pressure P

At equilibrium, μ_j' must be the same in all directions (i.e. all j's). Except for Δp and k, all terms are constant for a given stress field. This implies that

$$\Delta p - 2\,\gamma_{sl}\,k \;=\; \text{Constant}$$

One can therefore use the cases for which no tectonic stress is involved ($\Delta p = 0$) already obtained by von Bargen and Waff (1986) and Cheadle (1989) to calculate the value of that constant. The new curvature then becomes:

$$k' = (2\,\gamma_{sl}\,k^{o} - \Delta p) / 2\,\gamma_{sl}$$

where k^{o} is the curvature in a homogeneous stress field. Calculations of k' for increasing Δp are shown in Figure 43.

As mentioned above, a curvature larger than zero (axis of curvature in the fluid phase) is indicative of isolated pockets, while a negative curvature indicates interconnection (von Bargen and Waff, 1986; Figure 41). Figure 43 shows that otherwise interconnected pores, very small horizontal compressive stresses (200 Pa) can pinch off vertical pores that would otherwise be interconnected, while retaining horizontal pore interconnection.

Another possibility is for deviatoric stress to interconnect pores that were originally pinched-off. If the stress régime is extensional rather than compressional, small deviatoric stresses can change the mean curvature in the direction parallel to the es stress from positive to negative.

These two scenarios are strongly dependent upon the composition of the fluids at depth. For example, if the fluid is interconnected when no deviatoric stress is applied, then only in compressional areas should fluids be trapped, i.e. low-resistivity zones should only be seen where compression has occurred. Fluids should have escaped in extensional zones. However, lower crustal low-resistivity layers seem to be present in

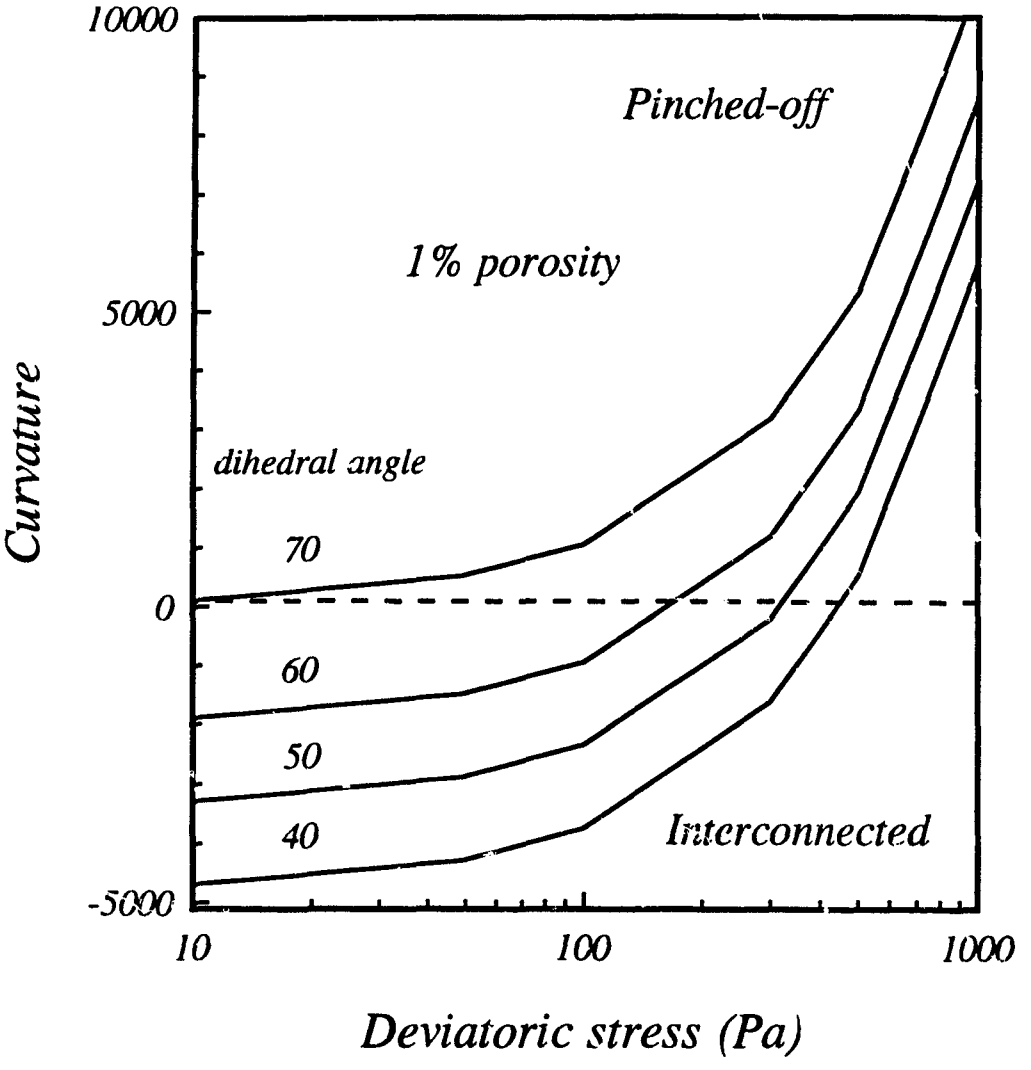

Figure 43 Influence of deviatoric stress on equilibrium pore curvature for selected values of dihedral angle. A negative curvature indicates that the fluid is interconnected.

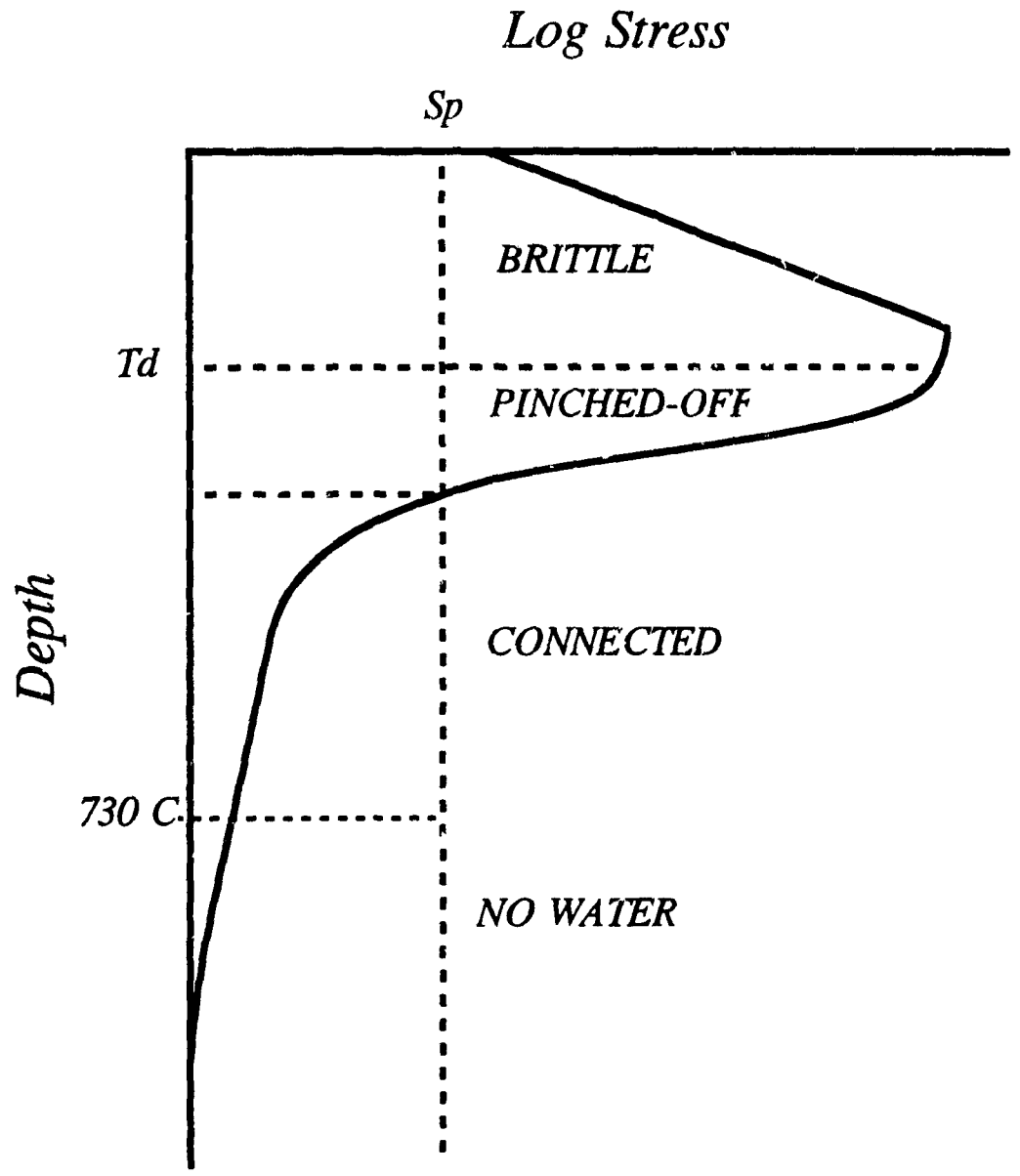

Figure 44 Stress-depth profile, from Kusznir and Park, 1986. Sp, stress required to pinch off the pores vertically (see Figure 43); Td, brittle-ductile transition temperature.

both compressional and extensional stress régimes. Thus, if the mechanism mentioned above is the most important for capping fluids, only when low-salinity water-rich fluids are present can horizontal interconnection operate in both compressional and extensional environments. Experimental evidence suggests that their median dihedral angle is about 60°, close to the pinch-off threshold for 1% porosity, implying that some pores are interconnected, others are not. Pores that are originally pinched-off will be interconnected in extensional regimes and pores that were initially interconnected will be pinched-off in compressional regimes. In either case, some of the fluid will be lost, for there will always be some degree of interconnection. This fluid loss will cease when the vertically interconnected pores will have lost enough fluid to pinch-off at a smaller dihedral angle.

Are the deviatoric stresses required to pinch-off or open the pores present in the lower crust? Figure 44 shows a crustal stress distribution profile 1 Ma after a horizontal compressional force is applied (see Kusznir and Park, 1986). The pattern is similar in magnitude for an extensional force. Note the logarithmic scale on the stress axis. As time progresses, crustal stress in the lower crust is dissipated and transferred to the upper crust (stress amplification), but in areas where forces are continuously acting (subduction zones, uplifted areas, etc.) or in areas where the lower crust is rich in strong plagioclase, such stresses may be maintained for substantial times. It should be emphasized here that the stresses required to change the curvature of equilibrium pores are very small (between 100 and 1000 Pa; Figure 43).

Equilibrium pores are expected to be present below the brittle-ductile transition. The zone in which stresses larger than the critical value required to pinch off the vertical pore interconnection acts as an impermeable barrier beneath which interconnected porosity is present. This pore interconnected layer may extend to approximately the 730°C isotherm, below which the rocks may be dehydrated. While the quantitative aspects of this model need to be refined for various crustal stress and thermal regimes, Figure 44 illustrates the plausibility of a stress induced mid- to lower crustal vertical permeability cap, and deep crustal horizontal pore interconnection. The eventual dissipation of the lower crustal stress in time, or a major change in the plate tectonic

régime that affects the stress can cause re-opening of the previously capped layers, and provoke rapid release of the fluids. An example where this situation may have occurred (Goldfarb et al., 1991) will be presented in the next chapter.

iv. Lower crustal shear processes

The association of the tops of the conductive and reflective layers with the temperature of the brittle-ductile transition also leads to the possibility of the alignment of originally isolated pockets of fluid by lower crustal shear. The lower crust (below the brittle-ductile transition in many areas) is generally the weakest part of the continental lithosphere through which stresses have to be transmitted (e.g. Kusznir and Park, 1986), and hence, under certain conditions, it can decouple the upper crust from the mantle. As horizontal motion occurs (e.g., in extensional areas, see Reston, 1990), the lower crust is deformed progressively in layers as the temperature of the brittle-ductile transition progresses downwards. This process is illustrated in Figure 45 The differential slip between the layers produces deep crustal shear zones and if high-pressure fluids are present, they may get trapped into these zones. Figure 46 shows in detail this process: (a) the pores are all interconnected in a ductile crust. As horizontal shearing occurs, the grain boundaries deform horizontally, and the pores are flattened (b). As this process continues, pores eventually become isolated vertically, the very high pore pressure gradients at grain edges pushing up the ductile matrix. This results in a series of interbedded horizontal channels of fluid with good horizontal interconnection (c), but with vertical migration greatly restrained. Fluids in such a configuration can explain both the deep crustal low-resistivity and the observed layered reflectivity, even though seismic methods can not resolve each of these channels individually.

Fluids in these shear zones should flow horizontally, in a direction parallel to the applied stress. This flow implies high fluid:rock ratios, and hence there is more risk for re-absorption of fluids through retrograde metamorphic reactions. This problem will be discussed in more detail in Chapter VI.

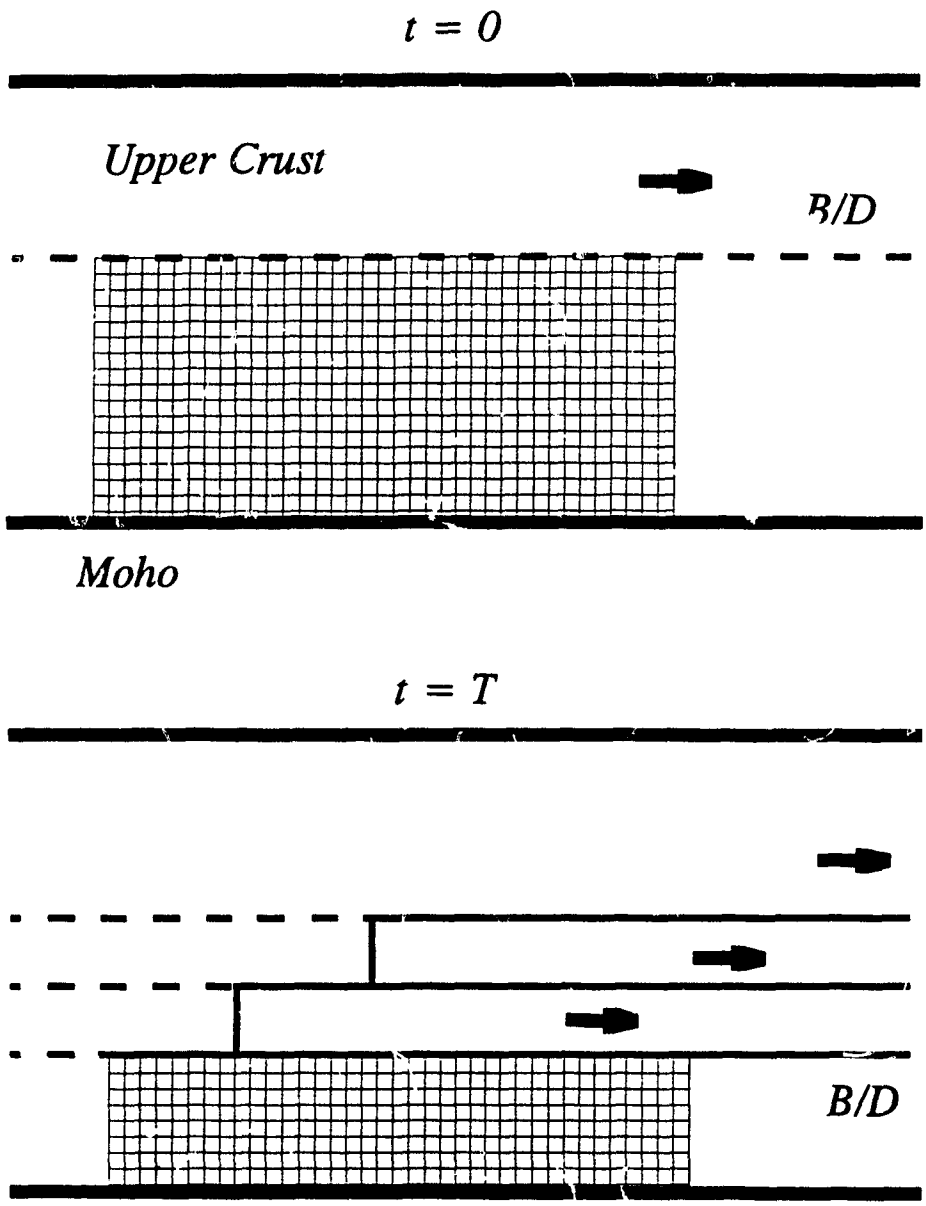

Figure 45 Lower crustal shear zone model. As the crust cools, it laminates and the pores are flattened in between the layers. Detailed explanations in text.

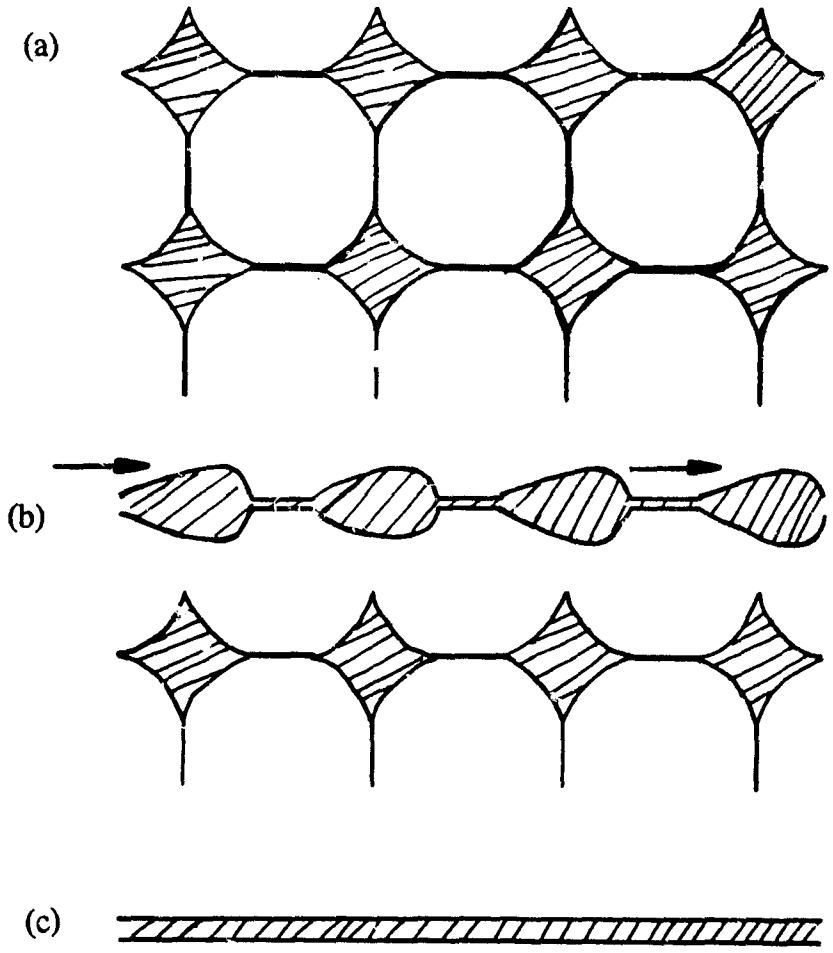

Figure 46 Detail of pore deformation by shear. (a) Equilibrium pores are well interconnected both horizontally and vertically, (b) as the crust cools, pores are flattened until forming channels (c).

CHAPTER VI ORIGIN AND NATURE OF LOWER CRUSTAL FLUIDS

The geophysical evidence presented in Chapters III and IV and the models presented in Chapter V supp. . the presence of aqueous fluids in the deep crust. Two very important aspects of the problem have however still not been discussed: what is the origin of the fluids? What is their composition? These questions will be addressed in this chapter.

i. Sources of fluids for the lower crust

Table 3 shows that lower crustal layers with inferred porosity are present in all types of geologic environments. This suggests either that there are many possible sources for free fluids in the deep crust, or that the source is not within the crust, but in the mantle. The most important sources are: a) wet rocks of oceanic origin, brought into the lower crust during episodes of crustal accretion and growth; b) fluids released from metamorphic dehydration reactions in progressively buried or heated rocks; c) water expelled from subducting slabs of oceanic crust; d) volatiles rising from the mantle. Each of these will be discussed below.

Oceanic crust rocks are formed at mid-oceanic ridges and have high porosity. Addition of oceanic crust is an important source of accretion. Most Phanerozoic continents grew by accretion of material separated from the mantle during subduction or arc magmatism (Taylor and McLennan, 1985) or by accretion of either unmetamorphosed or low grade rocks of oceanic origin (e.g. western North America). In both cases therefore, the added continental crust should contain substantial fluid, and some of which is probably unbound.

Prograde metamorphic reactions are accompanied by the release of volatiles, with water and carbon dioxide being the major constituents. In most continental areas, the crust is presently cooling from past thermal events. The one environment where tectonic activity first cools the crust then subsequently warms it i the ~200 km fore-arc areas of former subduction zones, where prograde metamorphism may currently be producing free water. The presence of free water is somewhat more problematic in a cooling crust:

it should be expelled or re-absorbed by retrograde metamorphism into hydrous silicates (e.g., Yardley, 1981). This retrograde cooling process may explain the inferred reduction in free water for Precambrian orogenic belts compared to Phanerozoic. However, most younger areas that have conductive and reflective lower crusts have also cooled since their last orogenic events (e.g. Western Europe). There also, fluids must have been added subsequently to maintain free fluid.

Recent oxygen isotope studies of mineralisation veins in the Juneau Gold Belt, Alaska (Goldfarb et al., 1991a; 1991b) contradict this theoretical conclusion. Goldfarb et al. (1991a) have found that low-salinity metamorphic waters there have remained at mid- to lower crustal pressure-temperature conditions for a very long period, perhaps from 110 to 56 Ma, during which the North American Cordillera was under compression. The fluids were not re-absorbed during that period, before finally escaping very rapidly around 55 Ma, coinciding with a change in motion of the Kula plate from compressional to transcurrent oblique. These fluids are found in rocks of metamorphic grade as high as amphibolite (Goldfarb et al., 1991a). This observation raises some questions about the dynamics of retrograde metamorphism. Note that these observations might however be only applicable in areas where subduction has occurred.

Another possibility is having the fluid phase not as nearly pure water, but as high salinity, the resulting reduced activity for the water may then stabilize this fluid phase so the reabsorption through formation of hydrous minerals does not occur. If this is not the case, then the presence of free water requires the addition of water in amounts sufficient to increase the total water content above the bound water required by the mineralogy stable at the local pressure-temperature conditions. For example pure amphibole contains about 2 wt% water; a granulite lower crust should have an even lower content of bound water (see also Figure 47).

Extra water can be brought into the crust by subduction and progressive dehydration of wet oceanic crust and oceanic sediments. The geophysical evidence for fluid input in a subduction zone, under Vancouver Island, has been discussed by Hyndman (1988). The landward limit of this fluid source has not yet been established, but results from Lewis et al. (1992) and from Chapter IV suggest that it might extend

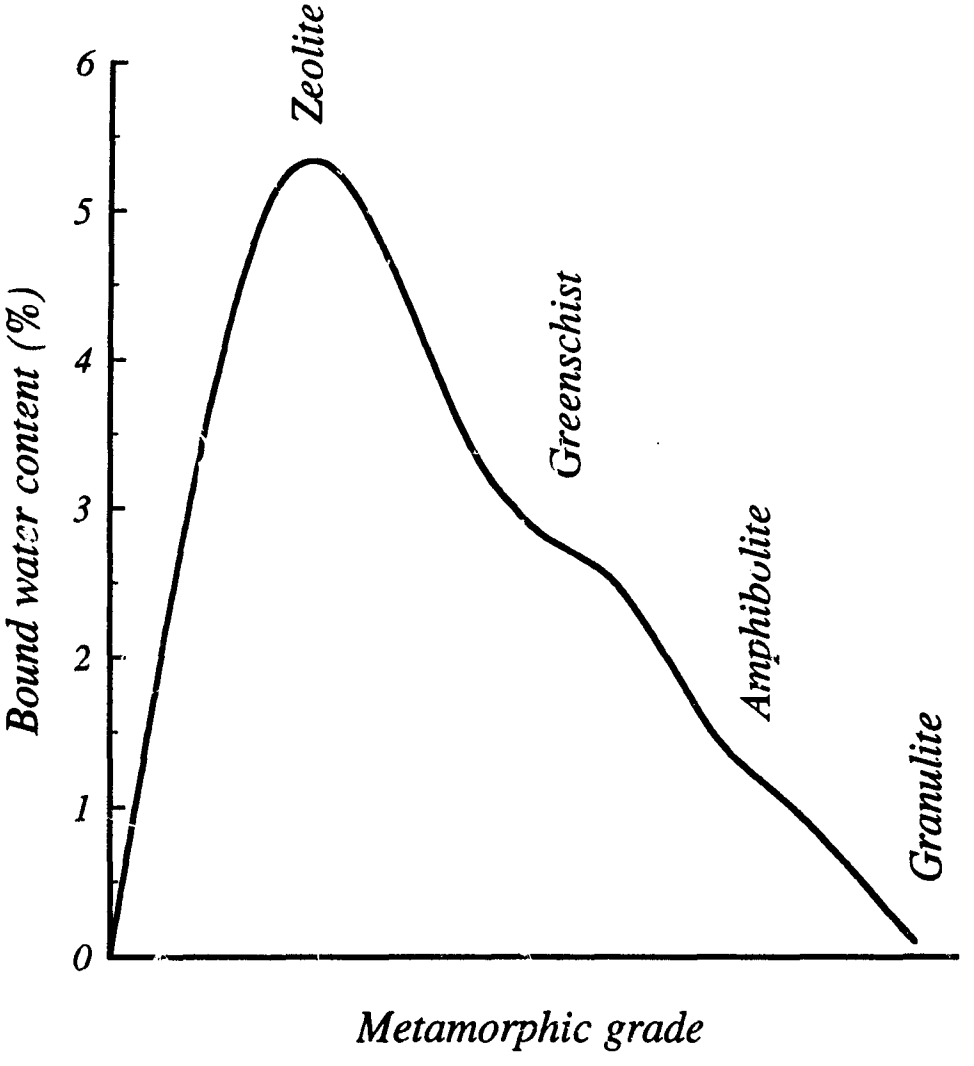

Figure 47 Water content vs metamorphic grade, from Fyfe et al. (1979). Greenschist to amphibolite facies are expected in present-day Phanerozoic lower crust.

a few hundred kilometres inland.

Another source of deep crustal fluids is the mantle (Kay and Kay, 1986). Seismic evidence suggests that the low-velocity zone of the upper mantle contains up to 5% basic melt (Anderson, 1989) at least in younger areas, which contains itself up to 2.5% free water (Yoder, 1976). This constitutes a substantial water reservoir, which can migrate into the lower crust as the melt cools, and then remained trapped by one of the mechanisms described earlier. This fluid production occurs in a cooling environment, in contrast to retrograde metamorphism that absorbs water upon cooling. This is an attractive mechanism to provide the extra fluids required if fluid reabsorption in retrograde metamorphism occurs.

ii. Composition of the conducting fluids

Most lines of geological evidence for deep crustal fluids - fluid inclusions, trace-element changes, stable isotope distributions - all argue for CO_2 as being the major fluid constituent in granulite terrains (Newton, 1989). The least equivocal sources of evidence are the fluid inclusions in minerals from high-grade terrains. They are usually CO_2-rich, but NaCl brine inclusions (30% wt NaCl) have been observed in metasedimentary granulites (Touret, 1986). It is still debated whether these brines could have survived the whole metamorphic process, or if they represent peak-metamorphic fluids (Touret, 1986). In either case, these results show that high-salinity brines are not affected by retrograde effects as these granulites cool.

Figure 48 shows the possible fluids under deep crustal pressure-temperature conditions. Only isochores (lines of constant density at given P,T conditions) passing through the box may represent fluids in the mid- to deeper crust. The isochores are based on composition of fluid inclusions and geobarometric and geothermometric determinations. Brine and low-density saline water affect parameters that can be observed geophysically: they especially should produce anomalously low electrical resistivities. On the other hand CO_2 itself has no appreciable effect in reducing the electrical resistivity.

At temperatures higher than about 280°C, CO_2 and H_2O are completely miscible.

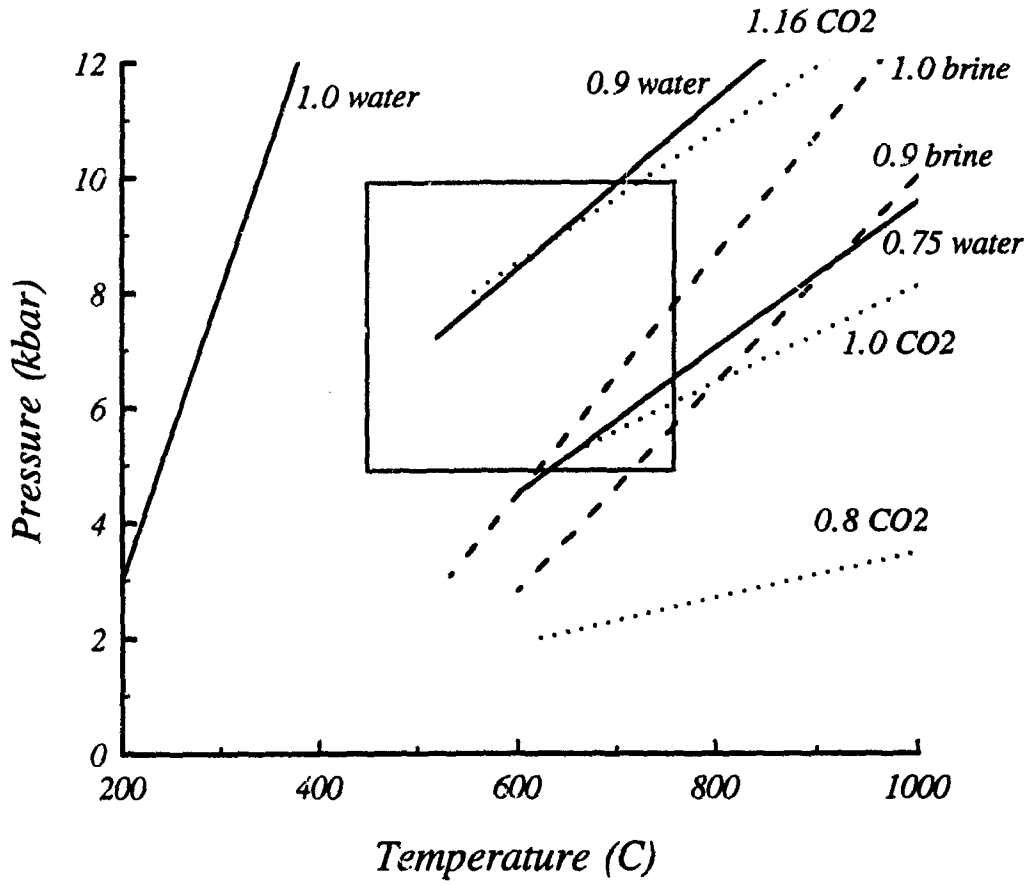

Figure 48 Isochores (pressure-temperature relations for constant density) of possible fluids under lower crustal conditions. Only the isochores passing inside the box are stable in the lower crust. From Touret (1986).

This situation can give rise to the dissolution reaction

$$CO_2(aq) + H_2O = HCO_3^- + H^+$$

the presence of the HCO_3^- ion can increase the electrical conductivity of the fluid (Nesbitt, 1992). An increase in pressure reduces the temperature of total miscibility, but an increase in NaCl concentration increases this temperature. The concentration of HCO_3^- however is strongly dependent upon temperature: the dissociation constant decreases with increasing temperature (Nesbitt, 1992). Hence, the production of HCO_3^- in a lower crustal environment ought not to be very important: it might however have a second order effect on the electrical resistivity of aqueous fluids. The concentration of NaCl remains the most important factor controlling the electrical resistivity of lower crustal fluids.

The salinity of the lower crustal fluids can also be constrained by the effect of salinity on the equilibrium pore geometries. Experimental data (see Chapter V) show that the higher the salinity, the smaller the dihedral angle. For brines ($c > 10$ wt% salt), this angle can be as low as 40°. Such a low dihedral angle ensures proper interconnection, even a very low porosities ($<< 1\%$), and hence reduces substantially the electrical resistivity of the rock. Fluids of moderate salinity (~ 3 wt%) also ought to be considered: experimental data show that they usually have mean dihedral angles slightly below 60° (critical value for interconnection at 1% porosity), and should therefore also be interconnected. However, the porosity required is larger (around 1%), and this increases dramatically the permeability, increasing the potential for fluid loss.

The physical state of the fluids is a fundamental, but too often neglected, parameter. It is usually assumed that fluids at lower crustal P, T conditions are in a supercritical phase, i.e. somewhere between liquid and gas, having a viscosity similar to that of a gas and a density closer to a liquid's (Kittel and Kroemer, 1980). Very little is known quantitatively about the properties of supercritical fluids that is of interest to earth scientists. Knight and Bodnar (1991) have studied the formation of synthetic fluid inclusions for varying salinity, and analyzed, amongst other parameters, the phase of the fluid. They have obtained the critical boundary for fluids of varying salinity (Figure 49). Another study of this problem by Bischoff (1991) for a smaller temperature range yielded

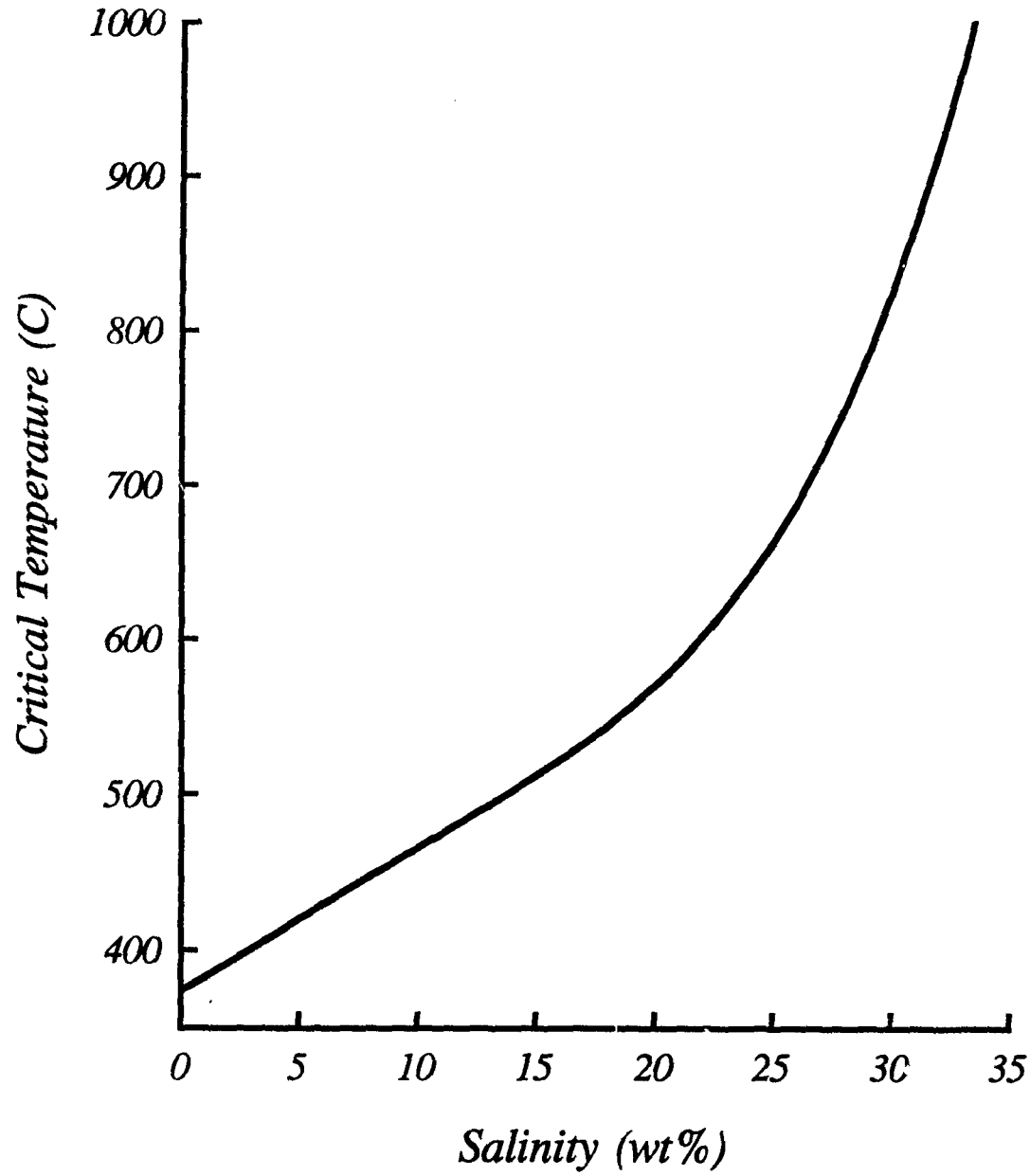

Figure 49 Effect of salinity on the critical temperature of aqueous fluids, from studies on synthetic fluid inclusions. From Knight and Bodnar (1989).

similar results. Seawater-salinity fluids have their critical point at a temperature of about 400°C, and hence should be in a supercritical state under lower crustal conditions. On the other hand, brines have their critical point at about 800°C, implying that they should still be liquid in the lower crust. This result has a crucial bearing on the trapping of the fluids: brines in the deep crust have the properties of liquids, i.e. high viscosity, high density, and hence can remain physically trapped into the crust for longer intervals of time (see equations page 87) than low-salinity supercritical fluids that have very low viscosity and lower density.

CHAPTER VII ALTERNATIVES TO THE SALINE FLUID HYPOTHESIS

As stated in the introduction, various mechanisms have been proposed to explain the anomalous in situ properties of the lower crust. The low electrical resistivity has been explained by the presence of graphite, metallic oxides and sulfides, or partial melt. However, only for graphite has a strong case been made. The lower crustal layered reflectivity has often been explained by layered magmatic underplating or by shear zones. A good case can be made for both mechanisms, but they are not necessarily incompatible with aqueous fluids.

i. Graphite

Interconnected graphite films have often been proposed as an alternative to fluids to explain the observed lower crustal low resistivity zones (Frost et al., 1989; Duba et al., 1989). It is an attractive model indeed: graphite is an extremely good conductor, it has been shown to cover grain boundaries in some sedimentary environments (black shales) and on one igneous example. There is an abundant supply of CO_2 in the deep crust that can be reduced to graphite. Observations show that graphite is stable in lower crustal environments (Glassley, 1982).

There are however many objections to the graphite model. First, it does not explain the observed low-velocity and reflective zones, since it has no noticeable effect on the elastic properties of a rock. An unreasonably large quantity of graphite is required to reduce the seismic velocity by the amounts estimated (Figure 50), and the resulting electrical resistivity is extremely low ($<<$ 1 ohm m), much lower than observed in electromagnetic surveys (10-100 ohm m; Figure 51).

It is difficult to reconcile the graphite model with some of the field observations pertaining to deep crustal resistivity. Lower crustal conductive layers have been shown to cross major terrane and structural boundaries (e.g. Jones et al., 1992 for the southern Canadian Cordillera; Bailey et al., 1989 for the Kapuskasing Structural Zone). A solid-conduction mechanism such as graphite should be greatly affected by structural changes. The thermal data also indicates that the lower crustal conductive layers are controlled by

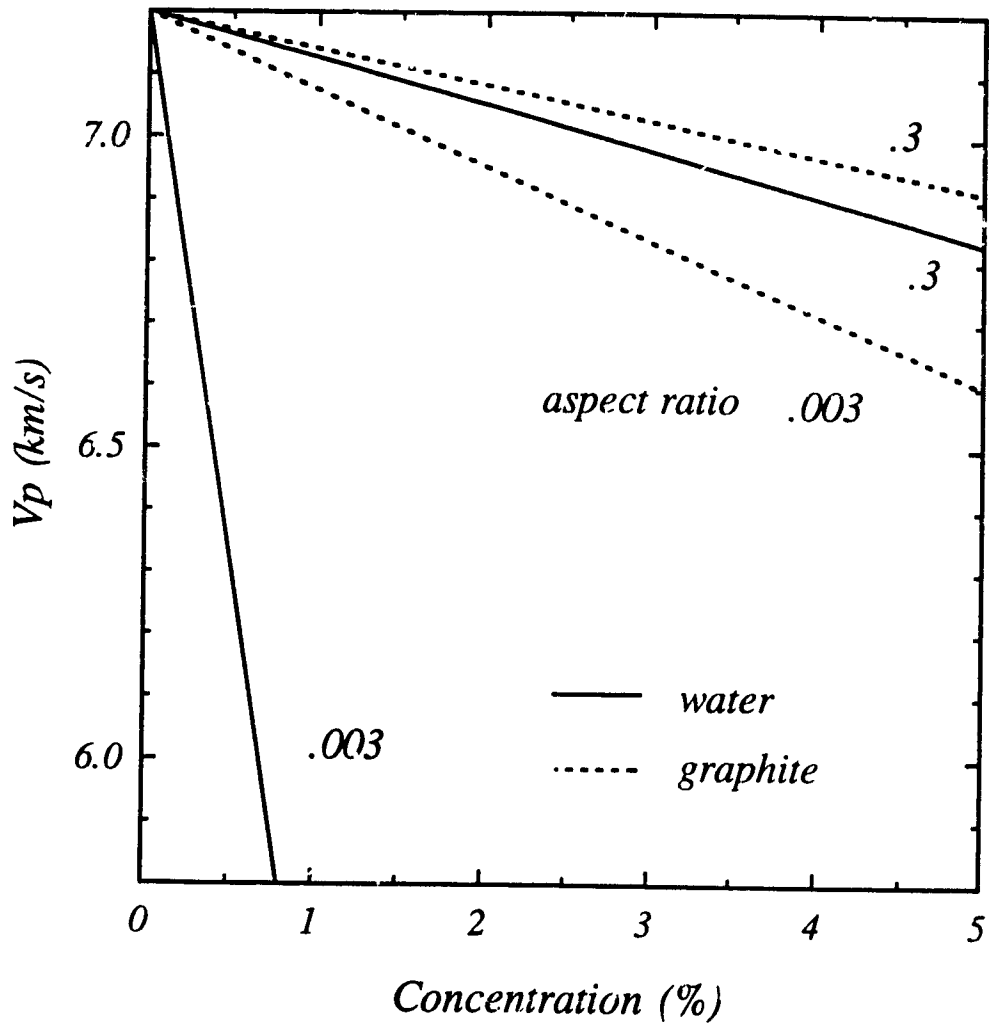

Figure 50 Velocity-concentration relations for graphitic inclusions, using the formalism of Kuster and Toksöz (1974), and comparison with water porosity.

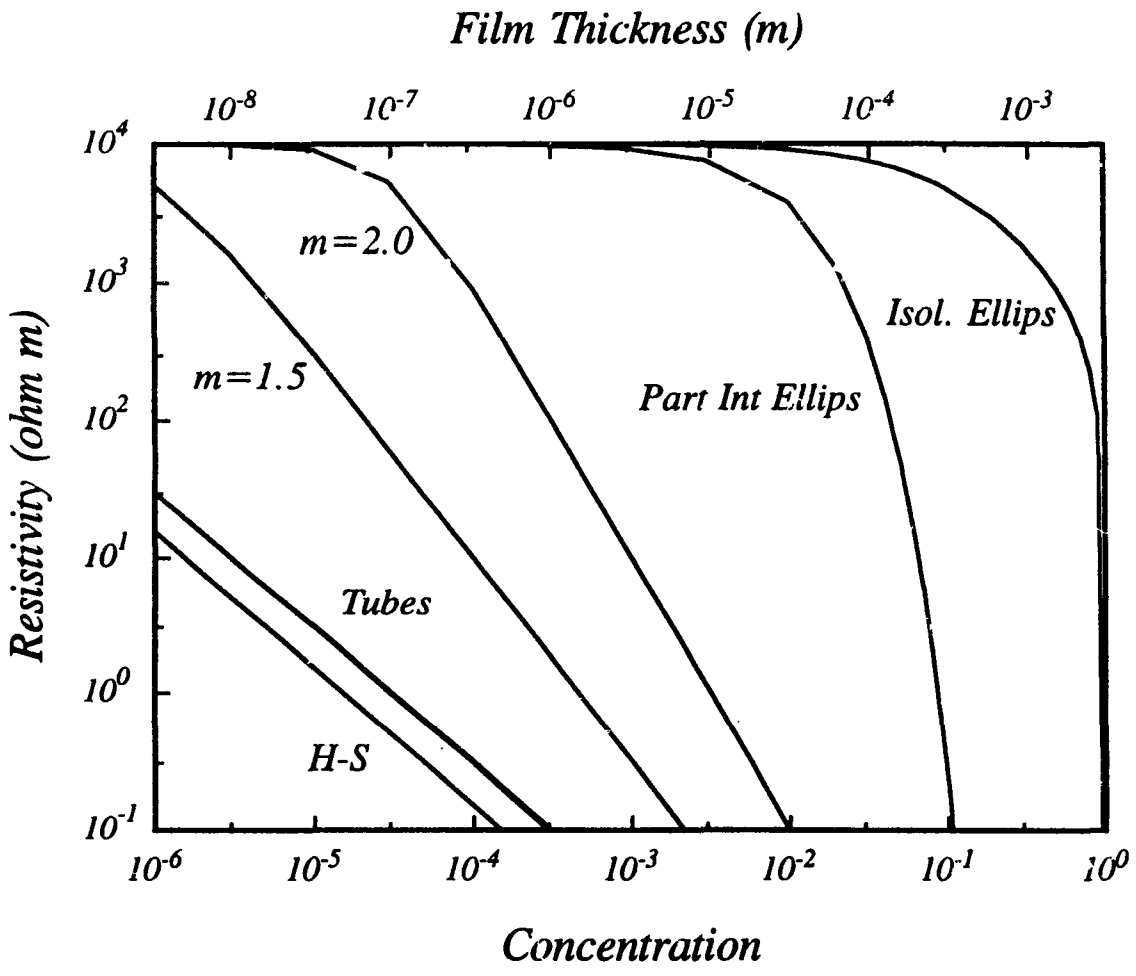

Figure 51 Resistivity-Concentration relations for graphitic inclusions. Geometries are the same as in Figure 13.

present-day temperature-pressure conditions: the higher the present surface heat flow, the shallower the conducting layer (e.g. Ádám, 1987; Chapter V). The graphite films might only be continuous (hence conducting) on large scales in the ductile crust: cooling in the upper crust may break the films (Frost et al., 1989). If the temperature increases, which is very likely to have happened for most crustal areas, it is difficult to conceive a reconnection of the graphite films.

The narrow range of observed resistivities for either Phanerozoic or Precambrian areas (about one order of magnitude, see Figure 16) is also difficult to explain with the graphite model. Since graphite is such a good conductor (10^{-5} ohm m), even small changes in graphite concentration should produce large changes in resistivity (Figure 51).

The graphite explanation is favoured by some metamorphic petrologists who base their reasoning on the evidence from fluid inclusions in exposed granulite terrains that have CO_2 as major fluid constituent. However, laboratory data on dihedral angle measurements (see Chapter V) indicate that CO_2-rich fluids invariably form isolated pockets at grain corners ($\theta > 60°$), and their isolation might explain why they persisted as fluid inclusions over long periods of time. This implies that any graphite formed by the reduction of CO_2 is in isolated form (i.e. resistive). Since the diffusivity of graphite is extremely low ($\sim 10^{-15}$ m^2/s; Watson, 1986), any graphite formed is unlikely to subsequently diffuse to form an interconnected film that can reduce the electrical resistivity. The diffusion time of graphite at mantle temperature over 1 cm^2 is about 0.3 Ma, and is certainly much longer at crustal temperatures, perhaps 30 or even 300 Ma. By that time the crust will have cooled and the films can not remain interconnected over long periods of time.

In a lower crustal environment, graphite can form in fluid-rich rock or in paths of crustal-scale fluid migration. The latter case requires an unusually high fluid:rock ratio to allow for deposition of graphite in a sufficient amount, since its concentration is extremely small. Another important problem is the reduction of CO_2 to produce graphite. Bryndzia and Wood (1990) present estimates of oxygen fugacity (fO_2) for deep crustal xenoliths. fO_2 values range from 0.3 to 10, showing that "continental amphibole-bearing xenoliths are among the most oxidized samples in their respective suite" (Bryndzia and

Wood, 1990). This observation provides strong direct evidence that the middle to lower crustal environment is indeed oxidizing. Graphite is stable (Glassley, 1982), but it can certainly not be produced in such oxidizing environments.

ii. Underplating

A popular explanation among crustal seismologists for the observed deep crustal high reflectivity is the underplating of the crust by mafic magmas derived from partial melting in the upper mantle. These are interpreted as being trapped around the level of the Moho or the lower crust. Warner (1990) has calculated reflection coefficients higher than 0.1 for mafic intrusions in a granitic or andesitic crust, sufficiently high to explain the lower crustal reflectivity. There is however little evidence from either xenoliths or exposed terrain rocks compositions for granitic or andesitic lower crust.

As pointed out earlier in Chapter VI, this underplating hypothesis is compatible with fluids in the lower crust. The presence of basaltic melt at shallow levels is not likely common, since the upper mantle temperatures are well below the melting point for basalt in most areas. This melting temperature can however be greatly reduced if small amounts of water are present and this water should end up in the lower crust.

There are some problems with the underplating hypothesis when analyzed in terms of the other geophysical parameters: first, it does not explain the observed lower crustal low resistivities; second, it is in contradiction with the observed low refraction velocities. As the mafic melt solidifies in a granitic on andesitic environment, it should increase the seismic velocity of the lower crust rather than reducing it.

Magmatic underplating is undoubtedly a very important contributor to the growth of the continental crust (Klemperer, 1989). Even though it is usually presented in opposition to the aqueous fluid explanation for lower crustal reflectivity (e.g. Warner, 1990), it is my contention that the two concepts in fact go hand in hand. Underplating is accompanied by an important amount of aqueous fluid.

iii. Shear zones

It has been argued by seismologists (e.g. Reston, 1988, 1990) that many of the commonly observed lower crustal reflections are produced by horizontal shear deformation of the lower crust. As stated earlier, the rheology of the lower crust differs greatly from that of the upper crust and upper mantle, and this difference may explain why the reflectivity is enhanced in the lower crust. A key observation pointed out by Reston (1988) is the continuity of the layered reflections in the dip direction, indicating that the ductile lower crust has been pervasively strained as differential motion occurred in shear zones (see Figure 4.5 for a sketch).

There are many ways shear zone can produce large impedance contrasts. by shearing out pre-existing heterogeneities to produce laminar or lenticular bodies (Warner, 1990), by causing grain-scale anisotropy in seismic velocity (Jones and Nur, 1984), by inducing high-pressure chemical changes in the rocks within the shear zone (Jones, 1986), or (as stated in Chapter V) by having free fluids within the shear zone. As temperature increases with depth, strain in the lower crust should become more and more pervasive (hence smaller) and one would expect reflections coefficients to decrease with depth. There does not seem to be much evidence that this is the case, although the diminution might be too small to be resolved within the capabilities of seismic processing. This might especially be the case if the crust is not exceptionally thick or the geothermal gradient not sufficiently high.

It is however worth noting that from all the mechanisms described above, only the presence of free fluids within the shear zone should give consistent impedance contrasts, since it does not depend entirely on the amount of strain in the lower crust; porosity plays a first-order role in reducing the velocity, the shearing mechanism mostly aligns it to produce layered reflections. Just as for underplating, shear zones, that are often presented as an alternative to aqueous fluids, are in fact perfectly compatible with them.

CHAPTER VII CONCLUSIONS

- A comparison of coincident deep crustal magnetotelluric and seismic refraction data with porosity models shows that electrical resistivity and seismic velocity appear to be related as predicted if they are both influenced by porosity.

- Analyses of seismic velocity and electrical resistivity in younger Phanerozoic areas yield porosity estimates in the range 0.5 to 1 per cent in pores of effective aspect ratio 0.01 to 0.03, as obtained from finite-element modelling of textural equilibrium pore geometries.

- The enhanced seismic reflectivity in the lower crust also correlates well with low electrical resistivity. In an example from the Canadian Cordillera examined in detail, high reflectivity and low resistivity layers correspond, within the resolution of the geophysical data inversions.

- The layers of inferred porosity are usually located just below the brittle-ductile transition at temperatures of about 400-450°C in the middle to lower crust. This suggests that the interconnected porosity is controlled by present temperature conditions and is restricted to the low-effective pressure régimes in the deep ductile crust.

- The porosity in the ductile lower crust is in textural equilibrium pores. The mineral grains will deform to the minimum energy configuration.

- Fluids can be kept at depth by deformation of equilibrium pores by small tectonic stresses reducing the vertical permeability, or by ductile shear processes aligning the pores horizontally.

- Whilst the geophysical data support the presence of free aqueous fluids in the lower crust, there is still a difficulty in reconciling free aqueous fluids with the expected retrograde metamorphic reactions that should take up water upon cooling. There must be enough water for free fluid to remain.

- Re-absorption will not happen if the porosity is a high-salinity, low-activity, H_2O-rich fluid.

- This high salinity fluid is in sub-critical, liquid phase at lower crustal temperatures, contrary to the previous assumption that lower-crustal aqueous fluids are

supercritical.

- High-salinity fluids have substantially higher viscosity than supercritical fluids, hence increasing their residence time in the ductile crust.

BIBLIOGRAPHY

Ádám, Á., 1978. Geothermal effects in the formation of electrically conducting zones and temperature distribution in the earth, *Physics of the Earth and Planetary Interiors*, **17**, P21-P28.

Ádám, Á., 1987. Are there two types of conductivity anomaly (CA) caused by fluid in the crust?, *Physics of the Earth and Planetary Interiors*, **45**, 209-215.

Allmendinger, R.W., Nelson, K.D., Potter, C.J., Barazangi, M., Brown, L.D., and Oliver, J.E., 1987. Deep seismic reflection characteristics of the continental crust, *Geology*, **15**, 304-310.

Anderson, D.L., 1989. *Theory of the Earth*. Blackwell, Boston.

Assumpção, M., and Bamford, D., 1978. LISPB-V. Studies of crustal shear waves, *Geophysical Journal of the Royal Astronomical Society*, **54**, 61-73.

Asudeh, I., 1982. Seismic structure of Iran from surface and body wave data. *Geophysical Journal of the Royal Astronomical Society*, **71**, 715-730.

Bailey, R.C., 1990. Trapping of aqueous fluids in the deep crust, *Geophysical Research Letters*, **17**, 1129-1132.

Bailey, R.C., Craven, J.A., McNae, J.C., and Polzer, B.D., 1989. Imaging of deep fluids in Archean crust, *Nature*, **340**, 136-138.

Bamford, D., Nunn, K., Prodehl, C., and Jacob, B., 1978. LISPB-IV. Crustal structure of northern Britain, *Geophysical Journal of the Royal Astronomical Society*, **54**, 43-60.

Barazangi, M., and Brown, L. (eds.). 1986a. *Reflection seismology: a global perspective*, Geodyn. Ser. vol. 13, Am. Geophys. Un., Washington.

Barazangi, M., and Brown, L. (eds.). 1986b. *Reflection seismology: the continental crust*, Geodyn. Ser. vol. 14, Am. Geophys. Un., Washington.

Barton, P., and Wood, R., 1984. Tectonic evolution of the North Sea basin: crustal stretching and subsidence, *Geophysical Journal of the Royal Astronomical Society*, **79**, 987-1022.

Benz, H.M., Smith, R.B., and Mooney, W.D., 1990. Crustal structure of the Northwestern Basin and Range Province from the 1986 program for array seismic studies of the continental lithosphere seismic experiment, *Journal of Geophysical Research*, **95**,

21823-21842.

Berdichevsky, M.N., and Dmitriev, V.I., 1976. Basic principles of interpretation of magnetotelluric sounding curves, in *Geoelectric and geothermal studies*, pp. 165-221, ed. Á. Ádám, Akadémiai Kiado, Budapest.

Berdichevsky, M.N., Vanyan, L.L., and Dmitriev, V.I., 1989. Methods used in the USSR to reduce near-surface inhomogeneity effects on deep magnetotelluric sounding, *Physics of the Earth and Planetary Interiors*, **53**, 194-206.

Berry, M.J., and Forsyth, D.A., 1975. Structure of the Canadian Cordillera from seismic refraction and other data, *Canadian Journal of Earth Sciences*, **12**, 182-208.

Berry, M.J., and Fuchs, K., 1973. Crustal structure of the Superior and Grenville provinces of the northeastern Canadian Shield, *Bull. Seis. Soc. Am.*, **63**, 1392-1432.

Bischoff, J.L., 1991. Densities of liquids and vapors in boiling NaCl-H_2O solutions: a PVTX summary from 300° to 500°C, *American Journal of Science*, **291**, 309-338.

Bittner, R., and Wever, Th., 1991. Energy histograms for the characterization of deep reflection seismic profiles, *Geophysical Journal International*, **105**, 37-43.

Blackwell, D.D., Steele, J.L., Frohme, M.K., Murphy, C.F., Priest, G.R., and Black, G.L., 1989. Heat flow in the Oregon Cascade Range and its correlation with regional gravity, magnetic, and geologic patterns, in *Geological, Geophysical, and Tectonic setting of the Cascade Range*, pp. 142-170, eds. Muffler, L.J.P., Weaver, C.S., and Blackwell, D.D., Open file report 89-178, U.S. Geological Survey.

Bloch, S., Hales, A.L., and Landisman, M., 1969. Velocities in the crust and upper mantle of southern Africa from multimode surface wave dispersion, *Bull. Seis. Soc. Am.*, **59**, 1599-1629.

Bloomer, J.R., Richardson, S.W., and Oxburgh, E.R., 1979. Heat flow in Britain: an assessment of the values and their reliability, in *Terrestrial heat flow in Europe*, pp. 293-300, eds. Čermak, V., and Rybach, L., Springer-Verlag, Berlin.

Boland, A.V., and Ellis, R.M., 1989. Velocity structure of the Kapuskasing Uplift, northern Ontario, from seismic refraction studies, *Journal of Geophysical Research*, **94**, 7189-7204.

Brace, W.F., Orange, A.S., and Madden, T.R., 1965. The effect of pressure on the electrical resistivity of water-saturated crystalline rocks, *Journal of Geophysical Research*, **70**, 5669-5678.

Bram, K., 1979. Heat flow measurements in the Federal Republic of Germany, in *Terrestrial heat flow in Europe*, pp. 191-196, eds. Čermak, V., and Rybach, L., Springer-Verlag, Berlin.

Brewer, J.A., Matthews, D.H., Warner, M.R., Hall, J., Smythe, D.K., and Whittington, R.J., 1983. BIRPS deep seismic reflection studies in the Caledonides, *Nature*, **305**, 206-210.

Brown, L.D., Chapin, C.E., Sanford, A.R., Kaufman, S., and Oliver, J., 1980. Deep structure of the Rio Grande Rift from seismic reflection profiling, *Journal of Geophysical Research*, **85**, 4773-4800.

Bryndzia, L.T., and Wood, B.J., 1990. Oxygen thermobarometry of abyssal spinel peridotites: the redox state and C-O-H volatile composition of the Earth's sub-oceanic mantle, *American Journal of Science*, **290**, 1093-1116.

Caner, B., Auld, D.R., Dragert, H., and Camfield, P.A., 1971. Geomagnetic depth sounding and crustal structure in western Canada, *Journal of Geophysical Research*, **76**, 7181-7201.

Cassidy, J.F., and Ellis, R.M., 1991. Shear wave constraints on a deep crustal reflective zone beneath Vancouver Island, *Journal of Geophysical Research*, **96**, 19843-19851.

Catchings, R.D., and Mooney, W.D., 1988. Crustal structure of the Columbia Plateau: evidence for continental rifting, *Journal of Geophysical Research*, **93**, 459-474.

Čermak, V., and Hurtig, E., 1979. Heat flow map of Europe, in *Terrestrial heat flow in Europe*, eds. Čermak, V., and Rybach, L., Springer-Verlag, Berlin.

Chapman, D.S., 1986. Thermal gradients in the continental crust, in *The Nature of the lower continental crust*, pp. 63-70, eds. Dawson, J.B., Carswell, D.A., Hall, J., and Wedepohl, K.H., Spec. Publ. 24., Geol. Soc., London.

Cheadle, M.J., 1989. Properties of texturally equilibrated two-phase aggregates, *Ph.D. Thesis*, University of Cambridge.

Christensen, N.I., 1979. Compressional wave velocities in rocks at high temperatures and pressures, critical thermal gradients, and crustal low-velocity zones, *Journal of Geophysical Research*, **84**, 6849-6857.

Christensen, N.I., 1982. Seismic velocities, in *Handbook of Physical properties of rocks*, pp. 1-228, ed. R.S. Carmichael, C.R.C. Press, Boca Raton, Florida.

Clowes, R.M., Gens-Lenartowicz, E., Demartin, M., and Saxov, S., 1987. Lithospheric structure in southern Sweden - results from FENNOLORA, *Tectonophysics*, **142**, 1-14.

Connerey, J.E.P., Nekut, A., and Kuckes, A.F., 1980. Deep crustal electrical conductivity in the Adirondacks, *Journal of Geophysical Research*, **85**, 2603-2614.

Cook, F.A., and Oliver, J.E., 1981. The late Precambrian-early Paleozoic continental edge in the Appalachian orogen, *American Journal of Science*, **281**, 993-1008.

Cook, F.A., Varsek, J.L, and Clowes, R.M., 1991. Lithoprobe reflection transect of southwestern Canada: Mesozoic Thrust and Fold Belt to mid-ocean ridge, in *Continental Lithosphere: Deep Seismic Reflections*, pp. 247-255, eds. Meissner, R., Brown, L., Dürbaum, H.J., Franke, W., Fuchs, K., and Siefert, F., Geodyn. Ser. vol. 22, Am Geophys. Un., Washington.

Cook, F.A., Varsek, J.L, Clowes, R.M., Kanasewich, E.R., Spencer, C., Parrish, R.R., Brown, R.L., Carr, S.D., Johnson, B.J., and Price, R.A., 1992. Lithoprobe crustal reflection cross section of the southern Canadian Cordillera I: Foreland Thrust and Fold Belt to Fraser River Fault, *Tectonics*, **11**, 12-35.

Cook, F.A., Simony, P.S., Coflin, K.C., Green, A.G., Milkereit, B., Price, R.A., Parrish, R.R., Patenaude, C., Gordy, P.L., and Brown, R.L., 1987. Lithoprobe southern Canadian Cordilleran transect: Rocky Mountain thrust belt to Valhalla gneiss complex, *Geophysical Journal of the Royal Astronomical Society*, **89**, 91-98.

Crawford, M.L., and Hollister, L.S., 1986. Metamorphic fluids: the evidence from fluid inclusions, in *Advances in physical geochemistry, volume 5*, pp. 1-35, eds. Walther, J.V., and Wood, B.J., Springer-Verlag, Berlin.

Cumming, W.B., Clowes, R.M., and Ellis, R.M., 1979. Crustal structure from a seismic refraction profile across southern British Columbia, *Canadian Journal of Earth Sciences*, **16**, 1024-1040.

Cunningham, P.S., Roecker, S.W., and Hatzfeld, D., 1986. Three-dimensional P and S wave velocity structures of southern Peru and their tectonic implications, *Journal of Geophysical Research*, **91**, 9517-9532.

Dahl-Jensen, T., Dyrelius, D., Juhlin, C., Palm, H., and Pedersen, L.B., Deep reflection seismics in the Precambrian of Sweden, *Geophysical Journal of the Royal Astronomical Society*, **89**, 371-378.

Dawson, J.B., Carswell, D.A., Hall, J., and Wedepohl, K.H. (eds), 1986. *The*

Nature of the lower continental crust, Spec. Publ. 24., Geol. Soc., London.

DEKORP Research Group, 1990. Results of deep-seismic reflection investigations in the Rhenish Massif, *Tectonophysics*, **173**, 507-515.

Dragert, H., Law, L.K., and Sule, P.O., 1980. Magnetotelluric soundings across the Pemberton Volcanic Belt, British Columbia, *Canadian Journal of Earth Sciences*, **17**, 161-167.

Drew, J.J., and Clowes, R.M., 1990. A re-interpretation of the seismic structure across the active subduction zone of western Canada, in *Studies of laterally heterogeneous structures using seismic refraction and reflection data*, pp. 115-132, ed. Green, A.G., Pap. 89-13, Geol. Surv. Can.

Dowling, F.L., 1970. Magnetotelluric measurements across the Wisconsin Arch, *Journal of Geophysical Research*, **75**, 2683-2698.

Duba, A., Huenges, E., Nover, G., Will, G., and Jödicke, H, 1988. Impedance of black shale from Münsterland 1 borehole: an anomalous good conductor?, *Geophysical Journal*, **94**, 413-419.

Dullien, F.A.L., 1979. *Porous media and pore structure*, Academic Press, New York.

Duncan, P.M., Hwang, A., Edwards, R.N., Bailey, R.C., and Garland, G.D., 1980. The development and application of a wide band electromagnetic sounding system using a pseudo-noise source, *Geophysics*, **45**, 1276-1296.

Edwards, R.N., Bailey, R.C., and Garland, G.D., 1981. Conductivity anomalies: lower crust or asthenosphere?, *Physics of the Earth and Planetary Interiors*, **25**, 263-272.

El-Isa, Z., Mechie, J., and Prodehl, C, 1987. Shear velocity structure of Jordan from explosion seismic data, *Geophysical Journal of the Royal Astronomical Society*, **90**, 261-281.

Eriksson, K.G., and Malmqvist, D., 1979. A review of the past and present investigations of heat flow in Sweden, in *Terrestrial heat flow in Europe*, pp. 267-277, eds. Čermak, V., and Rybach, L., Springer-Verlag, Berlin.

Fitterman, D.V., Stanley, W.D., and Bisdorf, R.J., 1988. Electrical structure of the Newberry Volcano, Oregon, *Journal of Geophysical Research*, **93**, 10119-10134.

Fountain, D.M., and Salisbury, M.H. 1981. Exposed cross-sections through the continental crust: implications for crustal structure, petrology and evolution, *Earth and*

Planetary Science Letters, **56**, 263-277.

Fowkes, F.M., 1965. Attractive forces at interfaces, in *Chemistry and physics at surfaces*, pp. 1-12, ed. Gushee, D.E., American Chemical Society, Washington.

Frost, B.R., Fyfe, W.S., Tazaki, K., and Chan, T., 1989. Grain-boundary graphite in rocks from the Laramie Anorthosite complex: implications for lower crustal conductivity, *Nature*, **340**, 134-136.

Fuchs, K., Bonjer, K.P., Gajewski, D., Lüschen, E., Prodehl, C., Sandmeier, K.J., Wenzel, F., and Wilhelm, H., 1987. Crustal evolution of the Rhinegraben area. 1. Exploring the lower crust in the Rhinegraben Rift by unified geophysical experiments, *Tectonophysics*, **141**, 261-275.

Furlong, K.P., and Fountain, D.M., 1986. Continental underplating: thermal considerations and seismic-petrologic consequences, *Journal of Geophysical Research*, **91**, 8285-8294.

Fyfe, W.S., Price, N.J., and Thompson, A.B., 1978. *Fluids in the Earth's crust*, Elsevier, Amsterdam.

Gajewski, D., and Prodehl, C., 1987. Seismic refraction investigation of the Black Forest, *Tectonophysics*, **142**, 27-48.

Gavrilenko, P., and Gueguen, Y., 1989. Pressure dependence of permeability: a model for cracked rocks, *Geophysical Journal International*, **98**, 159-172.

Gavrilenko, P., and Gueguen, Y., 1992. Fluid overpressure and pressure solution in the crust, *Geophysical Journal International*, in press.

Gregory, G.P., and Lanzerotti, L.J., 1982. Electrical conductivity structure in the lower crust, *Geophysical Surveys*, **4**, 467-500.

Griffin, W.L., and O'Reilly, S.Y., 1987. The composition of the lower crust and the nature of the continental Moho - xenolith evidence, in *Mantle xenoliths*, pp. 413-432, ed. Nixon, P.H., John Wiley and Sons, New York.

Giese, P., Ibbeken, S., Baier, B., and Schulze-Frerichs, K., 1990. Accompanying seismic refraction investigations along the profile DEKORP 2-North, *Geologische Rundschau*, **79**, 567-579.

Glassley, W., 1982. Fluid evolution and graphite genesis in the deep continental crust, *Nature*, **295**, 229-231.

Goldfarb, R.J., Newberry, R.J., Pickthorn, W.J., and Gent, C.A., 1991a. Oxygen, hydrogen and sulfur isotope studies in the Juneau Gold Belt, southeastern Alaska: constraints on the origin of hydrothermal fluids, *Economic Geology*, **86**, 66-80.

Goldfarb, R.J., Snee, L.W., Miller, L.D., and Newberry, R.J., 1991b. Rapid dewatering of the crust deduced from ages of mesothermal gold deposits, *Nature*, **354**, 296-298.

Goodwin, E.B., and McCarthy, J., 1990. Composition of the lower crust in west central Arizona from three-component seismic data, *Journal of Geophysical Research*, **95**, 20097-20109.

Gough, D.I., 1986. Seismic reflectors, conductivity, water and stress in the lower continental crust, *Nature*, **323**, 143-144.

Grant and West, G.F., 1965. *Interpretation theory in applied geophysics*, McGraw-Hill, New York.

Greensfelder, R.W., and Kovach, R.L., 1982. Shear wave velocities and crustal structure of the eastern Snake River Plain, Idaho, *Journal of Geophysical Research*, **87**, 2643-2653.

Gupta, M.L., 1989. Comparison of the thermal structure of the lithosphere of the Gondwanic shields and mobile belts (extended abstract), in *International symposium on the thermal evolution of the lithosphere and processes in the Earth's interior*, Acad. Sci. U.S.S.R., Moscow.

Haak, V., and Hutton, R., 1986. Electrical resistivity in continental lower crust, in *The Nature of the lower continental crust*, pp. 35-49, eds. Dawson, J.B., Carswell, D.A., Hall, J., and Wedepohl, K.H., Spec. Publ. 24., Geol. Soc., London.

Hermance, J.F., 1979. The electrical conductivity of materials containing partial melt: a simple model from Archie's Law, *Geophysical Research Letters*, **6**, 613-616.

Hermance, J., and Pedersen, J., 1980. Deep structure of the Rio Grande Rift: a magnetotelluric interpretation, *Journal of Geophysical Research*, **85**, 3899-3912.

Hirn, A., Jobert, G., Witttlinger, G., Xu, Z.H., and Gao, E.Y., 1984. Main features of the upper lithosphere in the unit between the High Himalayas and the Yarlung Zangbo Jian suture, *Annales Geophysicae*, **2**, 113-118.

Hirschleber, H.B., Lund, C.E., Meissner, R., Vogel, A, and Weinrebe, W., 1975. Seismic investigations along the Scandinavian "Blue Road" traverse, *Journal of Geophysics*, **41**, 135-148.

Holbrook, W.S., Gajewski, D., Krammer, A., and Prodehl, C., 1986. An interpretation of wide-angle compressional and shear wave data in southwest Germany: Poisson's ratio and petrological implications, *Journal of Geophysical Research*, **93**, 12081-12106.

Hutton, V.R.S., Ingham, M.R., and Mbipom, E.W., 1980. An electrical model of the crust and upper mantle in Scotland, *Nature*, **287**, 30-32.

Hyndman, R.D., 1988. Dipping seismic reflectors, electrically conductive zones and trapped water in the crust over a subducting plate, *Journal of Geophysical Research*, 93, 13391-13405.

Hyndman, R.D., and Hyndman, D.W., 1968. Water saturation and high electrical conductivity in the lower continental crust, *Earth and Planetary Science Letters*, **4**, 427-432.

Hyndman, R.D., and Klemperer, S.L., 1989. Lower crustal porosity from electrical measurements and inferences about composition from seismic velocities, *Geophysical Research Letters*, **16**, 255-258.

Hyndman, R.D., and Shearer, P.M., 1989. Water in the lower continental crust: modelling magnetotelluric and seismic reflection results, *Geophysical Journal International*, **98**, 343-365.

Hyndman, R.D., Lewis, T.J., and Marquis, G., 1991. Comment on "Origin of deep crustal reflections: implications of coincident seismic refraction and reflection data in Nevada" by Holbrook, Catchings and Jarchow, *Geology*, **19**, 1243-1244, 1991.

Jaupart, C., Francheteau, J., and Shen, X.J., 1985. On the thermal structure of the southern Tibetan crust, *Geophysical Journal of the Royal Astronomical Society*, **81**, 131-155.

Jiracek, G.R., 1990. Near-surface and topographic distortions in electromagnetic induction, *Surveys in Geophysics*, **11**, 163-203.

Jones, A.G., 1981. On a type classification of lower crustal layers under Precambrian regions, *Journal of Geophysics*, **49**, 226-233.

Jones, A.G., 1987. MT and reflection: an essential combination, *Geophysical Journal of the Royal Astronomical Society*, **89**, 7-18.

Jones, A.G., 1988. Static-shift of magnetotelluric data and its removal in a sedimentary basin environment, *Geophysics*, **53**, 967-978.

Jones, A.G., Olafsdottir, B., and Tikkainen, J., 1983. Geomagnetic induction studies in Scandinavia III. Magnetotelluric observations, *Journal of Geophysics*, **54**, 35-50.

Jones, A.G., Kurtz, R.D., Oldenburg, D.W., Boerner, D.E., and Ellis, R., 1988. Magnetotelluric observations along the LITHOPROBE southeastern Canadian Cordilleran transect, *Geophysical Research Letters*, **15**, 677-680.

Jones, A.G., Gough, D.I., Kurtz, R.D., DeLaurier, J.M., Boerner, D.E., Craven, J.A., Ellis, R.G., and McNeice, G.W., 1992. Electromagnetic images of regional structure in the southern Canadian Cordillera, *Geophysical Research Letters*, in press.

Jones, R.H., 1986. Seismic reflections from major faults, *Ph.D. Thesis*, University of Cambridge.

Jones, T.D., and Nur, A., 1984. The nature of seismic reflections from deep crustal fault zones, *Journal of Geophysical Research*, **89**, 3153-3171.

Jurewicz, S.R., and Jurewicz, A.J.G., 1986. Distribution of apparent angles on random sections with emphasis on dihedral angle measurement, *Journal of Geophysical Research*, **91**, 9277-9282.

Kaila, K.L., Roy Chowdhury, K., Reddy, P.R., Krishna, V.G., Narain, H., Subbotin, S.I., Sollogub, V.B., Chekunov, A.V., Kharetchko, G.E., Lazarenko, M.A., and Ilchenko, T.V., 1979. Crustal structure along the Kavali-Udipi profile in the Indian peninsular shield from deep seismic sounding, *Journal of the Geological Society of India*, **20**, 307-333.

Kariya, K.A., and Shankland, T.J., 1983. Electrical conductivity of dry lower crustal rocks, *Geophysics*, **48**, 52-61.

Kaufman, A.A., and Keller, G.V., 1981. *The magnetotelluric sounding method*, Elsevier, Amsterdam.

Kay, R.W., and Kay, S.M., 1986. Petrology and geochemistry of the lower continental crust: an overview, in *The Nature of the lower continental crust*, pp. 147-159, eds. Dawson, J.B., Carswell, D.A., Hall, J., and Wedepohl, K.H., Spec. Publ. 24., Geol. Soc., London.

Kean, A.E., and Long, L.T., 1980. A seismic refraction line along the axis of the southern Piedmont and crustal thickness in the southeast United States, *Earthquake Notes*, **51**, 3-13.

Kittel, C., and Kroemer, H., 1980. *Thermal Physics*, Freeman, San Francisco.

Klemperer, S.L., 1989. Deep seismic reflection profiling and the growth of the continental crust, *Tectonophysics*, **161**, 233-244.

Klemperer, S.L., 1987. A relation between heat flow and the seismic reflectivity of the lower crust, *Journal of Geophysics*, **61**, 1-11.

Klemperer, S.L., Hauge, T.A., Hauser, E.C., Oliver, J.E., and Potter, C.J., 1986. The Moho in the northern Basin and Range province, Nevada, along the COCORP 40°N seismic-reflection transect, *Geological Society of America Bulletin*, **97**, 603-618.

Knight, C.L., and Bodnar, R.J., 1989. Synthetic fluid inclusions: IX. Critical PVTX properties of NaCl solutions, *Geochemica et Cosmochemica Acta*, **53**, 3-8.

Kurtz, R.D., 1982. Magnetotelluric interpretation of crustal and mantle structure in the Grenville Province, *Geophysical Journal of the Royal Astronomical Society*, **70**, 373-397.

Kurtz, R.D., DeLaurier, J.M., and Gupta, J.C., 1990. The electrical conductivity distribution beneath Vancouver Island: a region of active plate subduction, *Journal of Geophysical Research*, **95**, 10929-10946.

Kuster, G.T., and Toksöz, M.N., 1974. Velocity and attenuation of seismic waves in two-phase media: part I. Theoretical formulations, *Geophysics*, **39**, 587-606.

Kusznir, N.J., and Park, R.G., 1986. Continental lithosphere strength: the critical role of lower crustal deformation, in *The Nature of the lower continental crust*, pp. 79-93, eds. Dawson, J.B, Carswell, D.A., Hall, J., and Wedepohl, K.H., Spec. Publ. 24., Geol. Soc., London.

Lachenbruch, A. H., and Sass, J.H., 1977. Heat flow in the United States and the thermal regime of the crust, in *The Earth's crust*, pp. 626-675, ed. Heacock, J.G., Geophys. Monog. Ser. No. 20., Am. Geophys. Un., Washington.

Laporte, D., and Watson, E.B., 1991. Direct observation of near-equilibrium pore geometry in synthetic quartizites at 600°-800°C and 2-10.5 kbar, *Journal of Geology*, **99**, 873-878.

Leaver, D.S., Mooney, W.D., and Kohler, W.M., 1984. A seismic refraction study of the Oregon Cascades, *Journal of Geophysical Research*, **89**, 3121-3134.

Lee, V.W., Mackwell, S.J., and Brantley, S.L., 1991. The effect of fluid chemistry on wetting textures in novaculite, *Journal of Geophysical Research*, **96**, 10

023-10 037.

Levander, A.R., and Kovach, R.L., 1990. Shear velocity structure of the northern California lithosphere, *Journal of Geophysical Research,* **95**, 19773-19784.

Lewis, T.J., 1991. Heat flux in the Canadian Cordillera, in *Neotectonics of North America*, pp. 445-456, eds. Slemmons, D.B., Engdahl, E.R., Zoback, M.D., and Blackwell, D.D., Geol. Soc. Am., Boulder, Colorado.

Lewis, T.J., Bentkowski, W.H., Davis, E.E., Hyndman, R.D., Souther, J.G., and Wright, J.A., 1988. Subduction of the Juan de Fuca plate: thermal consequences, *Journal of Geophysical Research*, **93**, 15207-15225.

Lewis, T.J., Bentkowski, W.H., and Hyndman, R.D., 1992. Crustal temperatures near the Lithoprobe Southern Canadian Cordilleran Transect, *Canadian Journal of Earth Sciences*, in press.

Lienert, B.R., and Bennett, D.J., 1977. High electrical conductivity in the lower crust of the northwestern Basin and Range: an application of inverse theory to a controlled source deep-magnetic-sounding experiment, in *The Earth's Crust*, pp. 531-552, ed. Heacock, J.G., Geophys. Monog. Ser. No. 20, Am. Geophys. Un., Washington.

Luetgert, J.H., Mann, C.E., and Klemperer, S.L., 1987. Wide-angle deep crustal reflections in the northern Appalachians, *Geophysical Journal of the Royal Astronomical Society*, **89**, 183-188.

Luosto, U., and Korhonen, H., 1986. Crustal structure of the Baltic Shield based on off-FENNOLORA refraction data, *Tectonophysics*, **128**. 183-208.

Lüschen, E., Wenzel, F., Sandmeier, K.J., Menges, D., Rühl, Th., Stiller, M., Janoth, W., Keller, F., Söllner, W., Thomas, R., Krohe, A., Stenger, R., Fuchs, K., Wilhelm, H., and Eisbacher, G., 1987. Near-vertical and wide-angle seismic surveys in the Black Forest, SW Germany, *Journal of Geophysics*, **62**, 1-30.

Lyons, J.A., Forsyth, D.A., and Mair, J.A., 1980. Crustal studies in the La Malbaie region, Québec, *Canadian Journal of Earth Sciences*, **17**, 478-490.

Majorowicz, J.A., and Gough, D.I., 1991. Crustal structures from MT soundings in the Canadian Cordillera, *Earth and Planetary Science Letters*, **102**, 444-454.

Maréschal, M., Chakridi, R., and Chouteau, M., 1989. A magnetotelluric survey across the Groundhog River block: progress report on the pseudo 1-D interpretation, in *KSZ workshop*, pp. 77-81, Lithoprobe.

Marquis, G., and Hyndman, R.D., 1992. Geophysical support for aqueous fluids in the deep crust: seismic and electrical relationships, *Geophysical Journal International*, **110**, 91-105.

Marquis, G., and Hyndman, R.D., 1991. Velocity-resistivity relations in the deep crust, in *Continental Lithosphere: Deep Seismic Reflections*, pp. 329-333, eds. Meissner, R., Brown, L., Dürbaum, H.J., Franke, W., Fuchs, K., and Siefert, F., Geodyn. Ser. vol. 22, Am Geophys. Un., Washington.

Matthews, D.H., 1986. Seismic reflections from the lower crust around Britain, in *The Nature of the lower continental crust*, pp. 11-22, eds. Dawson, J.B., Carswell, D.A., Hall, J., and Wedepohl, K.H., Spec. Publ. 24., Geol. Soc., London.

Mavko, G.M., 1980. Velocity and attenuation in partially molten rocks, *Journal of Geophysical Research*, **85**, 5173-5189.

McKenzie, D., 1984. The generation and compaction of partially molten rock, *Journal of Petrology*, **25**, 713-765.

Meissner, R., 1986. *The continental crust: a geophysical approach*, Academic Press, New York.

Meissner, R., Brown, L., Dürbaum, H.J., Franke, W., Fuchs, K., and Siefert, F. (eds), 1992. *Continental Lithosphere: Deep Seismic Reflections*, Geodyn. Ser. vol. 22, Am Geophys. Un., Washington.

Mereu, R.F., Mueller, St., and Fountain, D.M. (eds), 1989. *Properties and processes of the Earth's lower crust*, Geophys. Monogr. No. 51, Am. Geophys. Un., Washington.

Merzer, A.M., and Klemperer, S.L., 1992. High electrical conductivity in a model lower crust with unconnected, conductive, seismically reflective layers, *Geophysical Journal International*, **108**, 895-905.

Milkereit, B, and Spencer, C, 1989. Noise suppression and coherency enhancement of seismic data, in *Statistical applications in the earth sciences*, pp. 243-248, eds. Agterberg, F.P., and Bonham-Carter, G.F., Paper 89-9, Geol. Surv. Can.

Misener, A.D., Thompson, L.G.D., and Uffen, R.J., 1951. Terrestrial heat flow in Ontario and Québec, *Transactions American Geophysical Union*, **32**, 729-738.

Mooney, W.D., and Brocher, T.M., 1987. Coincident seismic reflection/refraction studies of the continental lithosphere; a global review, *Reviews of Geophysics*, **25**, 723-742.

Nesbitt, B.E., 1992. Electrical resistivities of crustal fluids, *Journal of Geophysical Research*, in press.

Newton, R.C., 1989. Metamorphic fluids in the deep crust, *Annual Review of Earth and Planetary Science*, **17**, 385-412.

Nikolaevsky, V.N., 1985. Mechanics of fluid-saturated geomaterials: discusser's report, in *Mechanics of geomaterials*, pp. 379-401, ed. Z. Bažant, J. Wiley and Sons.

O'Connell, R.J., and Budiansky, B., 1974. Seismic velocities in dry and saturated cracked solids, *Journal of Geophysical Research*, **86**, 5412-5426.

PASSCAL Basin and Range Group, 1988. The 1986 PASSCAL Basin and Range lithospheric seismic experiment, *EOS*, **69**, 593-598.

Percival, J.A., and Card, K.D., 1985. Structure and evolution of Archean crust in central Superior province, Canada, *Geological Association of Canada Special Paper No. 28*, 179-192.

Percival, J.A., Green, A.G., Milkereit, B., Cook, F.A., Geis, W., and West, G.F., 1989. Seismic reflection profiles across deep continental crust exposed in the Kapuskasing uplift structure, *Nature*, **342**, 416-420.

Pham, V.N., Boyer, D., Therme, P., Yuan, X.C., Li, L., and Jin, G.Y., 1986. Partial melting zones in the crust in southern Tibet from magnetotelluric results, *Nature*, **319**, 310-314.

Poll, H.E., Weaver, J.T., and Jones, A.G., 1989. Calculations of voltages for magnetotelluric modelling of a region with near-surface inhomogeneities, *Physics of the Earth and Planetary Interiors*, **53**, 287-297.

Quist, A.S., and Marshall, W.L., 1969. The electrical conductances of some alkali metal halides in aqueous solutions from 0 to 800°C and at pressures to 4000 bars, *Journal of Physical Chemistry*, **73**, 978-985.

Ranalli, G., 1987. *Rheology of the earth*, Allen and Unwin, Boston.

Rasmussen, T.M., Roberts, R.G., and Pedersen, L.B., 1987. Magnetotellurics along the Fennoscandian Long Range profile, *Geophysical Journal of the Royal Astronomical Society*, **89**, 799-820.

Reston, T.J., 1988. Evidence for shear zones in the lower crust offshore Britain, *Tectonics*, **7**, 929-945.

Reston, T.J., 1990. Shear in the lower crust during extension: not so pure and simple, *Tectonophysics*, **173**, 175-183.

Robinson, R., 1983. Velocity structure of the Wellington region, New Zealand, from local earthquake data and its implications for subduction tectonics, *Geophysical Journal of the Royal Astronomical Society*, **75**, 335-359.

Sapin, M., Wang, X.J., Hirn, A., and Xu, Z.H., 1985. A seismic sounding in the crust of the Lhasa Block, Tibet, *Annales Geophysicae*, **3**, 637-646.

Sastry, T.S., Prasad, S.N., Srivastava, B.J., and Someswara Rao, M., 1990. Vertical electric profile at Choutuppal (Hyderabad) in peninsular India, *Physics of the Earth and Planetary Interiors*, **59**, 229-232.

Schmelling, H., 1985. Numerical models on the influence of partial melt on elastic, anelastic and electrical properties of rocks. Part I: elasticity and anelasticity, *Physics of the Earth and Planetary Interiors*, **41**, 34-57.

Schmucker, U., 1988. *Ergänzende magnetotellurische Sondierungen im Rheingraben*, Inst. Geop. Univ. Göttingen.

Shankland, T.J., and Ander, M.A., 1983. Electrical conductivity, temperatures, and fluids in the lower crust, *Journal of Geophysical Research*, **88**, 9475-9484.

Shearer, P.M., 1988. Cracked media, Poisson's ratio, and the nature of the upper oceanic crust, *Geophysical Journal*, **92**, 357-362.

Sinno, Y.A., Daggett, P.H., Keller, G.R., Morgan, P., and Harder, S.H., 1986. Crustal structure of the southern Rio Grande Rift from seismic refraction profiling, *Journal of Geophysical Research*, **91**, 6143-6156.

Sinno, Y.A., and Keller, G.R., 1986. A Rayleigh wave dispersion study between El Paso, Texas and Albuquerque, New Mexico, *Journal of Geophysical Research*, **91**, 6168-6174.

Stanley, W.D., 1984. Tectonic study of the Cascade Range and Columbia Plateau in Washington State based upon magnetotelluric soundings, *Journal of Geophysical Research*, **89**, 4447-4460.

Sternberg, B.K., Washburne, J.C., and Pellerin, L., 1988. Correction for static shift in magnetotellurics using transverse electromagnetic soundings, *Geophysics*, **53**, 1459-1468.

Swanson Analysis Systems, 1989. *ANSYS engineering analysis system, user's*

manual, vol. I and II, Swanson Analysis Systems Inc., Houston, PA.

Taylor, S.R., and McLennan, S.M., 1985. *The continental crust, its composition and evolution*, Blackwell Scientific Publications, Oxford.

Tezkan, B., 1988. Electromagnetic sounding experiments in the Schwarzwald ntral gneiss massif, *Journal of Geophysics*, **62**, 109-118.

Thompson, A.B., and Connolly, I.A.D., 1990. Metamorphic fluids and anomalous porosities in the lower crust, *Tectonophysics*, **182**, 47-55.

Thompson, A.B., and Connolly, J.A.D., 1992. Migration of metamorphic fluid: some aspects of heat and mass transfer, *Earth Science Reviews*, **32**, 107-121.

Thompson, R.G., Nekut, A., and Kuckes, A.F., 1983. A deep crustal electromagnetic sounding in the Georgia Piedmont, *Journal of Geophysical Research*, **88**, 9461-9473.

Touret, J., 1986. Fluid inclusions in rocks from the lower continental crust, in *The Nature of the lower continental crust*, pp. 161-172, eds. Dawson, J.B., Carswell, D.A., Hall, J., and Wedepohl, K.H., Spec. Publ. 24., Geol. Soc., London.

van Zijl, J.S.V., 1977. Electrical studies of the deep crust in various tectonic provinces of southern Africa, in *The Earth's crust*, pp. 470-500, ed. Heacock, J.G., Geophys. Monog. No. 20., Am. Geophys. Un., Washington.

Volbers, R., Jödicke, H., and Untiedt, J., 1990. Magnetotelluric study of the earth's crust along the deep seismic reflection profile DEKORP 2-N, *Geologische Rundschau*, **79**, 581-601.

von Bargen, N., and Waff, H.S., 1986. Permeabilities, interfacial areas and curvatures of partially molten systems: results of numerical computations of equilibrium microstructures, *Journal of Geophysical Research*, **91**, 9261-9276.

Wannamaker, P.E., 1986. Electrical conductivity of water-undersaturated crustal melting, *Journal of Geophysical Research*, 91, 6321-6327.

Ward, G., and Warner, M., 1991. Lower crustal lithology from shear wave seismic reflection data, in *Continental Lithosphere: Deep Seismic Reflections*, pp. 343-349, eds. Meissner, R., Brown, L., Dürbaum, H.J., Franke, W., Fuchs, K., and Siefert, F., Geodyn. Ser. vol. 22, Am Geophys. Un., Washington.

Warner, M., 1990. Basalts, water, or shear zones in the lower continental crust?, *Tectonophysics*, **173**, 163-174.

Watson, E.B., 1986. Immobility of reduced carbon along grain boundaries in dunite, *Geophysical Research Letters*, **13**, 529-532.

Watson, E.B., and Brennan, J.M., 1987. Fluids in the lithosphere, 1. Experimentally-determined wetting characteristics of CO_2-H_2O fluids and their implications for fluid transport, host-rock physical properties, and fluid inclusion formation, *Earth and Planetary Science Letters*, **85**, 497-515.

Watt, J.P., Davies, G.F., and O'Connell, R.J., 1976. The elastic properties of composite materials, *Reviews of Geophysics*, **14**, 541-564.

Weaver, B.L., and Tarney, J., 1984. Major and trace element composition of the continental crust, *Physics and Chemistry of the Earth*, Chapter 7.

Weaver, J.T., and Agarwal, A.K., 1992. Automatic one-dimensional inversion of magnetotelluric data by the method of modelling, *Geophysical Journal International*, in press.

Wier, S., 1982. Surface-wave dispersion and earth structure in south-eastern China, *Geophysical Journal of the Royal Astronomical Society*, **69**, 33-47.

Wyllie, M.R.J., Gregory, A.R., and Gardner, L.W., 1956. Elastic wave velocities in heterogeneous and porous media, *Geophysics*, **21**, 41-70.

Yardley, B.W., 1981. Effect of cooling on the water content and mechanical behaviour of metamorphosed rocks, *Geology*, **9**, 405-408.

Yoder, H.S., 1976. *Generation of basaltic magma*, National Academy of Sciences, Washington.

Zelt, B.C., Ellis, R.M., Clowes, R.M., Kanasewich, E.R., Asudeh, I., Luetgert, J.H., Hajnal, Z, Ikami, A., Spence, G.D., and Hyndman, R.D., 1992. Crust and upper mantle velocity structure of the Intermontane Belt, southern Canadian Cordillera, *Canadian Journal of Earth Sciences*, in press.

Zucca, J.J., 1984. The crustal structure of the southern Rhinegraben from re-interpretation of seismic refraction data, *Journal of Geophysics*, **55**, 13-22.